Cosmological Phase Transitions: Extra Dimensions and Black Holes

Jonathan Manuel

Submitted for the degree of

Doctor of Philosophy

Theoretical Particle Physics Research Group

School of Mathematical and Physical Sciences

University of Sussex

23rd November 2020

Declaration

I hereby declare that this thesis has not been and will not be submitted in whole or in part to another University for the award of any other degree.

Results in this thesis were obtained in collaboration with Dr Barry Dillon, Dr Basem El-Menoufi and Dr Stephan Huber and published in the following papers:

- B. M. Dillon, B. K. El-Menoufi, S. J. Huber, and J. P. Manuel, "Rapid holographic phase transition with brane-localized curvature", Phys. Rev. D 98 no. 8, (2018) 086005, arXiv:1708.02953
- B. K. El-Menoufi, S. J. Huber, and J. P. Manuel, "Black holes seeding cosmological phase transitions", Submitted for publication, arXiv:2006.16275

My contribution to the first paper is essential throughout with the exception of Section 4.5, as labelled in this thesis. My contribution to the second paper is essential throughout.

Signature:

Jonathan Manuel

UNIVERSITY OF SUSSEX

Jonathan P. Manuel

Doctor of Philosophy

Cosmological Phase Transitions: Extra Dimensions and Black Holes

SUMMARY

Early Universe cosmological phase transitions, in particular first-order transitions which proceed through the nucleation of bubbles, provide an environment for interesting physics with potentially detectable consequences. This thesis focuses broadly on bubble nucleation rates and the determination of a successful transition. After providing the groundwork for understanding these transitions and their key characteristics, this work can be considered in two main parts: improving viability of the extra-dimensional holographic phase transition, and quantifying the effect of black holes acting as nucleation sites for thermal phase transitions.

Extra dimensional models recently gained traction as attractive options for solving the hierarchy problem, one of physics' most prominent issues. Finite temperature studies of the Randall-Sundrum model, one of the most popular models, revealed the existence of the *holographic phase transition*, a first-order transition described by the radion field. Typically, however, this transition struggles to complete while maintaining a consistent theory. Applying knowledge from more conventional settings, this thesis firstly describes work to alleviate this problem through the introduction of brane localised curvature, altering the kinetic term of the radion field. Ultimately, it is shown that nucleation rates sufficient for a successful phase transition can be achieved over a large region of parameter space.

Nevertheless, difficulties remain when describing the role of black holes in holographic phase transitions. Inspired by these issues, the second key work of this thesis studies the possibility of black holes acting as nucleation sites in thermal phase transitions. Within the thin-wall limit, it is found that lower mass black holes could drastically improve nucleation rates. Consequently, future studies of cosmological phase transitions should carefully consider the effect of black holes; particularly in regards to phenomenological outcomes such as gravitational waves.

Acknowledgements

Firstly, I would like to thank my supervisor of nearly five years Stephan Huber, who provided me with this great opportunity and has always supported my work. A special thank you also goes to Basem El-Menoufi who was like a second supervisor to me as well as a friend. His encouragement alongside the endless hours spent discussing details will be missed. Thanks as well go to Thomas Konstandin who acted as my supervisor during a fantastic placement at DESY, Hamburg.

Further, I would like to thank my fellow students at Sussex who all made my time more enjoyable. In particular, my office mates over the years Andy Bond, Djuna Croon, Daniel Cutting, Chris Harman, Gustavo Medina and Yannick Kluth for all the laughter and discussions alongside putting up with my annoying habits. A special mention must go to my eternal office mate Daniel Cutting, who has been there throughout all the struggles as well as the good times and has made this experience so much better.

Of course, I am also very grateful for all the support of my family for their unending support and belief in me. And I must mention my friends Bill, Gavin, Jack, Jeremy, Ranald, Ryan, Sam and Tim for providing laughter when I need it the most.

Finally, I must thank my partner Sarah who always provides boundless support for all my endeavours and always shows an interest by asking "What's new in the quantum world?"

Contents

1 Introduction **1**

2 Cosmological Phase Transitions **6**

2.1 Describing False Vacuum Decay . . . 7

2.1.1 Zero-Temperature . . . 8

2.1.2 Finite Temperature . . . 11

2.1.3 Thin-wall Approximation . . . 13

2.1.4 Numerical Solutions . . . 15

2.1.5 Transition Rate and Successful Phase Transitions . . . 15

2.2 Thermodynamic Features of the Phase Transition . . . 17

2.3 Gravitational Waves . . . 18

2.3.1 Collisions . . . 19

2.3.2 Sound Waves . . . 20

2.3.3 MHD Turbulence . . . 21

3 Holographic Phase Transitions **22**

3.1 Large Extra Dimensions . . . 22

3.2 Randall-Sundrum model of Extra Dimensions . . . 23

3.2.1 Solving Hierarchies . . . 26

3.2.2 The Radion and Stabilisation . . . 27

3.2.3 Cosmology of the RS model . . . 30

3.3 The Holographic Phase Transition . . . 30

3.3.1 Comparing Free Energies . . . 31

3.3.2 Dynamics of the Phase Transition . . . 34

3.3.3 Characteristics of the HPT . . . 37

3.3.4 Approaches to the Black Hole Kinetic Term . . . 38
3.4 Addressing the Problems . . . 40

4 Rapid Holographic Phase Transition with Brane-Localized Curvature 42
4.1 Introduction . . . 43
4.2 Effect of brane-localized curvature on the radion . . . 45
4.2.1 Radion kinetic term . . . 46
4.2.2 Stabilization and the radion potential . . . 49
4.3 Thermal phase transition: holographic description . . . 51
4.4 Dynamics of the phase transition at large N . . . 53
4.4.1 Qualitative discussion . . . 54
4.4.2 Including brane-localized curvature . . . 61
4.4.3 Alternative look at the black hole contribution . . . 65
4.5 Phenomenology of brane-localized curvature . . . 69
4.5.1 Radion phenomenology . . . 70
4.5.2 Spin-2 phenomenology . . . 72
4.6 Discussion . . . 74

5 An Unsatisfactory Solution 76
5.1 Deriving an Approximate Black Hole Kinetic Term . . . 76
5.2 Black Holes as Nucleation Sites . . . 77

6 Black Holes as Nucleation Sites 79
6.1 Including Gravity: Coleman-de Luccia . . . 79
6.2 Black Holes Nucleating Zero Temperature Phase Transitions . . . 82
6.2.1 An Initial Investigation . . . 82
6.2.2 Quantifying the Conical Singularities . . . 87
6.3 Application to Finite Temperature Phase Transitions . . . 91

7 Black Holes Seeding Cosmological Phase Transitions 93
7.1 Introduction . . . 94
7.2 Bubbles vs Bounces in QFT . . . 97
7.2.1 Tunneling in Quantum Mechanics . . . 97
7.2.2 Tunneling in Quantum Field Theory . . . 99

7.3 Black Holes and Cosmological Phase Transitions . . . 102
7.3.1 Thin-wall instantons . . . 103
7.3.2 Interlude: the Coleman-de Lucia solution . . . 106
7.3.3 Including Black holes . . . 107
7.3.4 Static bubbles & periodic bounces . . . 111
7.4 The Tunneling Exponent . . . 116
7.4.1 Quantitative analysis . . . 119
7.4.2 Bubble nucleation criteria with black holes . . . 121
7.4.3 Electroweak-like phase transition . . . 123
7.5 Routes for phenomenology . . . 127
7.5.1 Primordial Black Holes: Formation and Abundance . . . 127
7.5.2 Black Hole Decay via Hawking Radiation . . . 128
7.6 Discussion and prospects for gravitational waves . . . 129
7.7 Summary . . . 131

8 Conclusion **133**

Bibliography **137**

Chapter 1

Introduction

Following the discovery of symmetry restoration at high temperatures [1–6] cosmological phase transitions became viable events with interesting physical consequences such as the creation of cosmological magnetic fields [7], the generation of the baryon asymmetry [8–11] (see reviews [12–16]) and the production of a gravitational wave background [17–19] (see reviews [20–23]). Such transitions could take place throughout a vast range of scales: from QCD ($\sim$ 100 MeV) [24–26] to Grand Unified Theory (GUT) ($\sim 10^{15}$ GeV) [27]. A thorough review is [28].

While these transitions can take various forms - first-order, second-order and crossover - the focus here will be on first-order transitions in which a metastable state is separated from an energetically favourable state by a potential barrier, with the transition proceeding through the nucleation of bubbles. One of the most important contributions to the understanding of these phase transitions is the work of Coleman and Callan [29, 30]. Their theory of false vacuum decay describes the decay of such a metastable state through quantum tunnelling at zero temperature and remains the basis of contemporary studies. Following swiftly, motivated by the knowledge of symmetry breaking in the early universe, Linde [31, 32] adapted the formalism to finite temperature. These studies expressed the nucleation rate of bubbles per unit volume in the simple form

$$\frac{\Gamma}{\mathcal{V}} = A\, e^{-B} \ . \tag{1.1}$$

While the coefficient A is typically a complex and involved quantity to compute, the exponent B is comparably simple to calculate, relying solely on the finite temperature potential describing the field and the parameters therein.

One of the most well studied transitions, because of its known existence in some form, is the electroweak phase transition (EWPT). Despite not being first-order in the Standard Model [33–37] many simple extensions can change this [38–45]. Originally, one of the most exciting prospects of the EWPT was solving the baryon asymmetry; however, this has become increasingly difficult [16]. With the landmark discovery by LIGO [46], gravitational waves now rule as the popular phenomenological outcome. This is particularly the case for electroweak-scale phase transitions where the stochastic background produced from the expansion and collision of bubbles could be detectable [21–23] with the planned LISA observatory [47].

While the imminent era of gravitational wave-based astronomy provides reason to be excited for the many extensions of the electroweak phase transition, these may not be the only detectable electroweak-scale transitions.

Extra dimensional models have existed since the work of Kaluza and Klein in the 1920's. It is only rather recently however, that they have become a mainstream particle physics subject, particularly from a cosmological phase transition viewpoint. Such models are often offered as a potential solution to the hierarchy problem, the vast discrepancy between the weak and Planck scales. Typically, these involve adding one or more large spatial dimensions [48] affecting only gravity and altering its fundamental scale. However, the necessary size and number of extra dimensions has made these theories rather unfavourable. One of the most popular alternatives is the Randall-Sundrum (RS) model [49]. Consisting of a single warped, spatial extra dimension bordered by branes, masses are shifted without the need of a large extra dimension while the Standard Model is confined to a brane.

However, studies of the RS model cosmology revealed that deviations from standard cosmology ultimately occur above $\sim 1\,\text{TeV}$ [50–53]. Inspired by these difficulties, the seminal work of Ref. [54] developed an alternative approach from the basis of the Anti-de Sitter/Conformal Field Theory (AdS/CFT) correspondence [55] and holography - the relation between a $(d+1)$-dimensional gravitational model and a d-dimensional conformal field theory. It was revealed that the dominant phase at high temperatures is described by an AdS_5-Schwarzschild space in which the brane containing the Standard Model has been replaced by the horizon of a five-dimensional (5D) Schwarzschild black hole. The transition from this high temperature phase to the RS setup has become known as the holographic phase transition. From the four-dimensional (4D) viewpoint, as informed by holography, this corresponds to a CFT transitioning from a deconfined to a confined phase. Given that the aim of the RS

model is to solve the hierarchy problem, the scale of the transition is typically electroweak.

From the viewpoint of traditional cosmological phase transitions, the holographic phase transition is certainly peculiar. Rather than being described by a single scalar field, the RS model, with a certain brane separation parametrised by the radion field μ, is glued to the black hole configuration, parametrised by the T_H field representing the position of the black hole horizon and corresponds to the Hawking temperature. The result is a potential, given by the stitching together of the free energies of the two phases, with a large separation in minima compared to the size of the maximum dividing them. A study of the general outcomes of such potentials was given in Ref. [56]. In regards to the holographic phase transition, the result is a significant amount of supercooling [57–59]. Naturally, the resulting gravitational wave background has also been studied with promising prospects for upcoming space based detectors [57, 59]. A recent study [60] has considered the transition in the presence of strong backreaction, removing any previously present supercooling but remaining detectable at future gravitational wave observatories.

Nevertheless, two key issues plague the holographic phase transition. Firstly, the limit on the parameter N. Defined as the size of the gauge group in the corresponding CFT, N is related to the 5D gravitational mass scale through holography. A large N is necessary for the semi-classical gravitational description to be valid, yet harms prospects for a successful transition by increasing the transition exponent B. Many previous studies [57–59] have found tension here. Secondly, ambiguities exist in the description of the high temperature phase. The kinetic term of the T_H field is unknown and is approximated to be identical to that of the radion. Hence, the true form of potential is not known.

The second part of this thesis focuses on the impact of black holes acting as bubble nucleation sites during cosmological first-order phase transitions. Gravity was first considered in the context of false vacuum decay by Coleman and De Luccia [61]. While it was found that the Euclidean action B could be reduced when tunnelling from a space with positive to zero vacuum energy, the effect is negligible for almost all conceivable applications. Yet, this was only the beginning for gravity. Ref. [62] proposed the idea that black holes could act as nucleation sites for bubbles, much like impurities in traditional transitions. Using Israel's junction conditions [63], a thin-wall formalism was developed. Depending on whether the initial vacuum energy density is positive, zero or negative, the respective Schwarzschild metric describes the initial state. A bubble of the lower energy state then spherically symmetrically

forms around the black hole and expands. Applying this in a zero temperature setting, Ref. [62] found that the introduction of black holes could reduce the transition exponent by almost a factor of 2, providing remarkable improvements in bubble nucleation rates.

Despite the success of Ref. [62], it had two main drawbacks: an unchanging black hole mass between phases and neglecting conical singularities. While the first is rather self-explanatory, conical singularities arise when the inverse periods of the Euclidean times do not match the Hawking temperature of the black holes.

After a rather long absence, the topic of black holes as nucleation sites recently gained popularity due to the work of Ref. [64]. Developing a formalism inspired by Ref. [62], they solved both the issue of constant mass and conical singularities, the second by implementing the work of Ref. [65]. It became clear that conical singularities play an important role, while a remnant mass differing from the seed mass presented opportunities for even greater improvements in nucleation rates. In fact, it was found that such improvements can become arbitrarily high for small seed black hole masses. Just as with Ref. [62], this study was focused on zero temperature transitions and has been applied to the fate of the current Higgs vacuum [66, 67].

Given the remarkable consequences for nucleation rates, one has to wonder how black hole nucleation sites would affect finite temperature cosmological phase transitions. Similar changes could have profound consequences for the predicted gravitational wave background, altering bubble sizes and velocities at collision.

With these topics in mind, this thesis follows the following structure. Chapter 2 introduces cosmological transitions and the framework to describe them. In particular: finding bubble profiles and calculating the transition exponent, both numerically and using the thin-wall approximation; using the transition rate to determine a successful phase transition; and calculating the gravitational wave power spectrum.

Using these concepts, the holographic phase transition is introduced in Chapter 3. First, the premise of extra-dimensions is introduced before shifting focus to the Randall-Sundrum model. After outlining issues with the cosmology, the necessity for an alternative high temperature phase is apparent and the holographic phase transition is proposed. The potential governing the dynamics is derived and the main features, as well as the limitations, are discussed. Most importantly, the restrictions on N and ambiguities in the description of the high temperature phase are highlighted.

Chapter 4 presents published work [68] introducing brane-localised curvature as a method to solve the first of these restrictions. With this natural addition, it is found that a successful phase transition is now possible at a large N ($N \sim 10^2$). Nevertheless, the ambiguities of the high temperature phase remain and Chapter 5 briefly outlines attempts to solve this. While they are unsuccessful, the idea for investigating black holes as nucleation sites in cosmological phase transitions is born.

The role of gravity and black holes in false vacuum decay is introduced in Chapter 6. By outlining the thin-wall formalism developed and refined in Refs. [62, 64] the basis is provided for application to a finite temperature setting. Chapter 7 does just this, presenting work submitted for publication [69] studying the role of black holes acting as nucleation sites in cosmological phase transitions. It is found that smaller mass black holes have great potential for improving transition rates. While concrete conclusions cannot be made without specifying a primordial black hole distribution, the various transition scenarios and their consequences on the resulting gravitational wave spectrum are outlined.

Finally, Chapter 8 offers concluding remarks and a future outlook.

Chapter 2

Cosmological Phase Transitions

In particle physics, a phase transition describes the transition from one vacuum state to another. To describe a typical scenario imagine the potential describing a scalar field $V(\phi, T)$ in a cooling universe. At high temperatures there exists a single minimum of $V(\phi, T)$ in which the universe sits, known as the false vacuum. As the universe cools a new energetically favourable minimum begins to form, known as the true vacuum, and the state transitions from false to true vacuum. The nature of the phase transition depends on the characteristics of this transition. If it is a continuous process it is known as a second-order phase transition. If the change is discontinuous, however, it is known as a first-order phase transition. Figure 2.1 shows the two cases for the scalar field potential $V(\phi, T)$. The left-hand plot shows a second-

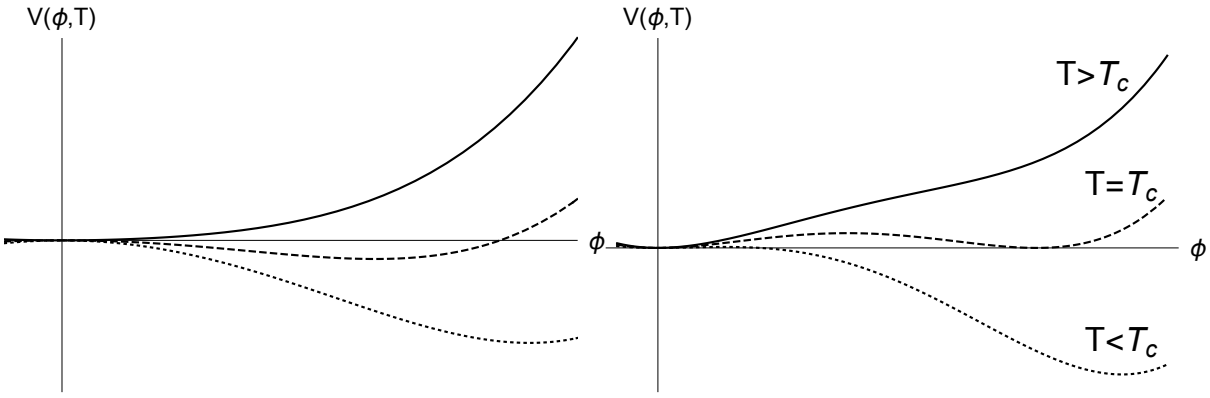

Figure 2.1: Left: Second-order phase transition for an example potential $V(\phi, T)$. Right: First-order phase transition for an example potential $V(\phi$,T). A first-order transition is signified by the presence of a barrier separating two minima. The critical temperature T_c is the temperature at which the two minima are degenerate.

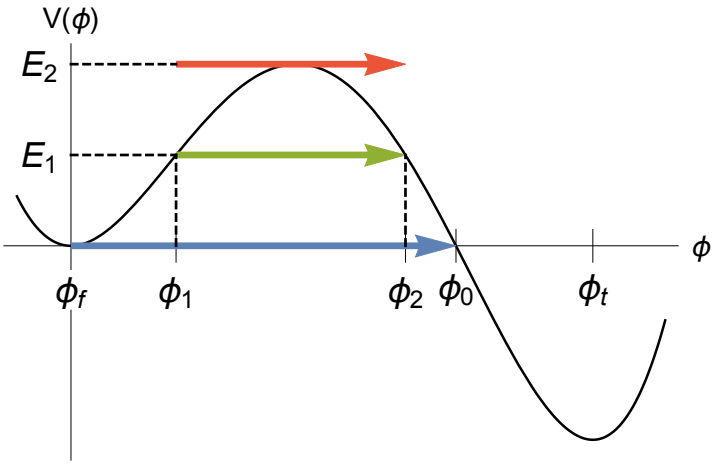

Figure 2.2: The three methods of decay of a false vacuum at finite temperature. Blue: Quantum decay from the ground state. Green: Quantum decay from a thermally excited state. Red: Thermal excitation over the barrier.

order transition where there is only ever one minimum and the emergence of the true vacuum is a continuous process. The right-hand plot instead shows a first-order transition. Here a barrier exists between the false and true vacua, allowing the coexistence of the two phases. At the critical temperature T_c the two minima are degenerate. Above T_c, the false vacuum is energetically favourable; below, the true vacuum is instead preferred and the transition begins. The transition occurs through the nucleation of bubbles, providing a unique physical environment. The focus of this thesis is first-order phase transitions.

2.1 Describing False Vacuum Decay

The method of decay from a false vacuum takes various forms depending on the temperature of the system. Taking an example scalar field potential $V(\phi)$, the coloured arrows in Figure 2.2 show the three methods. The aim is to quantify the probability of transition from the false vacuum ϕ_f to the true vacuum ϕ_t and the properties therein. Decay probability per unit time per unit volume is given by

$$\frac{\Gamma}{\mathcal{V}} = A\, e^{-B} \ . \tag{2.1}$$

Before moving onto the details of calculating the transition rate for each of the three methods, the basic idea of each will be introduced.

The first method is decay of the ground state at zero-temperature through quantum tun-

nelling, demonstrated by the blue line in Figure 2.2, and was first described by Coleman and Callan [29, 30]. Tunnelling occurs from the ground state at ϕ_f to ϕ_0, from which the state settles into the true vacuum ϕ_t.

Moving onto finite temperature processes, the second method is quantum tunnelling from a thermally excited state, shown by the green line in Figure 2.2. The ground state is thermally excited to a state with energy $E = E_1$ at ϕ_1 from which quantum tunnelling takes place, emerging at ϕ_2. This method is rarely discussed in the literature, as will be explained shortly.

Finally, if the temperature is large enough, thermal fluctuations can excite the ground state over the barrier, shown by the red line in Figure 2.2. This description was first developed by Linde [32]. It is important to highlight that, in contrast to the previous two methods, this involves no quantum tunnelling.

With the three methods introduced they will now be discussed in greater detail.

2.1.1 Zero-Temperature

Vacuum decay at zero-temperature in quantum field theory was first described by Coleman and Callan [29,30]. Building off the quantum mechanical description of a particle experiencing quantum tunnelling, an equivalent formalism of barrier penetration in quantum field theory was developed. The physical picture is described by the blue arrow in Figure 2.2; the aim is to describe the transition of the field from the false vacuum ϕ_f to the true vacuum ϕ_t through quantum tunnelling, with the intent of calculating the tunnelling rate given by Eq. (2.1). To begin, the exponent B will be calculated as given by Coleman [29], with A mentioned later as given by Coleman and Callan [30]. The scalar field is described by the Euclidean equation of motion

$$\left(\frac{d^2}{d\tau^2} + \nabla^2\right)\phi = \frac{dV(\phi)}{d\phi} \tag{2.2}$$

with the boundary conditions

$$\lim_{\tau\to\pm\infty} \phi(\tau, \vec{x}) = \phi_f \quad , \quad \lim_{|\vec{x}|\to\pm\infty} \phi(\tau, \vec{x}) = \phi_f \quad , \quad \frac{d\phi(0, \vec{x})}{d\tau} = 0 \quad . \tag{2.3}$$

Coleman named these solutions *bounces* and here they will be referred to as *infinite-period bounces*, a label that will commonly be used from now on.

Normalising the potential with respect to the false vacuum, $V(\phi) \to V(\phi) - V(0)$, the

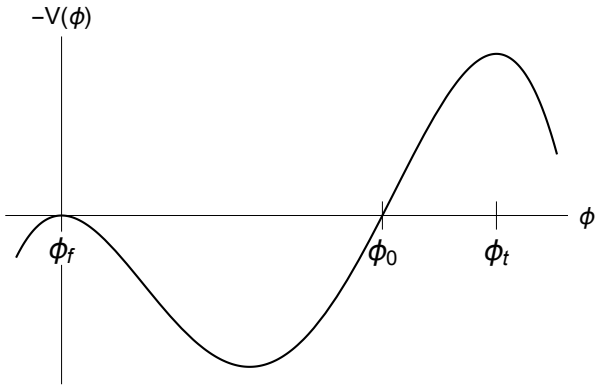

Figure 2.3: Inverse of an example potential $V(\phi)$. The equation of motion, Eq. (2.5), describes a particle moving in the inverse of the potential $V(\phi)$ with a damping term.

exponent of the decay rate B is the Euclidean action for the bounce

$$B = \int d^4x \left[\frac{1}{2} \left(\frac{d\phi}{d\tau} \right)^2 + \frac{1}{2} (\nabla\phi)^2 + V(\phi) \right] . \tag{2.4}$$

To get the true result for Γ it is necessary to sum over all contributions from all possible solutions of ϕ from Eq. (2.2). Thankfully, however, Coleman proved [29] that O(4)-invariant bounces provide the minimum of S_4 and therefore dominate the transition rate. In this case, the coordinate $\rho^2 = (\tau^2 + \vec{x}^2)$ can be used to simplify the equation of motion of Eq. (2.2) to

$$\frac{d^2\phi}{d\rho^2} + \frac{3}{\rho} \frac{d\phi}{d\rho} = \frac{dV(\phi)}{d\phi} , \tag{2.5}$$

with the boundary conditions

$$\lim_{\rho \to \infty} \phi(\rho) = \phi_f \quad , \quad \frac{d\phi(0)}{d\rho} = 0 \quad . \tag{2.6}$$

The final boundary condition is to ensure the solution is regular at the origin $\rho = 0$. In this scenario, the bounce action of Eq. (2.4) becomes

$$B = S_4(\phi) = 2\pi^2 \int_0^\infty d\rho \, \rho^3 \left[\frac{1}{2} \left(\frac{d\phi}{d\rho} \right)^2 + V(\phi) \right] . \tag{2.7}$$

The equation of motion can be understood by interpreting ϕ as the position of a particle and ρ as time. In this case, Eq. (2.2) describes a particle moving in the inverse potential $-V(\phi)$, as shown in Figure 2.3, with a damping force inversely proportional to ρ. The particle is released at rest, Eq. (2.3), and should return to rest in the false vacuum ϕ_f. The correct initial condition, ϕ_r, must lie in the range $\phi_0 < \phi_r < \phi_t$ due to the damping force. The

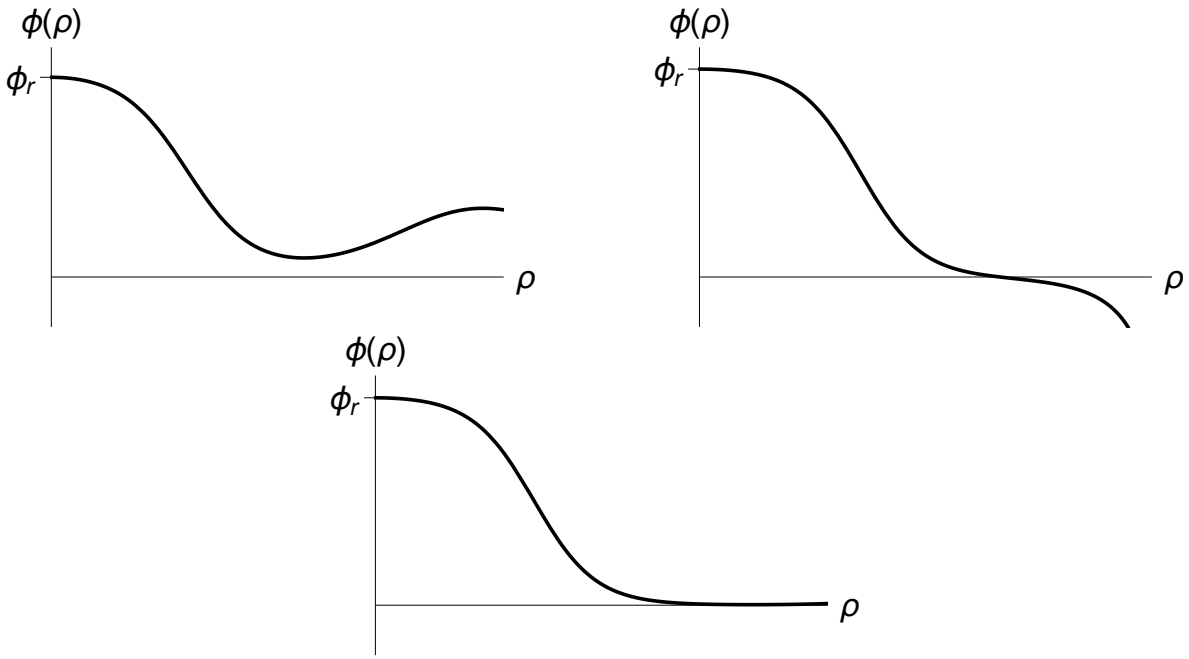

Figure 2.4: The three types of solution for the equation of motion Eq. (2.5) for three different release points ϕ_r in the range $\phi_0 < \phi_r < \phi_t$. Top Left: Undershoot; ϕ_r is too small to reach the peak of $-V(\phi)$ at ϕ_f and ends up oscillating in the minimum. Top Right: Overshoot; ϕ_r is too large, going over the maximum at ϕ_f. Bottom: Bubble; ϕ_r has just the right value such that the particle comes to a rest on top of the maximum.

three types of solution, with an initial release point $\phi_0 < \phi_r < \phi_t$, for Eq. (2.5) are shown in Figure 2.4. If ϕ_r is too small then the particle will undershoot, not having enough energy to climb the hill to ϕ_f, and oscillate in the valley, as shown by the top left plot of Figure 2.4. On the other hand, if ϕ_r is too large then it will simply have too much energy and overshoot the maximum at ϕ_f, as shown by the top right plot of Figure 2.4. When ϕ_r is chosen correctly however, the particle comes to rest on the maximum at ϕ_f, as shown in the bottom plot of Figure 2.4, and the bubble nature of the solutions becomes transparent. At large radial distance the state is that of the false vacuum ϕ_f. As the distance is reduced there is a region of rapidly changing $\phi(r)$ corresponding to the bubble wall. Smaller radial distances are inside the bubble and the state is now in the true vacuum.

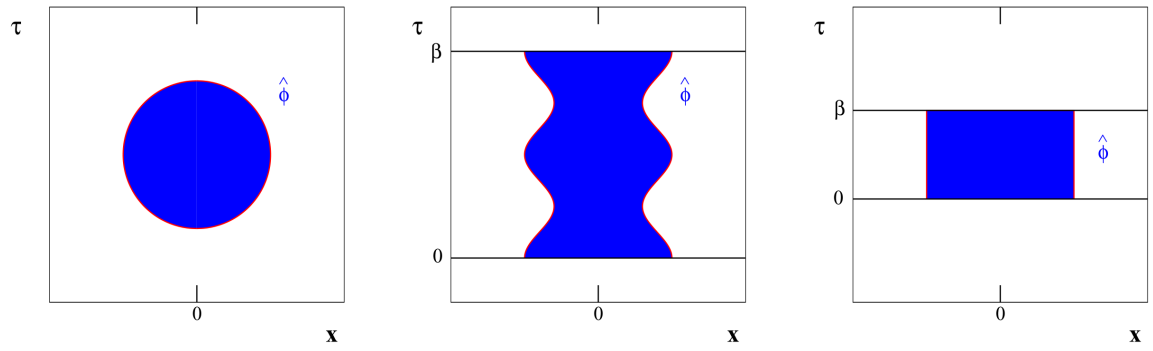

Figure 2.5: The solutions of the equation of motion Eq. (2.2) across a range of temperature regimes from Ref. [70]. Left: Zero-temperature. Middle: Intermediate temperature. Right: High temperature. The respective O(4) and O(3) symmetries at zero and high temperature are apparent.

2.1.2 Finite Temperature

The scenario of finite temperature introduces two alternative methods of vacuum decay, labelled thermally assisted tunnelling and thermal excitation; the green and red lines in Figure 2.2 respectively.

The most known and used is the case of thermal excitation as developed by Linde [32], describing the scenario when thermal fluctuations are large enough to excite the state over the potential barrier. Here, the zero-temperature description of Coleman and Callan is extended by noting that the Euclidean time has a period $\beta = 1/T$. Consequently, with symmetry in the time direction lost, the equations no longer have a time dependence and one should now look for O(3)-symmetric *static solutions* of Eq. (2.2) with a period $1/T$, in partnership with the finite temperature effective potential $V(\phi, T)$. The solution across a range of temperature regimes is shown in Figure 2.5. It is clear at zero-temperature the solution has O(4)-symmetry, whereas at high temperature this is reduced to O(3)-symmetry due to the periodisation of the Euclidean time. Due to this symmetry, the equations of motion of Eq. (2.2), with $r^2 = x^2$, simplify to

$$\frac{d^2\phi}{dr^2} + \frac{2}{r}\frac{d\phi}{dr} = \frac{dV(\phi, T)}{d\phi} \ , \tag{2.8}$$

with the boundary conditions

$$\lim_{r\to\infty} \phi(r) = \phi_f \quad , \quad \frac{d\phi(0)}{dr} = 0 \quad . \tag{2.9}$$

Comparing this to the zero-temperature result of Eq. (2.5) it is apparent that the only differ-

ences are the factor of 3 becoming 2 in the friction term and the effective potential becoming thermal. Additionally, the bounce action of Eq. (2.4) becomes

$$B = \frac{S_3(\phi)}{T} = \frac{4\pi}{T}\int_0^\infty dr\, r^2 \left[\frac{1}{2}\left(\frac{d\phi}{dr}\right)^2 + V(\phi, T)\right] \ , \tag{2.10}$$

where the $1/T$ factor arises from the periodicity of the Euclidean time coordinate $\int_0^\beta d\tau$.

The final method of transition is quantum tunnelling from a thermally excited state, a process labelled thermally assisted tunnelling and is represented by the green, middle line in Figure 2.2. As described earlier, the ground state of $E = 0$, at ϕ_f, is thermally promoted to an excited state of $E = E_1$, at ϕ_1, from which quantum tunnelling takes place, with the state emerging at ϕ_2. Given the finite temperature setting, the Euclidean time coordinate has a period $\beta = 1/T$ and the boundary conditions for the equation of motion are altered:

$$\frac{d^2\phi}{d\tau^2} + \nabla^2\phi - \frac{dV(\phi, T)}{d\phi} = 0 \ \ , \tag{2.11}$$

with the following boundary conditions

$$\lim_{|\vec{x}|\to\infty} \phi(\tau, \vec{x}) = \phi_f \ , \quad \frac{d\phi(0, \vec{x})}{d\tau} = 0 \ , \quad \frac{d\phi(\tau, \vec{0})}{dr} = 0 \ , \quad \lim_{\tau\to\pm\beta/2} \frac{d\phi(\tau, \vec{x})}{d\tau} = 0 \ \ . \tag{2.12}$$

Just as with the zero temperature case of Eqs. (2.2) and (2.3), these solutions bounce but now with a finite, rather than infinite, period of β. Hence, solutions of thermally-assisted tunnelling are labelled *finite-period bounces*. Studying Figure 2.5, finite-period bounces are portrayed by the middle plot describing solutions at intermediate temperatures. In the two previous methods of infinite-period bounces at zero-temperature and static solutions at finite temperature, the respective O(4) and O(3) symmetries allow great simplifications of the equation of motion Eq. (2.2) and Euclidean action Eq. (2.4). However, for finite-period bounces similar symmetry arguments cannot be made; there remains a dependence on time but it is not with an infinite period. Consequently, simplifications cannot be made and finding solutions becomes difficult. Accordingly, this method is very rarely discussed and used in the literature.

At this point it serves to briefly highlight the forms of the actions in Eqs. (2.7), (2.10). The first term, the gradient of the field $\phi(r)$, is only significantly non-zero across the bubble wall, clearly corresponding to a surface term. The second term, the potential $V(\phi)$, contributes over the full volume of the bubble.

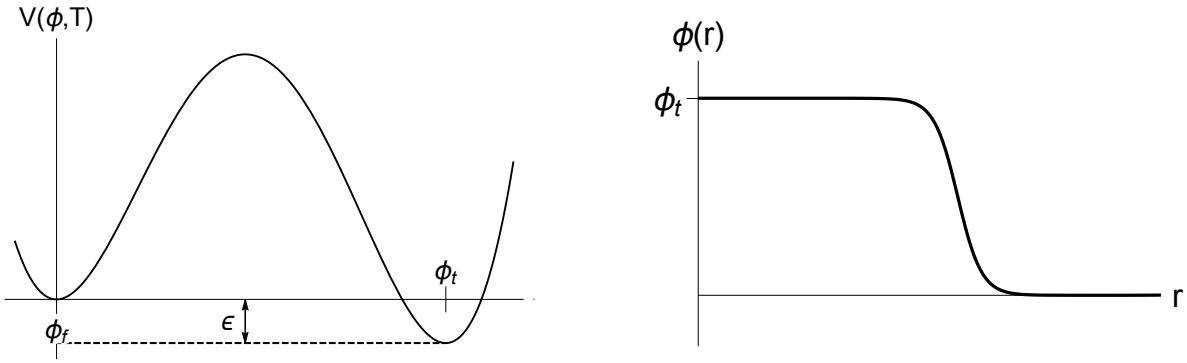

Figure 2.6: Left: An example potential in the thin-wall regime with the key characteristic of a small potential difference ϵ between the minima. Right: The corresponding example thin-wall bubble profile in which it is clear the size of the bubble is large compared to the wall width. In the thin-wall limit, the release point is approximately the true vacuum, $\phi_r \sim \phi_t$.

2.1.3 Thin-wall Approximation

In the limiting case when the difference between potential minima, $|V(\phi_t, T) - V(\phi_f, T)| = \epsilon$, is small compared to the potential barrier the problem is simplified and an analytic solution can be found. In this regime, shown in Figure 2.6 left, the bubble solutions have a large radius in comparison to the thickness of the bubble wall, as shown in Figure 2.6 right; a phenomenon that can be understood by again considering the dynamics of a particle in the inverse potential $-V(\phi, T)$. When ϵ is small the initial condition (or release point) ϕ_r must lie close to the maximum corresponding to the true vacuum ϕ_t. Consequently, the gradient felt by the particle from the potential is gentle and therefore spends a larger amount of time near ϕ_t. This translates to the extended plateau seen at lower r values in Figure 2.6, hence a larger bubble radius.

The large bubble radius allows simplification of the equations of motion of Eqs. (2.5) and (2.8) by noticing that the friction terms proportional to $1/r$ become negligible, reducing the equations to

$$\frac{d^2\phi}{dr^2} = \frac{dV(\phi, T)}{d\phi} \ , \tag{2.13}$$

the equation describing tunnelling in one-dimensional space. The solution of this equation is

$$r = \int_0^\infty \frac{d\phi}{\sqrt{2V(\phi, T)}} \tag{2.14}$$

where the corresponding one-dimensional action is

$$\begin{aligned} S_1 &= \int_0^\infty dr \left[\frac{1}{2} \left(\frac{d\phi}{dr} \right)^2 + V(\phi, T) \right] \\ &= \int_{\phi_f}^{\phi_t} d\phi \sqrt{2V(\phi, T)} \\ &\equiv \sigma \ , \end{aligned} \tag{2.15}$$

a quantity which is in fact the surface tension of the bubble wall, σ, and should be calculated in the limit $\epsilon \to 0$. In the thin-wall approximation the bounce action of Eq. (2.7) takes the form

$$S_4 = 2\pi^2 \sigma r^3 - \frac{\pi^2}{2} \epsilon r^4 \ . \tag{2.16}$$

The critical radius r_c can be found through extremisation of the action

$$r_c = \frac{3\sigma}{\epsilon} \ , \tag{2.17}$$

bearing the action

$$S_4 = \frac{27\pi^2 \sigma^4}{2\epsilon^3} \ . \tag{2.18}$$

The bubble action of Eq. (2.10) follows similar steps taking the form

$$S_3 = 4\pi\sigma r^2 - \frac{4\pi}{3} \epsilon r^3 \tag{2.19}$$

with a critical bubble radius

$$r_c = \frac{2\sigma}{\epsilon} \ , \tag{2.20}$$

leaving the final form

$$S_3 = \frac{16\pi\sigma^3}{3\epsilon^2} \ . \tag{2.21}$$

Studying Eqs. (2.16), (2.19), the surface and volume contributions highlighted earlier become clearer and their opposing effects revealed. At small r the surface term dominates and any bubbles formed will collapse. As r is increased the volume term eventually takes over and bubbles will expand. This behaviour is shown in Figure (2.7). The turning point between collapse and expansion is the critical radius r_c, a solution known as a critical bubble which corresponds to those of the equations of motion Eqs. (2.5), (2.8).

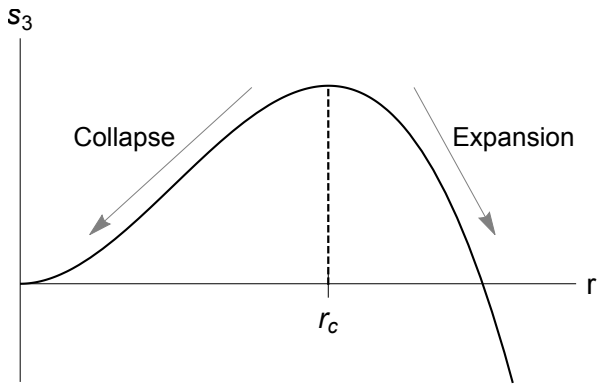

Figure 2.7: The thin-wall bubble action of Eq. (2.19). The location of the turning point is the critical bubble radius, r_c. Above r_c the bubble expands; below r_c the bubble collapses.

2.1.4 Numerical Solutions

Typically, the equations of motion of Eqs. (2.5) and (2.8) are impossible to solve analytically and, therefore, one must turn to numerical methods to find answers. As discussed and shown in Figure 2.4 this is a problem of finding the correct initial condition ϕ_r. Doing so numerically is frequently done using an overshoot-undershoot method. To begin, one chooses an initial ϕ_r and solves the equation of motion (Eq. (2.5) or (2.8)) to find the solution. This result will take one of the forms in Figure 2.4 and the initial condition is correspondingly altered; raise ϕ_r for an undershoot, lower ϕ_r for an overshoot. This process is iteratively repeated until a critical bubble to desired accuracy is found. The solution can then be substituted into the corresponding action Eq. (2.7) or (2.10), giving the exponent of the transition rate.

2.1.5 Transition Rate and Successful Phase Transitions

With methods for finding bubbles and calculating actions outlined, transition rates can be calculated. However, questions remain; what are relevant transition rates and how is a successful phase transition defined?

Acquiring a truly accurate value for the transition rate requires calculating the factor A in Eq. (2.1). It is typically argued that A is insignificant compared to the exponential and therefore it becomes only necessary to calculate B as previously outlined. Such logic is followed in this thesis, however, for completeness the forms for A in quantum and thermal transitions are included here. Coleman and Callan [30] focused solely on deriving A for zero-temperature

false vacuum decay, culminating in the expression

$$A = \left(\frac{S_4(\phi)}{2\pi}\right)^2 \left(\frac{\det'[-\Box + V''(\phi)]}{\det[-\Box + V''(\phi_f)]}\right)^{-1/2} , \tag{2.22}$$

where $\det'$ denotes the determinant computed with the zero eigenvalues omitted. Ref. [32] then demonstrates this can be estimated by realising that A has dimension m^4 and its value is determined by the three quantities $\phi(0)$, $\sqrt{V''(\phi)}$ and r. Hence, the ratio of determinants can be estimated by

$$\left(\frac{\det'[-\Box + V''(\phi)]}{\det[-\Box + V''(\phi_f)]}\right)^{-1/2} \sim \mathcal{O}\left(r^{-4},\, \phi^4(0),\, (V''(\phi))^2\right) , \tag{2.23}$$

and the transition rate takes the form

$$\Gamma \sim \mathcal{O}\left(r^{-4},\, \phi^4(0),\, (V''(\phi))^2\right) \left(\frac{S_4(\phi)}{2\pi}\right)^2 \mathrm{e}^{-S_4(\phi)} . \tag{2.24}$$

Linde [31, 32] additionally extends the description to finite temperature

$$A = T\left(\frac{S_3(\phi,T)}{2\pi T}\right)^{3/2} \left(\frac{\det'[-\Box + V''(\phi,T)]}{\det[-\Box + V''(\phi_f,T)]}\right)^{-1/2} , \tag{2.25}$$

which is again simplified through dimensional considerations and the ratio of determinants is estimated as

$$\left(\frac{\det'[-\Box + V''(\phi,T)]}{\det[-\Box + V''(\phi_f,T)]}\right)^{-1/2} \sim T^3 . \tag{2.26}$$

This leaves the finite temperature transition rate

$$\Gamma(T) \sim T^4 \left(\frac{S_3(\phi,T)}{2\pi T}\right)^{3/2} \mathrm{e}^{-S_3(\phi,T)/T} . \tag{2.27}$$

An estimate for a successful transition would be when at least one critical bubble is nucleated per Hubble volume. In this case Eq. (2.1) takes the form

$$\frac{\Gamma}{H^4} = \frac{A}{H^4}\,\mathrm{e}^{-B} \sim 1 , \tag{2.28}$$

where H is the Hubble constant. With the focus being finite temperature transitions, the coefficient takes a simplified form of Eq. (2.27), $A \sim T^4$, to give

$$\mathrm{e}^{-B} \sim \frac{H^4}{T^4} . \tag{2.29}$$

With the knowledge that during the radiation era $H = 1/(2t)$, the relationship between time and temperature

$$t = \xi\frac{M_p}{T^2} , \tag{2.30}$$

with

$$\xi = \left(\frac{45}{16\pi^3 g_*}\right)^{1/2} , \tag{2.31}$$

where g_* is the number of degrees of freedom at that temperature, is used to rewrite the equation in terms of more relevant parameters

$$\mathrm{e}^{-B} \sim g_*^2 \frac{T^4}{M_p^4} , \tag{2.32}$$

where the numerical factors have been dropped. Solving for B, the estimate for a successful phase transition is found

$$B \sim 170 - 2\ln g_* - 4\ln\left(\frac{T}{\mathrm{GeV}}\right) . \tag{2.33}$$

The temperature at which this condition is satisfied is known as the nucleation temperature T_n and is a key parameter when studying phase transitions.

2.2 Thermodynamic Features of the Phase Transition

It serves to highlight a few thermodynamic properties of the phase transition that can be important for physical consequences such as baryon asymmetry generation and gravitational wave production.

The first of these is the strength of the phase transition described as the ratio of the latent heat (density) to the radiation energy density in the high temperature symmetric phase [71–73] given by the expression

$$\alpha = \frac{\mathcal{L}(T)}{\rho_{\mathrm{rad}}} . \tag{2.34}$$

Latent heat is defined as the difference in enthalpy density

$$\mathcal{L}(T) = w(T, \phi_f) - w(T, \phi_t) , \tag{2.35}$$

where $w = \epsilon + p$ with

$$\epsilon(T, \phi) = \frac{3\pi^2}{90} g_* T^4 + V(\phi, T) - T\frac{\partial V}{\partial T} , \tag{2.36}$$

$$p(T, \phi) = \frac{\pi^2}{90} g_* T^4 - V(\phi, T) . \tag{2.37}$$

An alternative, and that which should be used when calculating gravitational wave spectra, is the ratio of the vacuum energy to the radiation energy density [72, 73]

$$\alpha = \frac{V_0}{\rho_{\mathrm{rad}}} , \tag{2.38}$$

where the vacuum energy is the difference in trace anomalies between the two phases divided by a factor of four

$$V_0 = \frac{1}{4}(\theta_f - \theta_t) \ , \tag{2.39}$$

with trace anomaly

$$\theta = \epsilon - 3p \ . \tag{2.40}$$

Importantly, the resulting expression is

$$\alpha = \frac{1}{\rho_{\text{rad}}} \left(-\Delta V(T) + \frac{1}{4} T \frac{\partial \Delta V(T)}{\partial T} \right) \Bigg|_{T_*} \ , \tag{2.41}$$

where T_* is the relevant temperature and is usually taken to be T_n and $\Delta V = V(\phi_t, T) - V(\phi_f, T)$.

The second important parameter is the (approximate) inverse duration of the phase transition. Taylor expanding the action $S(t)$ around a time t_*

$$S(t) \approx S(t_*) + \frac{dS}{dt}\bigg|_{t_*} (t - t_*) + \dots \ , \tag{2.42}$$

the negative coefficient of the second term gives the inverse time duration

$$\beta \equiv -\frac{dS}{dt}\bigg|_{t_*} \approx \frac{1}{\Gamma}\frac{d\Gamma}{dt}\bigg|_{t_*} \ . \tag{2.43}$$

By using $dT/dt = -TH$ a form in terms of the temperature is obtained

$$\frac{\beta}{H_*} = T_* \frac{dS}{dT}\bigg|_{T_*} \ . \tag{2.44}$$

This ratio β/H_* again plays an important role when calculating the gravitational wave spectrum.

Lastly, mentioned here because of its importance for most physical consequences is the velocity of the expanding bubble wall v_w. Calculation of wall velocity is a deeply involved process in which particle interactions at the interface on a microscopic level are needed, an exercise beyond the scope of this thesis. Therefore, it is rather typical for estimates or certain limits to be taken in the literature, in particular the runaway limit in which $v_w \to 1$. Further information can be found in the plethora of studies [45, 74–79].

2.3 Gravitational Waves

Gravitational waves (GWs) have become an important contemporary focus in the study of cosmological phase transitions thanks to the landmark first detection by LISA [46] and the

planned space-based observatories of the future [47]. While the focus of this thesis and the works within are not on gravitational wave production, the basics will be discussed such that dependencies on phase transition characteristics can be understood. During a first-order phase transition three main processes involved in the production of GWs have been outlined [21]:

- Collision of expanding bubble walls and shocks in the plasma.
- Sound waves left in the plasma after bubble collision.
- Magnetohydrodynamic (MHD) turbulence forming in the plasma after bubble collision.

The total gravitational wave power spectrum is then approximately the sum of these three contributions

$$h^2\Omega(f) \approx h^2\Omega_{\rm col}(f) + h^2\Omega_{\rm sw}(f) + h^2\Omega_{\rm turb}(f) \ . \tag{2.45}$$

Basics of each contribution will now be briefly discussed, while further details can be found in Refs. [20–23].

2.3.1 Collisions

The contribution of the scalar field to gravitational wave production comes from the collisions of the expanding bubbles. The envelope approximation [18, 19, 80–83] is a widely adopted approach modelling the expansion of bubbles as thin-shells which disappear once the transition is complete, the observation being that the emitted gravitational radiation mainly depends on the kinetic energy stored in the uncollided bubble regions. The GW power spectrum is given by [21]

$$h^2\Omega_{\rm env}(f) = 1.67\times10^{-5}\left(\frac{H_*}{\beta}\right)^2\left(\frac{\kappa_{\rm env}\alpha}{1+\alpha}\right)^2\left(\frac{100}{g_*}\right)^{1/3}\left(\frac{0.11v_w^3}{0.42+v_w^2}\right)S_{\rm env}(f) \tag{2.46}$$

with the spectral shape

$$S_{\rm env}(f) = \frac{3.8(f/f_{\rm env})^{2.8}}{1+2.8(f/f_{\rm env})^{3.8}} \ . \tag{2.47}$$

The current day peak frequency is

$$f_{\rm env} = 16.5\,\mu{\rm Hz}\left(\frac{f_*}{\beta}\right)\left(\frac{\beta}{H_*}\right)\left(\frac{T_*}{100\,{\rm GeV}}\right)\left(\frac{g_*}{100}\right)^{1/6} \ , \tag{2.48}$$

with the peak frequency at t_* given by

$$\frac{f_*}{\beta} = \left(\frac{0.62}{1.8-0.1v_w+v_w^2}\right) \ . \tag{2.49}$$

The efficiency factor $\kappa_{\rm env}$, which measures the conversion of latent heat into kinetic energy, depends on the wall velocity. Results from numerical fitting for differing regimes are shown in Appendix A of Ref. [20]. Stated here is the result for very large wall velocities ($v_w \to 1$), a limit often taken in the literature

$$\kappa_{\rm env} \simeq \frac{\alpha}{0.73 + 0.083\sqrt{\alpha} + \alpha} \ . \tag{2.50}$$

Knowledge of the relevant temperature T_*, phase transition strength α, inverse duration β/H_* and wall velocity v_w facilitates calculation of the gravitational wave spectrum due to bubble collisions

$$h^2\Omega_{\rm col}(f) \simeq h^2\Omega_{\rm env}(f) \ . \tag{2.51}$$

As noted by Ref. [22], for general thermal transitions, one expects $\kappa_{\rm col}$ to be small as v_w is limited and therefore the contribution to gravitational waves from collisions is small. On the other hand, vacuum transitions and those with a runaway bubble wall will have a large $\kappa_{\rm col}$ as essentially all latent heat goes into accelerating the bubble wall; hence, collisions provide the main source of gravitational waves there.

2.3.2 Sound Waves

Expansion and collision of bubbles results in sound waves taking the form of bulk motion in the plasma of the early universe. Although analytical studies have made some headway [84, 85], they are not in complete agreement with the numerical simulations which have shown that this long-lived source typically dominates contributions to the gravitational wave spectrum [72, 73, 86]. Fitting of these numerical results provides the power spectrum [22, 73]

$$h^2\Omega_{\rm sw}(f) = 8.5 \times 10^{-6} \left(\frac{H_*}{\beta}\right) \Gamma^2 \bar{U}_f^4 \left(\frac{100}{g_*}\right)^{1/3} v_w \, S_{\rm sw}(f) \tag{2.52}$$

where $\Gamma \approx 4/3$ is the adiabatic index and $\bar{U}_f^2 \approx (3/4)\kappa_f \alpha$ is the rms fluid velocity. The spectral shape is

$$S_{\rm sw}(f) = \left(\frac{f}{f_{\rm sw}}\right)^3 \left(\frac{7}{4 + 3(f/f_{\rm sw})^2}\right)^{7/2} \tag{2.53}$$

with the approximate peak frequency

$$f_{\rm sw} = 8.9\,\mu{\rm Hz}\, \frac{1}{v_w} \left(\frac{\beta}{H_*}\right) \left(\frac{T_*}{100\,{\rm GeV}}\right) \left(\frac{g_*}{100}\right)^{1/6} \ . \tag{2.54}$$

The efficiency factor κ_f follows the same description as for collisions. This form is limited to velocities about 10% or more away from the speed of sound or light and transition strengths

$\alpha \lesssim 0.1$. Upon comparison with the result from collisions Eq. (2.46), the power spectrum of sound waves is suppressed by one fewer power of $(\beta/H_*)^{-1}$, highlighting the longer lasting nature of this source.

2.3.3 MHD Turbulence

Turbulence in the plasma is also generated during the phase transition, in particular Kolmogorov-type turbulence [87]. The GW spectrum takes the form [21, 88, 89]

$$h^2\Omega_{\rm turb}(f) = 3.35\times10^{-4}\left(\frac{H_*}{\beta}\right)\left(\frac{\kappa_{\rm turb}\alpha}{1+\alpha}\right)^{3/2}\left(\frac{100}{g_*}\right)^{1/3} v_w\, S_{\rm turb}(f)\ . \tag{2.55}$$

The spectral shape is known exactly

$$S_{\rm turb}(f) = \frac{(f/f_{\rm turb})^3}{[1+(f/f_{\rm turb})]^{11/3}(1+8\pi f/h_*)}\ , \tag{2.56}$$

where h_* is the Hubble parameter at T_*

$$h_* = 16.5\,\mu{\rm Hz}\left(\frac{T_*}{100\,{\rm GeV}}\right)\left(\frac{g_*}{100}\right)^{1/6}\ , \tag{2.57}$$

and the peak frequency is

$$f_{\rm turb} = 27\,\mu{\rm Hz}\,\frac{1}{v_w}\left(\frac{\beta}{H_*}\right)\left(\frac{T_*}{100\,{\rm GeV}}\right)\left(\frac{g_*}{100}\right)^{1/6}\ . \tag{2.58}$$

Note, as with the sound wave contribution, there is a factor of $(\beta/H_*)^{-1}$ less suppression, indicative of a longer-lasting source. Additionally, there is a different dependence on the efficiency factor $\kappa_{\rm turb}$ compared to the other sources.

Dependence of the GW spectrum on thermodynamic parameters

With the formulae describing the gravitational waves sourced from first-order cosmological phase transitions in hand, the dependence on the thermodynamic parameters can be studied; namely, the transition strength α, inverse duration β/H_*, bubble wall velocity v_w and the relevant temperature which is taken to be the nucleation temperature $T_* = T_n$. Increases in transition strength α enhance the amplitude but have no effect on the peak frequency for each contribution. On the other hand, increases in β/H_* decrease the amplitude, with the effect more significant for collisions, and shifts the peak frequency to larger values. The relevant temperature T_* makes no changes explicitly to the amplitudes but again increases peak frequency. Lastly, increases in the wall velocity v_w increase the amplitude with the effect much more pronounced for collisions and turbulence. Increases here also reduce the peak frequency, although changes are much smaller for collisions.

Chapter 3

Holographic Phase Transitions

The contents of Chapter 2 outline a framework applicable to phase transitions throughout cosmological history. This chapter introduces the first of two main topics in this thesis - the holographic phase transition (HPT) [54]. Arising from finite temperature studies of one of the most popular extra-dimensional models, the Randall-Sundrum (RS) model, the holographic phase transition is rather different to more traditional cosmological phase transitions. As a consequence it can be highly supercooled and have prospects for a detectable gravitational wave spectrum [57–60]. Given the extra-dimensional foundation, an introduction to extra-dimensional models - in particular, the Randall-Sundrum model - is provided before discussing the holographic phase transition in detail. There have been a large number of reviews and lecture courses given on the topic of extra dimensions and some are given here for reference and further reading [90–96].

3.1 Large Extra Dimensions

Extra dimensional models recently gained popularity as solutions to the hierarchy problem, the large difference between the eletroweak $\sim 10^3$ GeV and Planck $\sim 10^{18}$ GeV scales. Initially, models of large extra dimensions [48, 97] introduced additional extra spatial dimensions into which gravity propagated. As a result, gravity appears weakened at shorter distances. A rough estimate for the size of additional extra dimensions can be given by [96]

$$R = \frac{1}{M_*}\left(\frac{M_p}{M_*}\right)^{2/n} , \tag{3.1}$$

where M_* is the fundamental scale of nature and n is the number of extra dimensions. To achieve a fundamental scale at the electroweak scale $M_* \sim$ TeV, the necessary size for different numbers of extra dimensions is estimated [96]

- $n = 1 \rightarrow R \sim 10^{15}\,\text{cm}$, which is very large and ruled out.
- $n = 2 \rightarrow R \sim 0.1\,\text{cm}$, which is barely ruled out by experiment.
- $n = 3 \rightarrow R \lesssim 10^{-6}\,\text{cm}$, which has not been tested.

Introducing at least three extra dimensions provides opportunities for solving the hierarchy problem. However, it can be argued that one should expect the size of the extra dimension to also be of the natural scale $R \sim 1/M_*$. Hence, all that's really happened is a shift of hierarchy from mass scales to R and M_*^{-1}. This is known as a problem of radius stabilisation and is difficult to solve in the models of Refs. [48, 97].

3.2 Randall-Sundrum model of Extra Dimensions

Further developing the theory of extra dimensions, Randall and Sundrum (RS) proposed a model of warped extra dimensions [49]. The physical setup is a single extra dimension compactified on a circle whose upper and lower halves are identified. Formally, this is a $S^1/\mathbb{Z}_2$ orbifold giving the relations

$$y \sim y + L\ , \quad y \sim -y\ , \tag{3.2}$$

where y is the coordinate of the extra dimension and $L = \pi R$ is its size. A graphical representation can be seen in Figure 3.1. The points $y = 0$ and $y = L$ are two fixed points on each of which lies a 3-brane, 3+1 dimensional spaces, enclosing the warped 5D bulk. Figure 3.2 shows the physical setup. The brane at $y = 0$ is known as the Planck, UV or hidden brane whereas the brane at $y = L$ is known as the TeV, IR or visible brane and is where, generally, the Standard Model (SM) is confined. Throughout the rest of this discussion the terms Planck and TeV brane will be used with the corresponding subscripts P and T for brane localised quantities.

The RS model is described by an action made of three components: a bulk term and two brane terms

$$S = S_{\text{bulk}} + S^{(i)}_{\text{brane}}\ . \tag{3.3}$$

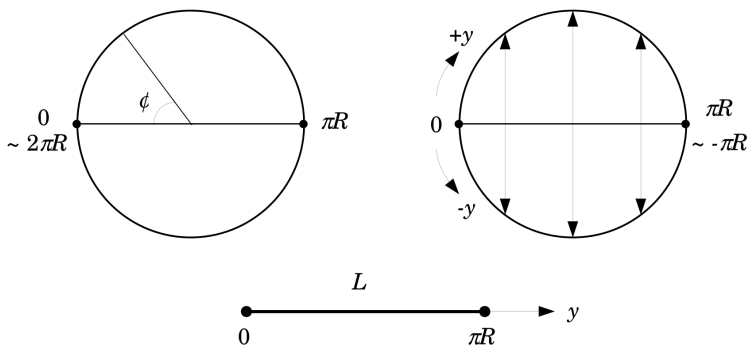

Figure 3.1: Graphical representation of the orbifolded extra dimension in the Randall-Sundrum model. Figure from Ref. [98].

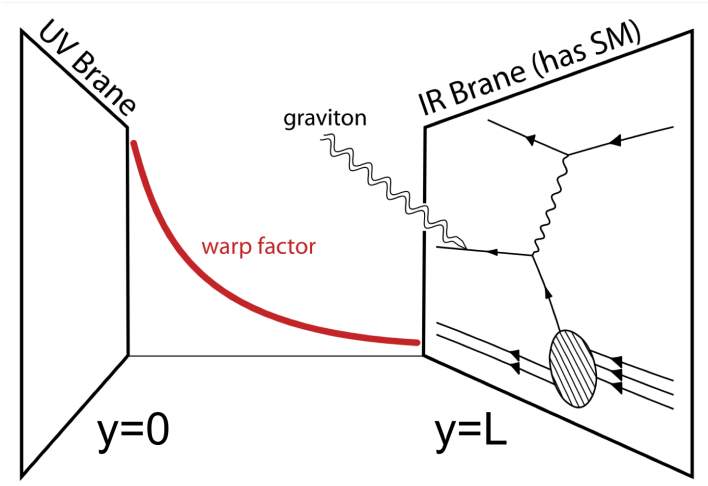

Figure 3.2: Setup of the Randall-Sundrum (RS) extra dimensional model. The extra dimension is warped and bounded by two 3-branes. Figure from Ref. [96].

The bulk term is a modified 5D Einstein-Hilbert action

$$S_{\text{bulk}} = \int d^4x \int_{-L}^{L} dy \, \sqrt{g} \, \left(2M_*^3 R - \Lambda\right) \ , \tag{3.4}$$

where M_* is the fundamental 5D mass scale, R is the Ricci scalar, Λ is the 5D cosmological constant and g is the determinant of the 5D metric. Meanwhile, the brane terms take the form

$$S_{\text{brane}}^{(i)} = -\int d^4x \int dy \, \sqrt{g} \, \lambda_i \, \delta(y - y_i) = -\int d^4x \, \sqrt{-g_i} \, \lambda_i \ , \tag{3.5}$$

where $i = P, T$ represents the Planck and TeV branes respectively such that $y_P = 0$ and $y_T = L$, with g_i the metric localised to that brane and λ_i the brane tension. The localised

metrics are given by

$$g^{(P)}_{\mu\nu}(x^\mu) \equiv g_{\mu\nu}(x^\mu, y=0) \quad , \quad g^{(T)}_{\mu\nu}(x^\mu) \equiv g_{\mu\nu}(x^\mu, y=L) \ . \tag{3.6}$$

To find the metric, it is assumed that the solution respects four-dimensional Poincare invariance in the x^μ-directions [49], beginning with the ansatz

$$ds^2 = \mathrm{e}^{-2A(y)}\eta_{\mu\nu}dx^\mu dx^\nu + dy^2 \ , \tag{3.7}$$

where $\eta_{\mu\nu} = \mathrm{diag}(-1,1,1,1)$ is the 4D Minkowski metric. Finding the form of $A(y)$ is therefore the task; the 5D Einstein equations are used with the ansatz

$$G_{MN} = R_{MN} - \frac{1}{2}g_{MN}R = -\frac{\Lambda}{4M_*^3}g_{MN} + \kappa^2 T_{MN} \ , \tag{3.8}$$

where $M, N = 0, 1, 2, 3, 5$ are the 5D indices (notice it is convention to skip the index 4) and $\kappa^2 = 1/(4M_*^3)$. In the original RS setup, $T_{MN} = 0$ and the 55-component provides the relation

$$G_{55} = 6A'^2 = \frac{-\Lambda}{4M_*^3} \ , \tag{3.9}$$

from which it is clear a real solution for A only exists if Λ is negative, demonstrating the bulk space is an anti-de Sitter space (AdS_5). Rearranging leaves

$$A'^2 = \frac{-\Lambda}{24M_*^3} \equiv k^2 \ , \tag{3.10}$$

where $k \equiv 1/l$ is known as the AdS curvature. Integrating the square root of this equation determines the form of A

$$A(y) = k|y| \ , \tag{3.11}$$

where $|y|$ ensures the solution respects the orbifold symmetry. Substituting into Eq. (3.7), the final form for the metric is found

$$ds^2 = \mathrm{e}^{-2k|y|}\eta_{\mu\nu}dx^\mu dx^\nu + dy^2 \ . \tag{3.12}$$

The factor multiplying the 4D coordinates is known as the "warp factor" and is responsible for the shifting of physical scales between the two branes.

Continuing, the 4D components, $\mu\nu$, of the Einstein equations remain

$$G_{\mu\nu} = \mathrm{e}^{-2A}(6A'^2 - 3A'')\eta_{\mu\nu} \ . \tag{3.13}$$

Following some algebra, one finds the relation

$$A'' = \frac{\lambda_P}{12M_*^3}\delta(y) + \frac{\lambda_T}{12M_*^3}\delta(y-L) \ . \tag{3.14}$$

Additionally, by differentiating Eq. (3.10) it can also be found

$$A'' = 2k\left(\delta(y) - \delta(y-L)\right) \ . \tag{3.15}$$

Equating the two forms of A'' leaves

$$24M_*^3 k(\delta(y) - \delta(y-L)) = \lambda_P\delta(y) + \lambda_T\delta(y-L) \ , \tag{3.16}$$

which, upon matching the coefficients of the delta terms, provides the necessary condition for satisfying the Einstein equations

$$\lambda_P = -\lambda_T = 24M_*^3 k \ , \tag{3.17}$$

a tuning inherent in the basic RS model; the brane tensions must be equal and opposite.

3.2.1 Solving Hierarchies

Consider the situation where matter fields are confined to the TeV brane at $y = L$. The Higgs scalar field has the action

$$\begin{aligned} S_H &= \int d^4x\,\sqrt{g_T}\left[g_T^{\mu\nu}D_\mu H^\dagger D_\nu H - \lambda\left(H^\dagger H - v_0^2\right)^2\right] \\ &= \int d^4x\,\mathrm{e}^{-4kL}\left[\mathrm{e}^{2kL}\eta^{\mu\nu}D_\mu H^\dagger D_\nu H - \lambda\left(H^\dagger H - v_0^2\right)^2\right] \ , \end{aligned}$$

where g_T is defined as in Eq. (3.6). Canonically normalising the Higgs field as $H = \mathrm{e}^{kL}\tilde{H}$, the action becomes

$$S_H = \int d^4x\,\left[\eta^{\mu\nu}D_\mu\tilde{H}^\dagger D_\nu\tilde{H} - \lambda\left(\tilde{H}^\dagger\tilde{H} - (\mathrm{e}^{-kL}v_0)^2\right)^2\right] \ . \tag{3.18}$$

The typical Higgs action is recovered with the crucial difference that the vacuum expectation value is now exponentially suppressed

$$v = \mathrm{e}^{-kL}v_0 \ . \tag{3.19}$$

Therefore, if the difference in scales was Planck to electroweak, that is $v_0 \sim 10^{18}\,\mathrm{GeV}$ and $v \sim \mathrm{TeV}$, then an exponent of approximately

$$kL \approx \ln(10^{15}) \approx 35 \ , \tag{3.20}$$

is needed. Considering k is of a similar order to the 5D Planck mass M_*, such drastic consequences only require a small extra dimension L. Additionally, perturbing the 5D action around the background metric reveals the relation between the 5D and 4D Planck masses

$$M_P^2 = \frac{M_*^3}{k}\left(1 - \mathrm{e}^{-2kL}\right) \ . \tag{3.21}$$

Given that the exponential is likely to be negligible, the scale of gravity is largely independent of the size of the extra dimension and the relation is approximately

$$M_P^2 \approx \frac{M_*^3}{k} \ . \tag{3.22}$$

3.2.2 The Radion and Stabilisation

Until this point, the size of the extra dimension L has been a free parameter and chosen to solve the hierarchy problem. Fluctuations in this radius are given by the scalar zero mode in the perturbations of the metric, with this scalar field known as the radion. Ref. [99] demonstrated the appropriate metric to describe the radion is

$$ds^2 = \mathrm{e}^{-2ky-2R(x)\mathrm{e}^{2ky}}\eta_{\mu\nu}dx^\mu dx^\nu + \left(1 + 2R(x)\mathrm{e}^{2ky}\right)^2 dy^2 \ , \tag{3.23}$$

leading to the radion itself being defined

$$\begin{aligned} \mu &= k\mathrm{e}^{d(x)} \\ &\simeq k\mathrm{e}^{-kL-R(x)\mathrm{e}^{2kL}} \ , \end{aligned} \tag{3.24}$$

where $d(x)$ is the proper length of the extra dimension. Further details can be found in Chapter 4. Problematically, the vanilla RS model contains no mechanism to generate an appropriate vacuum expectation value (VEV) for μ. Hence, not only is there no natural method of generating a hierarchy-solving radius, but the presence of a massless radion would also generate a long range force. Therefore, a dynamical radius stabilisation mechanism is needed.

Although there are possible alternatives [100, 101], the Goldberger-Wise (GW) mechanism [102] is a simple and popular choice. The idea is to add a massive scalar field φ to the bulk with interaction terms on the branes,

$$\begin{aligned} S = &\int d^4x \int_0^L dy\, \sqrt{g}\left(\frac{1}{2}g^{MN}\partial_M\varphi\partial_N\varphi - \frac{1}{2}m^2\varphi^2\right) \\ &- \int d^4x\sqrt{-g_P}\, V_P - \int d^4x\sqrt{-g_T}\, V_T \ , \end{aligned} \tag{3.25}$$

where $V_P = \lambda_P(\varphi^2 - \Phi_P^2)^2$, $V_T = \lambda_T(\varphi^2 - \Phi_T^2)^2$ describe the brane-localised interactions and m is the mass of the scalar field. Focusing on the bulk part, the equation of motion reads

$$\varphi'' - 4k\varphi' - m^2\varphi = 0 \ , \tag{3.26}$$

which gives the solution

$$\varphi(y) = \mathrm{e}^{2ky}\left[A\mathrm{e}^{vky} + B\mathrm{e}^{-vky}\right] \ , \tag{3.27}$$

with $v = \sqrt{4 + m^2/k^2}$. Given that the brane terms have been ignored, this result is only valid away from the boundaries of the extra dimension. Substituting this solution back into the action of Eq. (3.25) and integrating over the extra dimension reveals the 4D potential

$$V = k(v+2)A^2\left(\mathrm{e}^{2vkL} - 1\right) + k(v-2)B^2\left(1 - \mathrm{e}^{-2vkL}\right) \tag{3.28}$$

$$- \lambda_T\,\mathrm{e}^{-4kL}\left(\varphi^2(L) - \Phi_T^2\right)^2 - \lambda_P\left(\varphi^2(0) - \Phi_P^2\right)^2 \ . \tag{3.29}$$

Simplifying to the case in which λ_P and λ_T are large, it is clear from V that it is energetically favourable to have $\varphi(0) = \Phi_P$ and $\varphi(L) = \Phi_T$. Hence, Φ_P and Φ_T now describe the VEV of the scalar field φ on the Planck and TeV branes respectively. Eq. (3.27) then provides the conditions

$$A + B = \Phi_P \ , \tag{3.30}$$

$$\mathrm{e}^{2kL}\left[A\mathrm{e}^{vkL} + B\mathrm{e}^{-vkL}\right] = \Phi_T \ . \tag{3.31}$$

Solving these simultaneously in the limit $kL \gg 1$ gives the final forms of A and B

$$A = \Phi_T\,\mathrm{e}^{-(4+\epsilon)kL} - \Phi_P\,\mathrm{e}^{-(4+2\epsilon)kL} \ , \tag{3.32}$$

$$B = \Phi_P\left(1 + \mathrm{e}^{-(4+2\epsilon)kL}\right) - \Phi_T\,\mathrm{e}^{-(4+\epsilon)kL} \ , \tag{3.33}$$

where $\epsilon = v - 2 \simeq m^2/(4k^2)$ for $m/k \ll 1$. Finally, substituting these into Eq. (3.28) gives the potential for the radion

$$V(\mu) = \epsilon k^4\Phi_P^2 + \mu^4\left[(4+2\epsilon)\left(\Phi_T - \Phi_P\frac{\mu^\epsilon}{k^\epsilon}\right)^2 - \epsilon\Phi_T^2\right] \ , \tag{3.34}$$

where the brane VEVs have been made dimensionless via

$$\Phi_P \to k^{3/2}\Phi_P \quad , \quad \Phi_T \to k^{3/2}\Phi_T \ . \tag{3.35}$$

The dependence on the brane VEVs can be further elucidated by writing the potential in the form

$$V(\mu) = \epsilon k^4\Phi_P^2 + \mu^4\Phi_T^2\left[(4+2\epsilon)\left(1 - \left(\frac{\Phi_P}{\Phi_T}\right)\frac{\mu^\epsilon}{k^\epsilon}\right)^2 - \epsilon\right] \ . \tag{3.36}$$

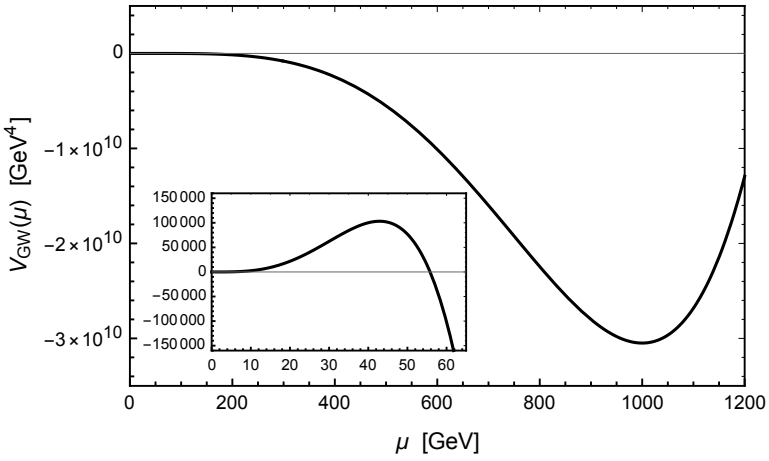

Figure 3.3: The GW potential of Eq. (3.34) with the example parameters $\Phi_T = 1$, $\Phi_P = 22.5$, $\epsilon = 0.1$ and $k = 10^{16}\,\text{GeV}$. The potential has been rescaled such that the false vacuum has a value of zero. The vast difference in the sizes of the maximum and minimum is clear.

By simply adding a massive scalar to the bulk, the GW mechanism has dynamically generated a potential for the radion μ, the minimum of which determines the size of the extra dimension through the radion VEV. An example GW potential can be seen in Figure 3.3. Interestingly, the GW potential possesses a maximum that is orders of magnitude smaller than the minimum.

For $\epsilon > 0$, the location of the turning points is

$$\mu_\pm = k\left(\frac{\Phi_T}{\Phi_P}\right)^{1/\epsilon}\left[\frac{(4+\epsilon) \mp \sqrt{\epsilon(4+\epsilon)}}{2(2+\epsilon)}\right]^{1/\epsilon}, \tag{3.37}$$

where μ_+ and μ_- are the locations of the maximum and minimum respectively. Given that $\epsilon \ll 1$ and k is in the region of M_*, achieving a reduction of scales necessitates $\Phi_T < \Phi_P$. Indeed $\mu_- \sim$ TeV can be achieved for e.g. $\Phi_T/\Phi_P \sim 1/10$ and $\epsilon \sim 1/20$; parameters of the order $\sim 0.1 - 1$ can solve the hierarchy.

The possibility of $\epsilon < 0$ also exists, corresponding to a negative m^2 for the GW field. In general this leads to the radion potential possessing no non-zero minimum. However, accounting for small changes in the TeV brane tension δT_T introduces a term $\delta T_T \mu^4$ to the potential, inducing a non-zero minimum and the turning points [54]

$$\mu_\pm = k\left(\frac{\Phi_T}{\Phi_P}\right)^{1/\epsilon}\left[\frac{(4+\epsilon) \mp \sqrt{\epsilon(4+\epsilon) - 4(\delta T_T/\Phi_T)}}{2(2+\epsilon)}\right]^{1/\epsilon}, \tag{3.38}$$

with $\delta T_T < \epsilon\Phi_T^2$ and $\delta T_T > -\Phi_T^2(4+\epsilon)$. Such a scenario allows for $\Phi_P < \Phi_T$ but of course introduces another free parameter.

It is important to note that the original approach by Goldberger and Wise neglected any backreaction of the GW field φ on the metric. This is valid when

$$\Phi_{P,T} \ll (M_* l)^{3/2} \ , \tag{3.39}$$

remembering $k = 1/l$. For a positive ϵ, $\Phi_P > \Phi_T$ and therefore Φ_P is the greatest threat to neglecting the backreaction. The opposite is true for negative ϵ.

3.2.3 Cosmology of the RS model

Attempts to understand the cosmology of extra dimensional models began with the work of Ref. [50] studying the case of branes with no cosmological constants. They find the standard cosmology of $H^2 \propto \rho$ is instead $H^2 \propto \rho^2$. Upon introduction of the brane cosmological constants however, Ref. [51] demonstrated the standard Friedmann equation is recovered with corrections of the order ρ^2; albeit, with the caveat of requiring tuned cosmological constants and a negative energy density in our universe. These issues are relieved if the extra dimension is dynamically stabilised [52], yet deviation from standard cosmology ultimately takes place above $T \sim 1$ TeV [53].

3.3 The Holographic Phase Transition

Persistent problems with the cosmology of the RS model, particularly at early times, motivated studies into viable alternative high temperature descriptions. Principal work of Ref. [54] demonstrated how the AdS/CFT (Anti-de Sitter/Conformal Field Theory) correspondence offers a useful 4D interpretation of the RS model, revealing the nature in 5D at high temperature. The AdS/CFT correspondence relates a $(d+1)$-dimensional gravitational model described asymptotically by AdS space to a d-dimensional conformal field theory [55]. The work of Ref. [54] finds its basis in the work of Witten [103] where attempts to extend the AdS/CFT correspondence resulted in the concrete example of a phase transition between AdS_{d+1} and AdS_{d+1}-Schwarzschild spaces. From a 4D viewpoint, the corresponding conformal field theory transitions between confined and deconfined spaces.

Of course the RS model is not simply AdS_5 space but a bulk AdS_5 space bordered by the Planck and TeV branes, resulting in some alterations [54, 104, 105]. Firstly, the addition of the Planck brane corresponds to a UV cutoff and the introduction of 4D gravity to the

4D CFT. Meanwhile, the addition of the TeV brane corresponds to some deformation of the CFT leading to a breakdown of the conformal invariance in the IR. Lastly, the addition of the GW stabilisation mechanism is associated to a quasi-marginal deformation of the CFT. Additionally, the radion field corresponds to the chemical potential in 4D.

With this knowledge, the finite temperature dynamics of the RS model, as described by Ref. [54], are as follows. At high temperatures the stable phase is described by an AdS_5-Schwarzschild (AdS-S) geometry, where the TeV brane is replaced by the horizon of a 5D Schwarzschild black hole (BH). The Hawking temperature of this black hole corresponds to the temperature of the 4D CFT. As the universe cools, the RS model becomes energetically favourable and a phase transition occurs. The TeV brane replaces the black hole horizon, the radion acquires a VEV and the distance between the two branes is stabilised. This phase transition is known as the holographic phase transition.

Before further discussing the specifics of the transition, it is important to understand the 5D classical gravity description is only accurate when the dual CFT is strongly coupled, defined by a large 't Hooft coupling $\lambda = N g_{\rm YM}^2$ and hence a large gauge group size $N \gg 1$. The two theories are related through

$$N^2 = 16\pi^2 (M_* l)^3 \ , \tag{3.40}$$

and therefore validity requires large $(M_* l)$. This is incredibly important and it will be seen that keeping a valid classical gravity description ($N \gg 1$) restricts the possibility for a successful phase transition.

3.3.1 Comparing Free Energies

To understand the nature of the phase transition it is first important to know which phase is energetically favourable at a given temperature; this is done by comparing free energies. For the RS setup the free energy is already known; it is the minimum of the GW potential, Eq. (3.36), $V(\mu_-)$ where μ_- is the location of the minimum as given in Eqs. (3.37) and (3.38).

Attempts to understand the black hole phase begin with the metric. As discussed, this is the AdS-S metric which is described by [106]

$$ds^2 = \frac{r^2}{l^2}\left(1 - \frac{r_0^4}{r^4}\right) dt^2 - \frac{l^2}{r^2}\left(1 - \frac{r_0^4}{r^4}\right)^{-1} dr^2 - \frac{r^2}{l^2}\sum_{i=1}^{3} dx_i^2 \ , \tag{3.41}$$

where r_0 is the event horizon of the black hole and $r_0 \leq r < \infty$. For $r_0 = 0$ this simply reduces to the pure AdS metric. Using analytic continuation $t \to -i\tau$ the Euclidean metric can be

found, where the inverse period of Euclidean time τ is equal to the temperature, $\beta^{-1} = T$. In fact, the metric of Eq. (3.41) is only a valid solution of the Einstein equations when the period takes a specific value, namely the inverse of the Hawking temperature [107]

$$\beta^{-1} = \frac{r_0}{\pi l^2} \equiv T_H \ . \tag{3.42}$$

If this is not true a conical singularity arises. Naturally, studying finite temperature dynamics means the temperature of the system T is free and is therefore not necessarily equal to the Hawking temperature T_H. Hence, there is a conical singularity in Euclidean coordinates at the horizon. Thankfully, Ref. [65] offers a solution, demonstrating that the integral of the Ricci scalar is

$$\int d^4x \sqrt{g}\, R \sim 4\pi(1-\alpha) \tag{3.43}$$

where α is the conical deficit angle with the value $\alpha = \beta/\beta_H = T_H/T$. The action corresponding to the cone is therefore

$$\begin{aligned} S_{\text{cone}} &= 2M_*^3 \int dx^5 \sqrt{-g}\, R \\ &= 2M_*^3 \frac{r_0^3}{l^3}\, 4\pi\left(1 - \frac{T_H}{T}\right) \\ &= 8\pi^4 (M_* l)^3\, T_H^3 \left(1 - \frac{T_H}{T}\right) \ . \end{aligned} \tag{3.44}$$

Finally, the free energy of the cone is found using $F = -T \cdot S$, giving

$$F_{\text{cone}} = 8\pi^4 (M_* l)^3\, T_H^4 \left(1 - \frac{T}{T_H}\right) \ . \tag{3.45}$$

With the conical contributions understood, the remaining contribution from the black hole can be calculated and is simply the difference in free energies between the AdS_5-Schwarzschild and AdS_5 spacetimes, $F_{\text{AdS-S}} - F_{\text{AdS}}$. With $R = -20/l^2$ for both the AdS-S and AdS metrics, the gravitational action of Eq. (3.4) takes the form

$$S = -\frac{16M_*^3}{l^2} \int d^5x \sqrt{-g} \ , \tag{3.46}$$

and the free energies are therefore

$$F_{\text{AdS-S}} = \frac{16TM_*^3}{l^2} \int_0^{1/T} dt \int_{r_0}^{\Lambda} dr\, \frac{r^3}{l^3} \ , \tag{3.47}$$

$$F_{\text{AdS}} = \frac{16TM_*^3}{l^2} \int_0^{1/T'} dt \int_0^{\Lambda} dr\, \frac{r^3}{l^3} \ , \tag{3.48}$$

where, again, the relation $F = -T \cdot S$ has been used. The cutoff Λ is introduced because both integrals are divergent, yet by now calculating the difference and taking $\Lambda \to \infty$ a finite value is found. Comparison of the free energies requires imposing that the geometries of the two solutions at the cutoff surface $r = \Lambda$ must be equal, giving

$$\begin{aligned}
\sqrt{g_{\mathrm{tt}}^{\text{AdS-S}}(r=\Lambda)}\,\beta_{\text{AdS-S}} &= \sqrt{g_{\mathrm{tt}}^{\text{AdS}}(r=\Lambda)}\,\beta_{\text{AdS}} \\
\sqrt{1-\frac{r_0^4}{\Lambda^4}}\,\frac{1}{T} &= \frac{1}{T'} \\
\left(1-\frac{r_0^4}{2\Lambda^4}\right)\frac{1}{T} &\simeq \frac{1}{T'}\ ,
\end{aligned} \tag{3.49}$$

where Taylor expansion has been used to find the last line. Using this result and taking the difference in free energies

$$\begin{aligned}
F_{\text{AdS-S}} - F_{\text{AdS}} &\simeq \frac{16M_*^3}{l^2}T\left[\frac{1}{4l^3}(\Lambda^4 - r_0^4)\frac{1}{T} - \frac{\Lambda^4}{4l^3}\frac{1}{T'}\right] \\
&= \frac{16M_*^3}{l^2}\left[\frac{1}{4l^3}(\Lambda^4 - r_0^4) - \frac{\Lambda^4}{4l^3}\left(1-\frac{r_0^4}{2\Lambda^4}\right)\right] \\
&= -2\pi^4(M_*l)^3T_H^4\ ,
\end{aligned} \tag{3.50}$$

taking $\Lambda \to \infty$ for the final line. Finally, adding the conical contribution of Eq. (3.45) gives the free energy of the high temperature phase

$$F_{\text{BH}} \equiv F_{\text{AdS-S}} - F_{\text{AdS}} + F_{\text{cone}} = 6\pi^4(M_*l)^3T_H^4 - 8\pi^4(M_*l)^3TT_H^3\ . \tag{3.51}$$

Determining the energetically favourable phase requires comparing the minima of the free energies which, for F_{BH}, is when $T_H = T$, corresponding to the absence of a conical singularity. Hence, the minimum of the black hole phase reads

$$F_{\text{BH}}^{\text{min}} = -2\pi^4(M_*l)^3T^4\ . \tag{3.52}$$

The minimum of the free energy in the two phases is now known: $V(\mu_-)$ for the RS phase, $F_{\text{BH}}^{\text{min}}$ for the black hole phase. The temperature at which the two phases are energetically favourable, known as the critical temperature T_c, is found by equating the two

$$T_c = \left(\frac{|V(\mu_-)|}{2\pi^4(M_*l)^3}\right)^{1/4}\ . \tag{3.53}$$

For $T > T_c$ the black hole phase is energetically favourable. Below T_c a transition to the RS setup occurs.

3.3.2 Dynamics of the Phase Transition

The minima of the two phases are separated by a barrier; therefore, a first-order phase transition proceeding through bubble nucleation occurs. These bubbles interpolate between the AdS-S spacetime and the stabilised RS setup. The dynamics of the low temperature phase are described entirely by the radion μ and its potential, Eq. (3.36). The radion gains a non-zero VEV and stabilises the extra dimension. The dynamics of the high temperature phase are described by the free energy of the black hole, Eq. (3.51), parametrised by T_H, which can be thought of as playing the role of a field. Typically, as described in Chapter 2, the false and true vacua are described by the same field. Unusually, here the dynamics are described by two fields, μ and T_H. How are the two connected? As outlined by Ref. [54], the two phases, and their topologies, can be deformed into one another by moving the horizon to $r = 0$ and then moving the TeV brane back from $r = 0$. The bubble therefore interpolates between the phases as follows. The centre of the bubble describes the black hole phase with the horizon and Planck brane. Moving out from the centre, the horizon recedes to $r = 0$. The configuration eventually arrives at pure AdS, at which point the TeV brane then approaches from $r = 0$. Finally, far outside the bubble, the TeV brane is stabilised at a finite r. To summarise, the RS model with a stabilised TeV brane, parametrised by the radion μ, is glued to the black hole configuration, parametrised by the Hawking temperature T_H, through pure AdS which is recovered for both $\mu \to 0$ and $T_H \to 0$.

Given that the configurations are glued in this manner, a potential describing the dynamics can be found by combining the free energies [54] (which, from now on, will be written as potentials) of Eq. (3.36) and Eq. (3.51). Repeated here for clarity

$$V_{\mathrm{RS}}(\mu) = \mu^4 \Phi_T^2 \left[(4+2\epsilon) \left(1 - \left(\frac{\Phi_P}{\Phi_T} \right) \frac{\mu^\epsilon}{k^\epsilon} \right)^2 - \epsilon \right] , \tag{3.54}$$

$$V_{\mathrm{BH}}(T_H, T) = 6\pi^4 (M_* l)^3 T_H^4 - 8\pi^4 (M_* l)^3 T T_H^3 , \tag{3.55}$$

these result in a combined potential [58]

$$V(\psi, T) = 2\pi^4 (M_* l)^3 T^4 + \begin{cases} V_{\mathrm{RS}}(\psi) & \psi \geq 0 \\ V_{\mathrm{BH}}(\psi, T) & \psi < 0 \end{cases} , \tag{3.56}$$

where the first term is simply $-F_{\mathrm{BH}}^{\mathrm{min}}$ and is present to set the false vacuum to zero potential.

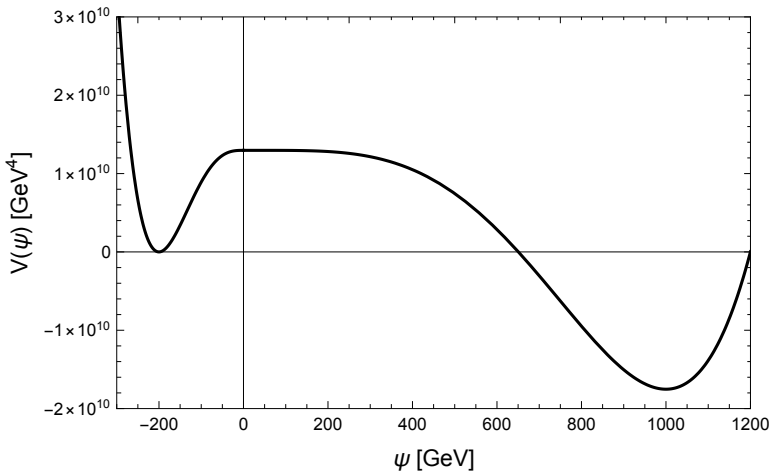

Figure 3.4: A plot of the combined potential of Eq. (3.56) for $\Phi_T = 1$, $\epsilon = 0.1$, $(M_* l) = 0.55$ and $T = 200$ GeV.

The field ψ is defined

$$\psi \equiv \begin{cases} \mu & \text{for } \psi \geq 0 \\ -T_H & \text{for } \psi < 0 \end{cases} . \tag{3.57}$$

An example of the combined potential of Eq. (3.56) is seen in Figure 3.4. This now resembles the typical scenarios discussed in Chapter 2, a potential parametrised by a single field ψ. For $\psi < 0$ the potential is described by the black hole phase, where the potential at the minimum has been offset to zero. For $\psi \geq 0$ the potential is described by the GW potential.

The regular prescription of Chapter 2 can now be followed. However, there is a crucial approximation made in Eq. (3.56) - the μ and T_H fields have the same kinetic term. While the kinetic term for the radion is derived [52, 105, 108] to be

$$\mathcal{L} = -12\sqrt{-g}\,(M_* l)^3\,(\partial_\alpha \mu)(\partial^\alpha \mu)\ , \tag{3.58}$$

$$\equiv Z^2 \frac{1}{2}(\partial_\alpha \mu)(\partial^\alpha \mu)\ , \tag{3.59}$$

the equivalent task for T_H would involve finding a complete solution of the Einstein equations describing the bubble [54], an incredibly difficult task. Therefore, combining the fields as in Eq. (3.57) and using the subsequent potential of Eq. (3.56) is not strictly correct; the scale of the left hand side of Figure 3.4, $\psi < 0$, is unknown.

To perform an agnostic analysis, one can just write the Lagrangians

$$\mathcal{L}_{\rm BH} = Y^2 \frac{1}{2}(\partial T_H)^2 - V_{\rm BH}(T_H, T) \tag{3.60}$$

$$= Y^2 \left[\frac{1}{2}(\partial T_H)^2 - \frac{V_{\rm BH}(T_H, T)}{Y^2}\right] , \tag{3.61}$$

$$\mathcal{L}_{\rm RS} = Z^2 \frac{1}{2}(\partial \mu)^2 - V_{\rm RS}(\mu) \tag{3.62}$$

$$= Z^2 \left[\frac{1}{2}(\partial \mu)^2 - \frac{V_{\rm RS}(\mu)}{Z^2}\right] . \tag{3.63}$$

where the second forms, which have factored out the kinetic term coefficients, can be used for a typical analysis as outlined in Chapter 2. The transition rate is given by

$$\Gamma \sim \mathrm{e}^{-B} \tag{3.64}$$

where B is the Euclidean action computed from the bubble and a prefactor is assumed to be subdominant. Concentrating on the finite temperature O(3)-invariant solutions, the bubble is found by now solving the differential equation

$$\partial^2 \psi + \frac{2}{r}\partial\psi = \begin{cases} \frac{1}{Z^2}\frac{\partial V}{\partial \psi} & \psi \geq 0 \\ \frac{1}{Y^2}\frac{\partial V}{\partial \psi} & \psi < 0 \end{cases} , \tag{3.65}$$

where $V(\psi, T)$ is from Eq. (3.56). The Euclidean action is made up of two contributions, from the RS and black hole sides, given by

$$S_3^{\rm BH} = 4\pi \cdot Y^2 \cdot \int_{r(\psi=0)}^{r(\psi=-T)} dr\, r^2 \left[\frac{1}{2}(\partial\psi)^2 + \frac{1}{Y^2}V(\psi, T)\right] , \tag{3.66}$$

$$S_3^{\rm RS} = 4\pi \cdot Z^2 \cdot \int_{0}^{r(\psi=0)} dr\, r^2 \left[\frac{1}{2}(\partial\psi)^2 + \frac{1}{Z^2}V(\psi, T)\right] , \tag{3.67}$$

where r is the radial coordinate and the quantity relevant for tunnelling is then $B = S_3/T = (S_3^{\rm BH} + S_3^{\rm RS})/T$. The same approach can be translated to the O(4)-invariant solutions. Finally, the condition for successful tunnelling is approximated by Eq. (2.33) with $g_* \sim 100$ and $T_c \sim 100$ GeV, giving

$$\frac{S_3}{T} \lesssim 140 . \tag{3.68}$$

Following this framework, one can take arbitrary forms of the kinetic term factors Y and Z and calculate the tunnelling properties. While the radion kinetic term is known, Eq. (3.58), the ambiguity of the black hole kinetic term Y is a key issue that has prompted a number of different approaches from the literature [54, 57–59]. Before examining these separate approaches however, the general results and features that make the holographic phase transition interesting will be discussed.

3.3.3 Characteristics of the HPT

Several works have studied the characteristics of the holographic phase transition [54, 57–59]. To attain some basic understanding of the roles the parameters play in the tunnelling probability, the thin-wall formulae of Refs. [54, 57] can be used. Within the confines of their approximation ignoring the width of the BH side, the thin-wall formula for the O(3)-symmetric Euclidean action reads

$$S_3 = \frac{16\pi}{3}\left(\frac{3N^2}{2\pi^2}\right)\frac{\sigma^3}{(\Delta V)^2}\ , \tag{3.69}$$

$$\approx \frac{2.95\,N^{7/2}}{\epsilon^{9/8}\,\Phi_T^{3/2}}\frac{T_c/T}{\left(1-(T/T_c)^4\right)^2}\ , \tag{3.70}$$

where $\sigma = \int_0^{\mu_-} d\mu\sqrt{2V_{\rm RS}(\mu)}$ is the surface tension calculated using just the GW potential at the critical temperature, ΔV is the difference between the BH and GW minima, and $(2N^2/2\pi^2)$ comes from the canonical normalisation of μ. The factors of ϵ and Φ_T arise from both σ and ΔV. More specifically, as stated in Ref. [54], these are given by $\sigma \simeq \sqrt{2}\epsilon^{3/4}\Phi_T\mu_-^3$ and $\Delta V = \epsilon^{3/2}\Phi_T^2\mu_-^4[1-(T/T_c)^4]$. It is clear how increasing N hinders the tunnelling probability. However, it is necessary to have a large N for the semi-classical gravity description to remain valid. This tension consistently plagues HPT success. However, ϵ and Φ_T could yet come to the rescue. While $\epsilon \ll 1$ is a condition from the derivation of the GW potential, small increases can still aid tunnelling. Meanwhile, Φ_T offers a promising solution - any increase greatly reduces S_3/T. Indeed, following a full numerical analysis, Ref. [57] supports these conclusions.

From this position it appears there is no issue with having a large N, one can just raise Φ_T accordingly and still find tunnelling. Of course it is never so simple, using the GW effective potential for the radion requires negligible backreaction on the metric, Eq. (3.39). Given the relation to N through Eq. (3.40) the backreaction limits read

$$\Phi_{T,P} \ll \frac{N}{4\pi}\ . \tag{3.71}$$

Hence, $\Phi_{T,P}$ are always severely constrained and any possible gains are limited. The backreaction constraint is most limiting for $\epsilon > 0$. Here $\Phi_P > \Phi_T$ (from Eq. (3.37)) and therefore Φ_T is limited by the size of Φ_P rather than its own value. Consequently, Ref. [57] found that, for $\epsilon > 0$ nucleation never takes place in a regime where backreaction can be ignored. Turning to the case of $\epsilon < 0$, where it is necessary to introduce the new parameter δT_T, it is now true

that $\Phi_T > \Phi_P$ and the previous issue is avoided - the backreaction constraint is weakened. Hence, Ref. [57] finds a successful transition is possible for $N \lesssim 12$.

Indeed, this reliance on negative ϵ, and the relaxation on backreaction constraints it provides, to achieve a successful transition is present throughout the literature. Two further studies [58, 59], soon to be discussed for their alternative approaches when describing the BH contribution, follow a similar theme: successful tunnelling can only occur for $\epsilon < 0$ and $N \lesssim 8$. Whether $N \sim 8$ presents a scenario where the semi-classical gravitational description remains valid is open to discussion, but it is nevertheless too close for comfort. A full numerical study of the dependence of the Euclidean action on the parameters N, Φ_T and ϵ can be found in Chapter 4.

It is clear that finding a successful transition is difficult while maintaining a valid theory, but what are the traits of a successful HPT? Refs. [57–59] all find that, unlike a standard electroweak-scale transition, a large amount of supercooling, $T_n \ll T_c$, is present. The source is the flatness of the nearly-conformal radion potential, which can be written

$$V(\mu) = \mu^4 \cdot P\left[\left(\frac{\mu}{k}\right)^{\epsilon}\right] \ , \tag{3.72}$$

where conformality is broken by the small parameter ϵ. Here, the maximum μ_+ and minimum μ_- can lie far apart, offering an alternative dependence of the Euclidean action on the temperature. Greater detail can be found in Ref. [56] which studied the cosmological consequences of such nearly-conformal potentials.

Drastic reductions in nucleation temperature will have significant consequences for any gravitational waves produced, see Refs. [57, 59], and any other phase transitions proceeding the HPT, see Ref. [58] for an application to the electroweak phase transition and baryogenesis.

3.3.4 Approaches to the Black Hole Kinetic Term

Issues with the kinetic term of the T_H field describing the black hole contribution, as previously mentioned, remain a stumbling block on the path to a wholly reliable analysis. Given the lack of a concrete solution, the studies of Refs. [54, 57–59] each take an alternative approach. The respective details are discussed to highlight the ambiguities at play.

Neglecting the BH Side: To begin, Refs. [54] and [57] work off the assumption that the black hole side is likely negligible. Considering the radion kinetic term is proportional to

$(M_* l)^3 \sim N^2$, it is clear that both free energies depend on N^2 and can be rescaled: $\tilde{F}_{\rm RS} \equiv F_{\rm RS}/N^2$ and $\tilde{F}_{\rm BH} \equiv F_{\rm BH}/N^2$. Comparing the two free energies at the critical temperature T_c, where the depths of their minima are equal, the only factor in determining their relevance is the location of their minima (width). The location of $F_{\rm BH}^{\rm min}$ is simply T_c, whereas $F_{\rm RS}^{\rm min}$ is located at $\mu_- \sim 1\,\text{TeV} \gg T_c$. Hence, the width of the black hole side is assumed negligible compared to that of the RS side, as seen in Figure 3.4, and can be neglected. At temperatures below T_c the radion minimum will become deeper compared to the BH minimum and the conclusion will only be reinforced. Ref. [57] performs a numerical study in this regime revealing successful nucleation is possible for $\epsilon < 0$ and $N \lesssim 12$. Nevertheless, their approach remains an approximation in that it assumes there are no other factors in the kinetic term for T_H which could make it numerically relevant.

Using the Combined Potential: Instead of completely ignoring the width of the BH side, Ref. [58] follows the suggestion of Ref. [54] in forming a combined potential of the BH and RS fields, as given in Eq. (3.56). Given the absence of the true form, the BH kinetic term is approximated to be identical to that of the radion, Eq. (3.58). With a complete potential a full numerical analysis, as outlined in Chapter 2, can be performed. Again focusing on the negative ϵ scenario, they find the transition is significantly supercooled and a successful transition is only possible for an even more constraining $N \lesssim 6$.

Boundary Condition on the Equation of Motion: The focus of Ref. [59] was to partially take into account backreaction by reconciling the radion effective potential with the superpotential method [109,110] which fully considers backreaction but provides no effective potential itself. During their study however, a novel approach to considering the BH side was introduced. While the specific shape of the BH side is not considered, the depth is used as a boundary condition when solving the radion equation of motion. As discussed in Chapter 2, the dynamics of the equation of motion (see top line in Eq. (3.65) for the radion) are those of a ball rolling in the inverse potential; the goal is finding the release point such that the ball stops on the "hilltop" of the false vacuum. In the holographic phase transition however, only the RS side of the potential is accurately known. Hence, only dynamics up to $\mu = 0$ (approaching from $\mu > 0$), and not beyond, are known - in reality the field would need to evolve further to the BH minimum. Ref. [59] attempts to capture some of these dynamics by demanding that, upon reaching $\mu = 0$, the field have the kinetic energy necessary to "jump" and stop on top of

the BH minimum, Eq. (3.52). Explicitly, the solution of the finite temperature O(3)-invariant equation of motion for the radion

$$\partial^2\mu + \frac{2}{r}\partial\mu = \frac{\partial V_{\rm RS}(\mu)}{\partial\mu} \ , \tag{3.73}$$

must satisfy

$$Z^2\frac{1}{2}\left(\partial\mu\right)^2\big|_{\mu=0} = \left|F_{\rm BH}^{\rm min}\right| \ , \tag{3.74}$$

where, as a reminder, Z is the kinetic term of radion field as given in Eq. (3.58). With this approach Ref. [59] finds a result very similar to Ref. [58]. Thermal transitions are still only possible for $N \lesssim 7$, despite relaxing the backreaction constraints, with supercooling by orders of magnitude. Again, this study focuses on a negative ϵ.

3.4 Addressing the Problems

The numerous approaches just described offer scenarios for successful tunnelling but are restrained to relatively low N, leaving the theory open to validity doubts, and negative ϵ. Chapter 4 presents published work [68] attempting to solve these two issues through the introduction of TeV-brane localised curvature. A natural extension to the RS model, TeV-brane localised curvature [111] is described by the action

$$S_{\rm IR} = \frac{M_{\rm IR}^2}{2}\int d^4x\,\sqrt{g_T}\,R(g_T) \ , \tag{3.75}$$

where the mass scale $M_{\rm IR}$ is a new free parameter in the model. In the context of the phase transition, this addition makes a simple yet important change to the kinetic term of the radion

$$\mathcal{L}_{\rm RS} = Z^2\frac{1}{2}(\partial\mu)^2 \ , \tag{3.76}$$

where

$$Z = \sqrt{24(M_* l)^3(1-\theta_{\rm IR})} \quad , \quad \theta_{\rm IR} \equiv \frac{M_{\rm IR}^2 k}{M_*^3} \ . \tag{3.77}$$

Aside from the limit $\theta_{\rm IR} < 1$, $\theta_{\rm IR}$ is a free parameter. From Eq. (3.67) it is clear that the Euclidean action is proportional to Z^2. The simple addition of brane localised curvature provides a parameter which can directly lower S_3 and improve transition rates.

Chapter 4 demonstrates how the introduction of brane localised curvature opens up the viable parameter space for successful tunnelling to the positive ϵ and large N regions. This

work does not attempt to address the issues concerning the BH kinetic term, instead utilising and comparing the approaches of Ref. [59], introducing a boundary condition, and Ref. [58], using a combined potential.

Note that the published work in Chapter 4 uses some slightly different conventions to those in this chapter. In particular, note the differences between the 5D Einstein-Hilbert actions in Eq. (3.4) and Eq. (4.3), and the definition of N in Eq. (3.40) and Eq. (4.1).

Chapter 4

Rapid Holographic Phase Transition with Brane-Localized Curvature

Barry M. Dillon[1], Basem Kamal El-Menoufi[2], Stephan J. Huber[2], and Jonathan P. Manuel[2]

[1]Centre for Mathematical Sciences, Plymouth University, Plymouth, PL4 8AA, United Kingdom

[2]Department of Physics & Astronomy, University of Sussex, Falmer, Brighton, BN1 9QH, United Kingdom

Phys. Rev. D98 (2018) no.8, 086005

arXiv:1708.02953

Abstract

We study the finite-temperature properties of the Randall-Sundrum model in the presence of brane-localized curvature. At high temperature, as dictated by AdS/CFT, the theory is in a confined phase dual to the planar AdS black hole. When the radion is stabilized, *á la* Goldberger-Wise, a *holographic* first-order phase transition proceeds. The brane-localized curvature contributes to the radion kinetic energy, substantially decreasing the critical bubble energy. Contrary to previous results, the phase transition completes at much larger values of N, the number of degrees of freedom in the CFT. Moreover, the

field value of the bulk scalar on the TeV-brane is allowed to become large, while remaining consistent with back-reaction constraints. Assisted by this fact, we find that for a wide region in the parameter space tunneling happens rather quickly, i.e. the nucleation temperature becomes of the order of the critical temperature. At zero temperature, the most important signature of brane-localized curvature is the reduction of spin-2 Kaluza-Klein graviton masses and a heavier radion.

4.1 Introduction

The possibility that physical reality might consist of extra spatial dimensions has intrigued theoretical physicists since at least the work of Kaluza and Klein. The modern excitement about extra dimensions re-surfaced when it was realized they offer a simple solution to the hierarchy problem [48]. Most prominent is the proposal by Randall and Sundrum [49] in which the bulk of spacetime is a slice of AdS_5 bordered by two branes in which, unlike gravity, matter is confined to propagate only on the TeV brane. The hierarchy between the weak and Planck scales dynamically emerges due to the effect of gravitational redshift: mass scales on the TeV brane are exponentially redshifted by the warp factor.

The cosmology of extra-dimensional models came under scrutiny immediately after their proposal. In the absence of brane cosmological constants, the extra dimension leads to unconventional cosmology on the brane, i.e. $H \propto \rho$ [50]. Nevertheless, in the Randall-Sundrum (RS) model standard cosmology could be recovered at low energy but at the cost of requiring finely-tuned energy densities on the two branes [51] and negative energy matter content in our universe. This fine tuning is lifted if the extra dimension is dynamically stabilized [52], yet, deviation from standard cosmology ultimately takes place at early times above $\sim 1\,\text{TeV}$ [53]. The above problems evidently prompt questions about the high temperature dynamics of the Randall-Sundrum I (RSI) model.

Creminelli et al. sought to address these issues by employing the AdS/CFT correspondence [54]. The holographic description of the RSI model has been discussed extensively in the literature [104, 105]. Most importantly, the dual strongly coupled conformal field theory (CFT) is *confining* where the spin-2 bound states are conjectured to be dual to the Kaluza-Klein (KK) spin-2 spectrum of the 5D theory. At high temperature, as familiar from QCD, one should expect the theory to undergo a phase transition and enter a *de-confined phase*. In fact, Witten [112] considered a similar situation using the AdS/CFT dictionary to study

the phase transition of a large-N gauge theory defined on $\mathbb{S}^3$. On the gravity side, the high temperature phase is the AdS-Schwarzschild black hole while the low temperature phase is thermal AdS. This is the well-known Hawking-Page phase transition [113].

The physics in our situation is now transparent: at high temperatures, the RSI is unstable and the theory must undergo a phase transition. Similar to the Hawking-Page phase transition, the high temperature phase is described by the planar AdS black hole [106]. However, unlike Hawking-Page, the planar AdS black hole is stable at any finite temperature *unless* the extra dimension in the RSI solution is dynamically stabilized [54]. The metric fluctuations contain a scalar degree of freedom, i.e. the radion, that controls the physical size of the extra dimension. A stabilization mechanism, e.g. Goldberger-Wise [102], generates a potential for the radion that renders the phase transition possible as we shall see below.

Several works have been devoted to study the dynamics of the holographic phase transition [54,57–59] and, albeit introducing various twists, two general properties of the phase transition (PT) were found to hold true regardless of the details. First, the PT is strongly first order with substantial amounts of supercooling. Second, the system gets stuck in the false vacuum if the ratio of the 5D Planck mass to the bulk cosmological constant is larger than $\mathcal{O}(1)$, taking the best case scenario [59]. Although it might be desirable for certain applications to have large amounts of supercooling, the second property threatens the framework consistency, in particular, the holographic interpretation of the transition. Effective field theory lore tells us that the Einstein-Hilbert action dominates the dynamics on the gravity side only if the ratio of the 5D Planck mass to the cosmological constant is large. Precisely, AdS/CFT asserts the correspondence [55]

$$N^2 = 4\pi^2 (M_\star l)^3 + 1 \quad , \tag{4.1}$$

where $M_\star$ is the 5D Planck mass, l is the AdS radius and N is the number of CFT degrees of freedom. Ideally, for the classical gravity description to be meaningful, one must have $(M_\star l) \gg 1$ or large N. At large N, the 4D field theory is strongly coupled which is essential for understanding the phase transition.

In this paper, we consider a minimal extension to the RSI set-up, namely a TeV-brane localized curvature [111]

$$S^{\rm G}_{\rm IR} = \frac{M^2_{\rm IR}}{2} \int d^4x \sqrt{g_L}\, R(g_L) \tag{4.2}$$

where $M_{\rm IR}$ is a mass scale comprising the new parameter in the model, g_L is the induced metric on the TeV brane and R is the Ricci scalar built from the induced metric. Naturally, one should expect $M_{\rm IR}$ to be of the same order of magnitude as other mass scales in the model, i.e. the 5D Planck mass and the bulk cosmological constant. We are concerned with the finite temperature aspects of the model, in particular the dynamics of the holographic phase transition. We shall see that the kinetic energy of the radion receives a non-trivial modification due to Eq. (4.2) and allows for a large-N phase transition to proceed over a wide range of parameters appearing in the radion potential. Moreover, the model accommodates a wide range of nucleation temperatures: A large amount of supercooling is achieved if the mass-squared of the bulk scalar field is small compared to the AdS curvature.

The plan of the paper is as follows. In Section 4.2, we define the radion and derive its kinetic Lagrangian employing the orbifold formulation of the RSI model. We then move to construct the radion potential induced via the Goldberger-Wise mechanism. Section 4.3 is devoted to determining the free energies and discussion of the modeling of the phase transition and its holographic interpretation. Section 4.4 offers a detailed study of the dependence of the tunneling rate on the various model parameters paying special attention to the role brane-localized curvature plays in the phase transition. The phenomenological consequences of Eq. (4.2) and possible collider signatures of the radion are the subject of Section 4.5. Our conclusions are given in Section 4.6.

4.2 Effect of brane-localized curvature on the radion

In this section we derive the effective 4D Lagrangian for the radion including the brane-localized curvature. The radion is a scalar degree of freedom that controls the physical size of the extra dimension. The brane-localized curvature contributes to the kinetic energy of the radion, thereby introducing a non-trivial modification to its effective Lagrangian. In the absence of a stabilization mechanism the radion is strictly massless. We employ a bulk scalar field, *á la* Goldberger and Wise [102], to generate a potential for the radion. We review the computation of the potential starting from the Charmousis-Gregory-Rubakov (CGR) wave-function [99].

4.2.1 Radion kinetic term

It is important to derive the radion kinetic term in detail because it is instructive to point out the difference in the result obtained from the orbifold picture of the RSI model to that obtained in the so-called interval approach [114, 115]. In the orbifold picture, the action of the theory is composed of bulk and boundary parts as

$$S^{\rm G}_{\rm bulk} = \frac{M_\star^3}{2}\int d^4x \int_{-L}^{L} dy\,\sqrt{G}\left(R + 12\,k^2\right), \quad k^2 \propto \Lambda \tag{4.3}$$

and

$$S^{\rm G}_{{\rm B}_i} = -\sigma_i \int d^4x \int_{-L}^{L} dy\,\sqrt{g_i}\,\delta(y-y_i), \quad y_i = 0, L \tag{4.4}$$

where the Planck (TeV) brane is located at the orbifold fixed point $y = 0\,(L)$ and g_i denotes the induced 4D metric on the branes. The extra dimension is compactified on an $\mathbb{S}^1/Z_2$ orbifold and the theory admits a static solution

$$ds^2 = e^{-2k|y|}\eta_{\mu\nu}dx^\mu dx^\nu - dy^2 \tag{4.5}$$

provided the brane tensions are fine-tuned to obtain flat brane geometries

$$\sigma_0 = -\sigma_L = 6kM_\star^3 \quad . \tag{4.6}$$

The background solution remains intact even with the introduction of the brane-localized curvature

$$S^{\rm G}_{\rm IR} = \frac{M_{\rm IR}^2}{2}\int d^4x\sqrt{g_L}\,R(g_L) \quad , \tag{4.7}$$

as one could easily see by noticing that the induced metric on the TeV brane is flat. The 4D Planck mass has a dependence on the new mass scale, $M_{\rm IR}$, as

$$M_{\rm Pl}^2 = \frac{M_\star^3}{k}\left(1 - e^{-2kL} + e^{-2kL}\,\frac{M_{\rm IR}^2 k}{M_\star^3}\right) \quad , \tag{4.8}$$

where, with $e^{-2kL} \ll 1$, the dependence is indeed very mild.

It is useful to pause and comment on the holographic description of brane-localized curvature. The RS models are thought to be dual to strongly coupled 4D theories that are approximately conformal between $M_\star$ and the Kaluza-Klein scale. The presence of UV and IR branes explicitly breaks conformal symmetry, and matter fields on the UV (IR) brane are

seen as dual to fundamental (composite) fields in the dual theory. Hence, the massless graviton (UV localized) is thought to be mostly fundamental, while the Kaluza-Klein gravitons (IR localized) are thought to be mostly composite. In the absence of the IR brane ($L \to \infty$) the dual theory would be conformal at all energies below $M_\star$, and the effective Planck mass would be $M_{\rm Pl}^2 = M_\star^3/k$. In the dual theory the bulk Einstein-Hilbert action arises dynamically via loops of CFT fields cut off at $M_\star$, while the spontaneous breaking of conformal invariance, due to the presence of the IR brane, generates a $-e^{-2kL}M_\star^2/k$ correction to $M_{\rm Pl}^2$. Now, the presence of an IR brane kinetic term also corrects the effective Planck mass, Eq. (4.8), thus in terms of the dual theory it should be thought of as arising due to modified dynamics associated with the breakdown of conformal invariance in the IR. For a more thorough discussion on the CFT interpretation we refer the reader to [116].

Formally, the radion is the scalar zero-mode in the metric perturbations. Physically, radion fluctuations control the size of the extra dimension. It was shown in Ref. [99] that an appropriate ansatz for scalar perturbations is

$$ds^2 = e^{-2ky-2F}\eta_{\mu\nu}dx^\mu dx^\nu - (1+2F)^2 dy^2, \quad F \equiv F(x^\mu, y) \tag{4.9}$$

where F is related to the physical radion field as we show below. In the absence of Eq. (4.7), one could determine the radion wave-function by either solving the linearized Einstein equations or simply working on the action level. For example, one could expand the actions in Eqs. (4.3) and (4.4) to quadratic order in $F(x^\mu, y) \equiv f(y)R(x)$. The wave-function is then determined by simply demanding the quadratic fluctuations to be massless, which yields the following differential equation for the wave-function in the bulk

$$400k^2 f^2 + 48 f\ddot{f} + 36\dot{f}^2 - 368 k f\dot{f} = 0 \tag{4.10}$$

with the following unique solution respecting the orbifold boundary conditions[1]:

$$f(y) = e^{2k|y|} \quad . \tag{4.11}$$

The same solution is recovered from the equations of motion; see, e.g., Ref. [99]. The situation is drastically different in the presence of brane curvature: Eq. (4.11) does *not* solve the linearized equations of motion. Nevertheless, this poses no concern. First, the theory is

[1]The brane terms resulting from Eq. (4.4) force the boundary conditions, automatically satisfied by Eq. (4.11).

ultimately defined via a path integral that only employs the action as the fundamental object. Second and more importantly, the wave-function in Eq. (4.11) is physically motivated as it yields a degree of freedom whose value measures the size of the extra dimension.

To derive the kinetic term of the radion, there is a subtle issue that we wish to point out. The available derivation in the literature starts by first expanding the action to quadratic order in fluctuations, i.e. $F(y, x^\mu)$, and proceeds using the CGR wave-function to integrate along the extra dimension thereby obtaining the usual kinetic term. In fact, this procedure is inaccurate for the purpose of studying the phase transition and is adequate only when discussing radion phenomenology at zero temperature. In a nutshell, the procedure of expanding the action to second order in F leads to a non-standard kinetic term of the form $(\partial\mu)^2/\mu^2$. As we shall see below, this problem is artificial and an exact computation yields a proper kinetic term for the radion.

Now we plug Eq. (4.9) into (4.3) without any expansion. A straightforward computation yields

$$S^{\rm G}_{\rm bulk} = \frac{M_\star^3}{2}\int d^4x \int_{-L}^{L} dy \left[6e^{-2k|y|}e^{-2F}(1-2F)(\partial_\alpha F)(\partial^\alpha F) - 8k^2(1-2F)\, e^{-4k|y|}e^{-4F}\right] \tag{4.12}$$

where we have integrated by parts and utilized Eq. (4.11) to considerably simplify the term inside brackets. Because of orbifold boundary conditions, there are terms in the action proportional to delta functions but they all cancel identically with the brane actions in Eq. (4.4). Lastly, we need to carry out the integral over y which prompts us to recall the definition of the radion field. Precisely,

$$\mu(x) \equiv k e^{-kd(x)} \tag{4.13}$$

where $d(x)$ is the proper length of the extra dimension

$$kd(x) = k\int_0^L dy(1+2F) = kL + R(x)(e^{2kL}-1) \quad . \tag{4.14}$$

Now the integral in Eq. (4.12) is performed via a change of variables

$$k\bar{y} = ky - e^{2ky}R(x) + R(x) \tag{4.15}$$

and one finds

$$\mathcal{L} = \frac{6M_\star^3}{k^3}\,\frac{1}{2}(\partial_\alpha\mu)\,(\partial^\alpha\mu) \tag{4.16}$$

where we used that $e^{2kL} \gg 1$ and ignored a self-interaction term $\mathcal{O}(\mu^4)$. Adding Eq. (4.7) now leads to our main result

$$\mathcal{L} = \mathcal{Z}^2 \, \frac{1}{2} (\partial_\alpha \mu) \, (\partial^\alpha \mu) \tag{4.17}$$

where

$$\mathcal{Z} \equiv \sqrt{\frac{6M_\star^3}{k^3}(1-\theta_{\rm IR})}, \quad \theta_{\rm IR} \equiv \frac{M_{\rm IR}^2 k}{M_\star^3} \, , \quad \xi_{\rm IR} \equiv 1 - \theta_{\rm IR} \quad . \tag{4.18}$$

Notice here that the sole effect of Eq. (4.7) is to modify the kinetic energy of the physical radion. Indeed, we demand that $\theta_{\rm IR} < 1$ to insure the radion is not a ghost. Our result differs from that obtained by employing the interval approach [115], which hinges on solving the linearized equations of motion in the presence of Eq. (4.7). In addition, notice the interval approach parametrizes the scalar perturbations differently than Eq. (4.9). We stick to the CGR wave-function, and the corresponding kinetic term, since it allows for a transparent relation between $F(x, y)$, the radion and the size of the extra dimension.

4.2.2 Stabilization and the radion potential

We shall see in the next section that the high temperature phase of the theory, holographically dual to the planar AdS black hole, is stable at any temperature and no phase transition can occur. This completely changes once the extra dimension in the Randall-Sundrum set-up is stabilized. Indeed even in the zero-temperature realization of the model, stabilization is required to invoke a dynamical mechanism generating the large hierarchy between the weak and Planck scales in a natural way.

The mechanism of Goldberger and Wise is minimal and serves our purposes. It relies on adding a bulk scalar field that develops a non-trivial profile along the extra dimension. Using this profile in the Goldberger-Wise action, a potential for the radion field is generated with a global minimum thus dynamically fixing the size of the extra dimension.

Here, we derive the radion potential using the correct metric ansatz for the scalar perturbation. In the bulk, the scalar field equation is

$$(\Box + m^2)\varphi(y) = 0 \tag{4.19}$$

which is evaluated using the metric in Eq. (4.9) and leads to

$$(1+2F)\varphi'' - 4(1+2F)(k+F')\varphi' - 2F'\varphi' = (1+2F)^3 m^2 \varphi \quad , \tag{4.20}$$

where a prime denotes derivative with respect to y. Remarkably, the bulk equation could be solved exactly with the coordinate transformation

$$k\bar{y} = ky + e^{2ky}R(x) - R(x) \tag{4.21}$$

which turns the equation simply to

$$\ddot{\varphi} - 4k\dot{\varphi} = m^2\varphi, \quad \dot{\varphi} \equiv \partial_{\bar{y}}\varphi \quad . \tag{4.22}$$

We see that the coordinate transformation has changed the independent variable to be the proper distance along the extra dimension, i.e. $\bar{y}$. Now, the solution is rather simple,

$$\varphi(\bar{y}) = e^{2k\bar{y}}\left[Ae^{\nu k\bar{y}} + Be^{-\nu k\bar{y}}\right], \quad \nu \equiv \sqrt{4 + \frac{m^2}{k^2}} \tag{4.23}$$

where A and B are integration constants to be fixed by boundary conditions. The exact forms of the boundary actions do not concern us as they merely enforce the boundary conditions. We can easily switch back to the coordinate y to determine the constants

$$\varphi(y=0) = \Phi_P \ , \quad \varphi(y=L) = \Phi_T \quad . \tag{4.24}$$

The potential of the radion is determined by plugging the solution back into the action and integrating over the extra dimension. Precisely, we have

$$V(\mu) = \int_0^L dy\ e^{-4ky-4F}(1+2F)\left[(1+2F)^{-2}\varphi'^2 + m^2\varphi^2\right] \ , \tag{4.25}$$

which is evaluated most simply by switching to $\bar{y}$ to yield

$$V(\mu) = k(\nu+2)A^2\big(e^{2\nu kd(x)} - 1\big) + k(\nu-2)B^2\big(1 - e^{-2k\nu d(x)}\big) \ , \tag{4.26}$$

where

$$A + B = \Phi_P \ , \quad Ae^{\nu kd(x)} + Be^{-\nu kd(x)} = e^{-2kd(x)}\Phi_T \quad . \tag{4.27}$$

So far, no approximations have been made. We can follow Goldberger and Wise to solve for the constants in the limit of large extra dimension, i.e. $kd(x) \gg 1$, which indeed is a valid limit given that we want to solve the hierarchy problem. Another convenient limit is that of small $\epsilon \equiv m^2/4k^2$ that enables the extraction of analytic results. In terms of the physical radion, we finally have

$$V(\mu) = \epsilon k^4\Phi_P^2 + \mu^4\left[(4+2\epsilon)\left(\Phi_T - \Phi_P\frac{\mu^\epsilon}{k^\epsilon}\right)^2 - \epsilon\Phi_T^2\right] \tag{4.28}$$

where the brane vacuum expectation values (VEVs) are made dimensionless via

$$\Phi_P \to k^{3/2}\Phi_P, \quad \Phi_T \to k^{3/2}\Phi_T \quad . \tag{4.29}$$

We shall thoroughly discuss the constraints on the brane VEVs in Section 4.4. This completes our derivation of the radion effective Lagrangian.

4.3 Thermal phase transition: holographic description

It is mandatory to study the finite temperature behavior of the RS model if it were to describe the early universe. This endeavor was initiated in Ref. [54] concluding that finite-temperature effects tend to destabilize the extra dimension. At low enough temperature (below a TeV) and in the absence of a stabilization mechanism, a temperature-dependent potential for the radion is induced through its coupling to the heavy KK gravitons. When the latter are integrated out and a thermal average of the effective action is performed, a correction of the form $(-T^8/\mu^4)$ appears [54]. Clearly, the latter correction renders the RS set-up unstable by pushing the branes away from each other.

The authors of Ref. [54] turned to the AdS/CFT correspondence to understand the high temperature phase of the model. The RSI is conjectured to be dual to a strongly coupled CFT [104, 105]. The introduction of branes is then seen to break conformal symmetry. The Planck brane explicitly breaks the symmetry by introducing a UV cut-off while coupling the CFT to 4D gravity. The TeV brane, on the contrary, signals the spontaneous breakdown of the symmetry in the IR where the scale of symmetry breaking is set precisely by the size of the extra dimension. Matter fields on the TeV brane, as well as KK states, are dual to bound states in the 4D theory.

The finite temperature physics of the RSI model becomes very transparent if one recalls the exact AdS/CFT dictionary [103]

$$Z_{\rm CFT}[g] = Z_{\rm gravity}[G] \tag{4.30}$$

where the rhs denotes the thermal partition function of a quantum theory of gravity formulated on AdS space with metric G that induces a boundary metric g. In the saddle-point approximation to the partition function, one finds all solutions to the Euclidean Einstein equations representing thermal equilibrium. The partition function is then a sum over these disconnected saddles, ideally taking loop fluctuations into account. In our case, there are two

solutions that represent states of thermal equilibrium; the RSI model with two branes and the planar AdS black hole. This observation, first made in Ref. [54], is key to unveiling the high temperature characteristics of the model, and the physics turns out to be quite similar to the Hawking-Page phase transition.

Let us recall the AdS planar black hole [106]. The metric reads

$$ds^2 = \frac{r^2}{l^2}\left(1 - \frac{r_0^{D-2}}{r^{D-2}}\right)dt^2 - \frac{l^2}{r^2}\left(1 - \frac{r_0^{D-2}}{r^{D-2}}\right)^{-1} dr^2 - \frac{r^2}{l^2}\sum_{i=1}^{3} dx_i^2 \tag{4.31}$$

where the transverse dimensions, i.e. x_i, could be made compact by restricting the range of coordinates. There exists a single horizon at $r = r_0$ with $\mathbb{R}^3$ topology. The parameter r_0 is related to the ADM mass per unit transverse volume

$$\frac{\mathcal{M}}{V} = \frac{3M_\star^3 r_0^4}{2l^5} \quad . \tag{4.32}$$

Armed with the two solutions, we need to compare their respective free energies to decide on the relative stability of each phase. The Euclidean approach to black hole thermodynamics commences with introducing the Euclidean section via an analytic continuation $t \to -i\tau$. The periodicity of imaginary time is fixed so as to avoid a conical singularity [107], i.e.

$$\beta = \frac{\pi l^2}{r_0} \quad . \tag{4.33}$$

The contribution of the saddle-point to the free energy is given by the Euclidean action, i.e. $\beta F(\beta) = \mathcal{S}_E$. The free energy of the black hole diverges as $r \to \infty$, so we subtract off the pure AdS contribution

$$F_{\text{pBH}} - F_{\text{AdS}} = -\frac{\pi^4}{2}(M_\star l)^3 T^4 \quad . \tag{4.34}$$

Notice that the temperature of AdS is not fixed by any requirement. The relation between the black hole and AdS temperatures, as devised by Hawking and Page [113], is found by equating the proper length of the thermal circle at spatial infinity. The conclusion from Eq. (4.34) is very elegant: unlike the AdS-Schwarzschild black hole, the planar black hole is always stable and never decays to thermal AdS.

The free energy of the RSI solution is more subtle. Simply put, the computation yields a finite result while thermal AdS yields a divergent contribution. The situation is easily remedied by simply sending the Planck brane to infinity to coincide with the AdS boundary.

To see this, we introduce a new coordinate, $ky = -\ln(kr)$, which turns Eq. (4.5) into

$$ds^2 = \frac{r^2}{l^2}dt^2 - \frac{l^2}{r^2}dr^2 - \frac{r^2}{l^2}\sum_{i=1}^{3} dx_i^2 \tag{4.35}$$

which is the same as AdS except that $r \in [r_{\rm TeV}, \infty)$. Upon including the Hawking-Gibbons-York boundary term for the TeV brane, one simply finds

$$F_{\rm RS} - F_{\rm AdS} = 0 \tag{4.36}$$

which means again that no phase transition could proceed and the theory stays in the deconfined phase at any temperature. Indeed, there is a caveat to this result: the situation drastically changes once stabilization is taken into account upon adding the bulk scalar. The simplest way to see this is by inspecting the induced radion potential in Eq. (4.28) which contributes to the free energy of the RSI phase inciting a phase transition at a critical temperature

$$T_{\rm c}^4 = \frac{2V(\mu_-)}{\pi^4 (M_\star l)^3} \tag{4.37}$$

where μ_- denotes the radion VEV.

In the five-dimensional description used here, the phase transition is characterized by a jump in the radion field, which therefore takes the role of the order parameter. As we explained, the five-dimensional phase transition corresponds in the dual theory to a (de)-confinement transition of the strongly coupled theory. At high temperatures, the system has a nearly conformal symmetry, which spontaneously breaks when the strong sector confines. This symmetry breakdown will generate a composite pseudo-Goldstone boson, i.e. the dilaton. The VEV of the dilaton field sets the confinement scale, and so can be interpreted as the order parameter on the four-dimensional side [117].

4.4 Dynamics of the phase transition at large N

We saw in the last section that the stabilization-induced radion potential triggers a first order phase transition to proceed from the high temperature black hole phase to the low temperature RSI phase. In this section, we study the dynamics of the phase transition. First, we illuminate how the various parameters of the model affect the features of the phase transition. Second, we discuss the effect of brane-localized curvature by making $\xi_{\rm IR} \neq 1$, where $\xi_{\rm IR}$ is defined in Eq. (4.18).

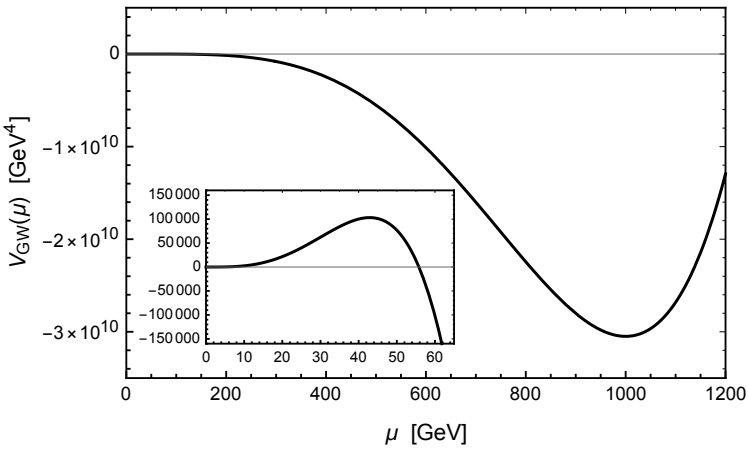

Figure 4.1: A plot of the radion potential, described by Eq. (4.38), for $\Phi_T = 1$, $\epsilon = 0.1$ and $(M_\star l) = 0.55$. The inset shows the size and location of the maximum.

4.4.1 Qualitative discussion

It is instructive at this stage to discuss in detail the effect various parameters have on the strength of the phase transition. To this end, we start by rewriting the radion Lagrangian

$$\mathcal{L} = \mathcal{Z}^2 \frac{1}{2}(\partial\mu)^2 - \Phi_T^2 \left[(4+2\epsilon) \left(1 - (\Phi_P/\Phi_T)\frac{\mu^\epsilon}{k^\epsilon} \right)^2 - \epsilon \right] \mu^4 \quad , \tag{4.38}$$

where we explicitly uncover that Φ_T, unlike Φ_P, plays a dominant role in the dynamics. The generic features of the potential are displayed in Figure 4.1. Most importantly, for any positive ϵ the potential possesses a global maximum and a minimum. The values of Φ_T and ϵ predominantly control both the position of, as well as the value of the potential at the extrema.

As it stands, this Lagrangian is still not adequate to discuss the tunneling process. We need to subtract off the energy of the false vacuum, i.e. Eq. (4.34), which serves as a temperature-dependent offset when computing the bubble action. This leaves the potential

$$V(\mu, T) = \Phi_T^2 \left[(4+2\epsilon) \left(1 - (\Phi_P/\Phi_T)\frac{\mu^\epsilon}{k^\epsilon} \right)^2 - \epsilon \right] \mu^4 + \frac{\pi^4}{2}(M_\star l)^3 T^4 \ . \tag{4.39}$$

In conventional tunneling problems the potential describes the whole scenario and one uses a bounce solution to find a bubble profile that ends in the false vacuum with zero kinetic energy. The case at hand is drastically different since, as we explained, we do not consider the contribution of the black hole to the tunneling rate and our potential therefore only describes the dynamics of the radion. To handle this problem, we follow the approach used by Ref. [59]

which tacitly takes care of this issue. As in the usual bounce solution approach the radion is released somewhere between the extrema of the potential and is then required to tunnel to $\mu = 0$. However, given that $\mu = 0$ is not the false vacuum we demand the radion field reaches this point with enough kinetic energy to jump over and mount on top of the black hole free energy, the correct false vacuum. Precisely, the bubble profile now obeys the boundary condition [59]

$$\xi_{\rm IR}\,\frac{1}{2}(\partial_\alpha\mu)(\partial^\alpha\mu)|_{\mu=0} = \frac{\pi^4}{12}T^4 \quad , \tag{4.40}$$

which consequently introduces a non-trivial temperature dependence in the tunneling rate in addition to the temperature dependent offset now in the potential. Once the parameters $(M_\star l)$, Φ_T and ϵ are fixed, Eq. (4.40) associates each release point μ_r to a temperature value. We believe the treatment outlined in Ref. [59] is the most suitable in our situation given our inability to include the black hole phase in computing the tunneling rate.

Radion field configurations are found by using the boundary condition, Eq. (4.40), in conjunction with solutions of the canonically normalized O(3) equation of motion

$$\partial_r^2\mu + \frac{2}{r}\cdot\partial_r\mu = \frac{1}{\mathcal{Z}^2}\cdot\frac{\partial V(\mu,T)}{\partial\mu} \tag{4.41}$$

where $\mathcal{Z}$ and $V(\mu,T)$ are given by Eqs. (4.17) and (4.39) respectively, although note that the temperature dependent offset plays no role here. Eq. (4.41) is solved for a range of release points μ_r which in turn translate to a range of temperatures through Eq. (4.40). The solutions and corresponding temperatures are then used to find the O(3) bounce action from

$$\frac{S_3}{T} = \frac{4\pi}{T}\cdot\mathcal{Z}^2\cdot\int dr\; r^2\left[\frac{1}{2}(\partial_r\mu)^2 + \frac{1}{\mathcal{Z}^2}\cdot V(\mu,T)\right] . \tag{4.42}$$

The tunneling rate per unit volume reads

$$\Gamma = A(T)\,e^{-S_3/T}, \tag{4.43}$$

where by dimensional analysis we shall estimate $A(T)\sim(\mu_-)^4$. The requirement of nucleating one critical bubble per unit Hubble volume then translates into

$$\frac{S_3}{T} \leq 4\log\left(\frac{M_P}{T_c}\right) + 4\log\left(\frac{\mu_-}{T_c}\right), \tag{4.44}$$

where the cosmology is radiation-dominated. Hence, if we take T_c to be of the same order as μ_-, we obtain $S_3/T \lesssim 140$. This is the value we use throughout our study although a lower T_c, attainable in most of our parameter space, considerably relaxes the nucleation condition.

Including the false vacuum offset, it is illustrative to split the bounce action into two contributions

$$\frac{S_3}{T} = \frac{E}{T} + \frac{2\pi^5}{3}(M_\star l)^3 \,(r_c T)^3 \quad , \tag{4.45}$$

where E and r_c are, respectively, the energy and radius of the critical bubble. In such a form it becomes apparent that the factors influencing the bounce action are E, T, and r_c. Each of these factors has a non-trivial dependence on the input parameters which we discuss below.

At first sight, it appears from our potential and boundary condition that we have five free parameters,

$$\left(\xi_{\rm IR}, (M_\star l)^3, \Phi_T, \Phi_P/\Phi_T, \epsilon\right) \quad , \tag{4.46}$$

and we plan to discuss each extensively.[2] The new parameter $\xi_{\rm IR}$ is left to the next subsection and so, for now, we fix $\xi_{\rm IR} = 1$, restoring the usual scenario [54, 57–59]. In fact, solving the hierarchy problem imposes a constraint that the global minimum of the potential must lie at the TeV scale. This fixes the ratio Φ_P/Φ_T as follows: the global extrema of the potential are located at

$$\mu_\pm = k\left(\frac{\Phi_T}{\Phi_P}\right)^{1/\epsilon}\left[\frac{(4+\epsilon) \mp \sqrt{\epsilon(4+\epsilon)}}{2(2+\epsilon)}\right]^{1/\epsilon} \quad , \tag{4.47}$$

where, for $\epsilon > 0$, μ_+ and μ_- are the maximum and minimum respectively. Hence, once ϵ and $(M_\star l)$ are fixed[3], the ratio Φ_P/Φ_T is uniquely determined once we make our choice of $\mu_- = 1\,\text{TeV}$.

$(M_\star l)$ *factor.* The value of $(M_\star l)$ (corresponding to the number of colors in the CFT Eq. (4.1)) plays a crucial role in the phase transition. In Figure 4.2, the effect of $(M_\star l)$ on E, T and r_c is shown for various release points. Each factor displays a dependence on $(M_\star l)$ either explicitly, implicitly through $\mathcal{Z}$, or both. The rapid increase in the bubble energy, E, is due to both the $\mathcal{Z}$ factor and the increase in r_c. For r_c, the only dependence on $(M_\star l)$ comes through $\mathcal{Z}$. Finally, the increase in $(M_\star l)$ for a fixed release point decreases the temperature. It is interesting to note that the combination $r_c T$ does not scale significantly with $(M_\star l)$.

[2] When exploring the dependence on these parameters we ignore back-reaction constraints to streamline the discussion, but we ultimately take them into account in the following subsection.

[3] Throughout this section, a choice of $(M_\star l)$ determines k by requiring the 4D Planck mass, Eq. (4.8), to be 10^{18}GeV.

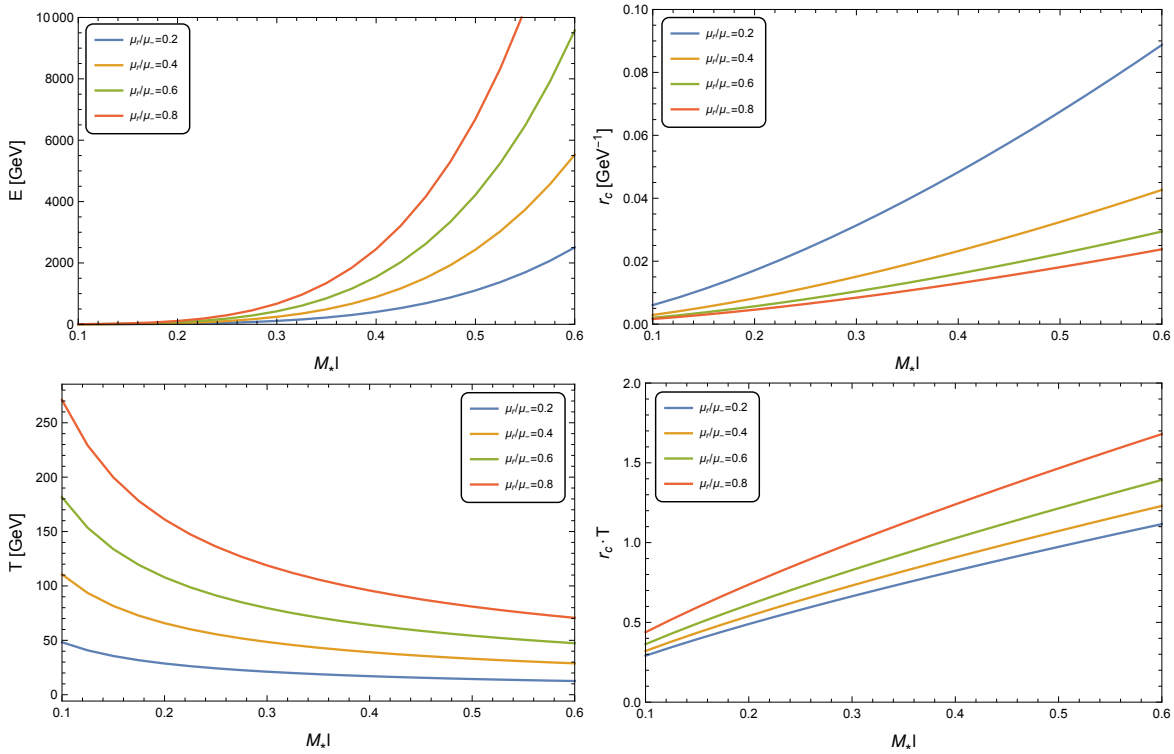

Figure 4.2: The dependence of various quantities in the bounce action S_3/T of Eq. (4.45) on $(M_\star l)$ for a range of release points. We take the benchmark values $\epsilon = 0.05$ and $\Phi_T = 1$.

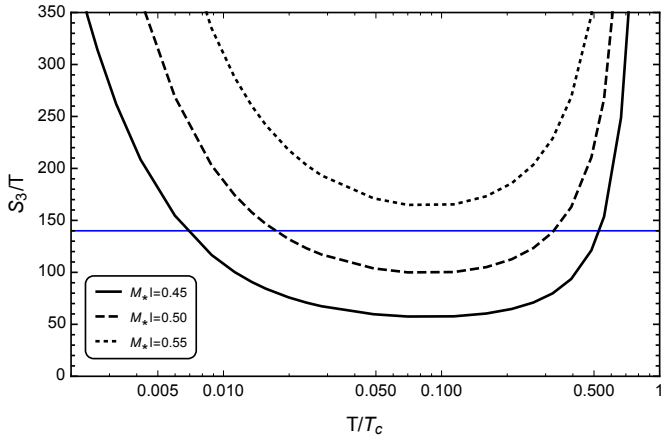

Figure 4.3: The bounce action S_3/T for various values of $(M_\star l)$ with the benchmark values $\epsilon = 0.05$ and $\Phi_T = 1$, where the blue line represents the nucleation condition. It is clear that increasing $(M_\star l)$ hinders the tunneling.

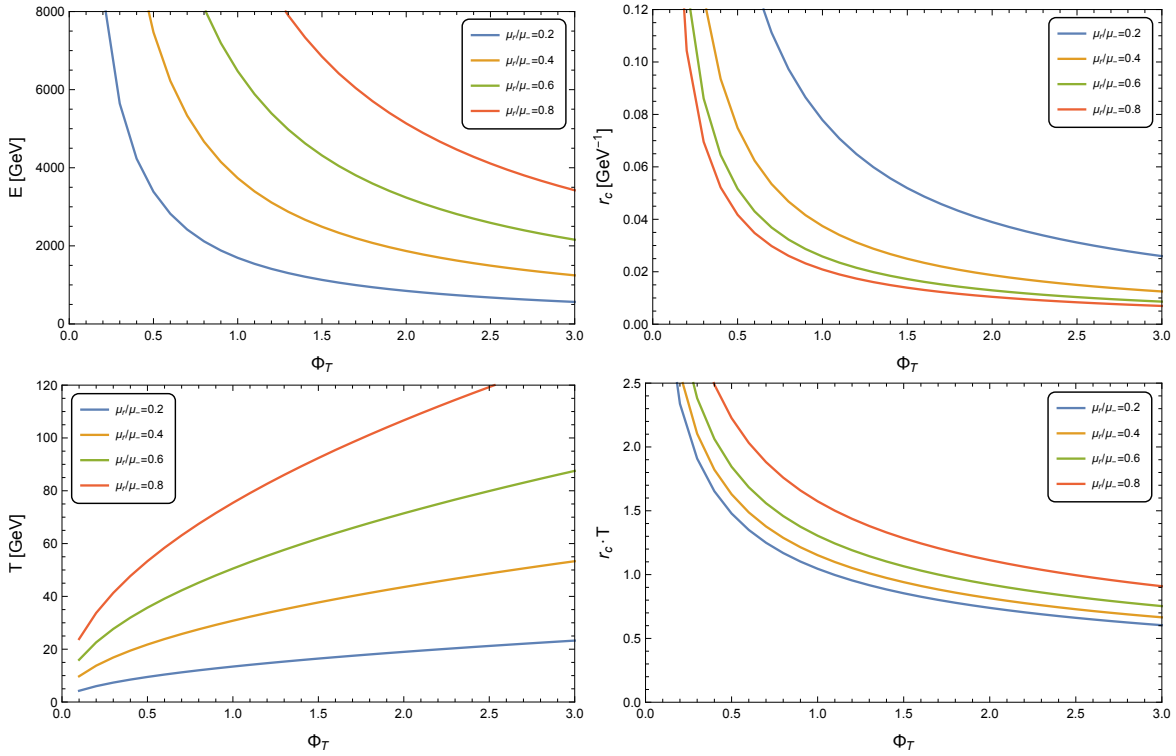

Figure 4.4: The dependence of various quantities in the bounce action S_3/T of Eq. (4.45) on Φ_T for a range of release points. We take the benchmark values $\epsilon = 0.05$ and $(M_\star l) = 0.55$.

In Figure 4.3, we show the tunneling exponent for various values of $(M_\star l)$. Here, the devastating effect of large $(M_\star l)$ on the tunneling rate is clear. An incremental increase causes the system to get stuck in the false vacuum. This tension has been noted in Refs. [54, 57–59] to be the most unpleasant feature of the phase transition. In fact, large $(M_\star l)$ (or N) is required for the semiclassical analysis to be reliable. We shall see below how the inclusion of $\xi_{\rm IR}$ drastically changes the situation.

Effect of Φ_T. The parameter Φ_T plays a major role in determining the tunneling rate. Increasing Φ_T renders the potential deeper at the minimum, thereby considerably facilitating the tunneling to occur. We see in Figure 4.4 the effect of increasing Φ_T on the various quantities in Eq. (4.45). As we shall explain below, with $\xi_{\rm IR} = 1$ the condition of limited back-reaction on the background geometry prohibits us from leveraging the effect of Φ_T. Arguably, the most important effect of brane-localized curvature will be to enable us to prop up Φ_T consistent with back-reaction constraints. Figure 4.5 shows the dramatic effect increasing Φ_T has on aiding nucleation.

ϵ *parameter*. The choice of ϵ has a strong impact on the strength of the phase transition.

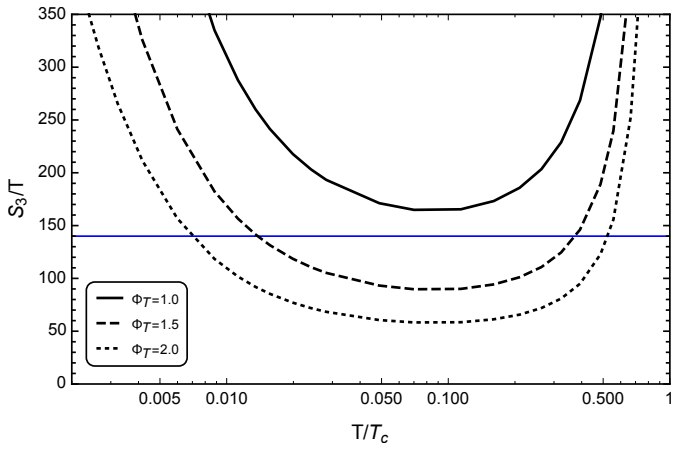

Figure 4.5: The bounce action S_3/T for various values of Φ_T with the benchmark values $\epsilon = 0.05$ and $(M_\star l) = 0.55$, where the blue line represents the nucleation condition. It is clear that increasing Φ_T significantly improves nucleation rates.

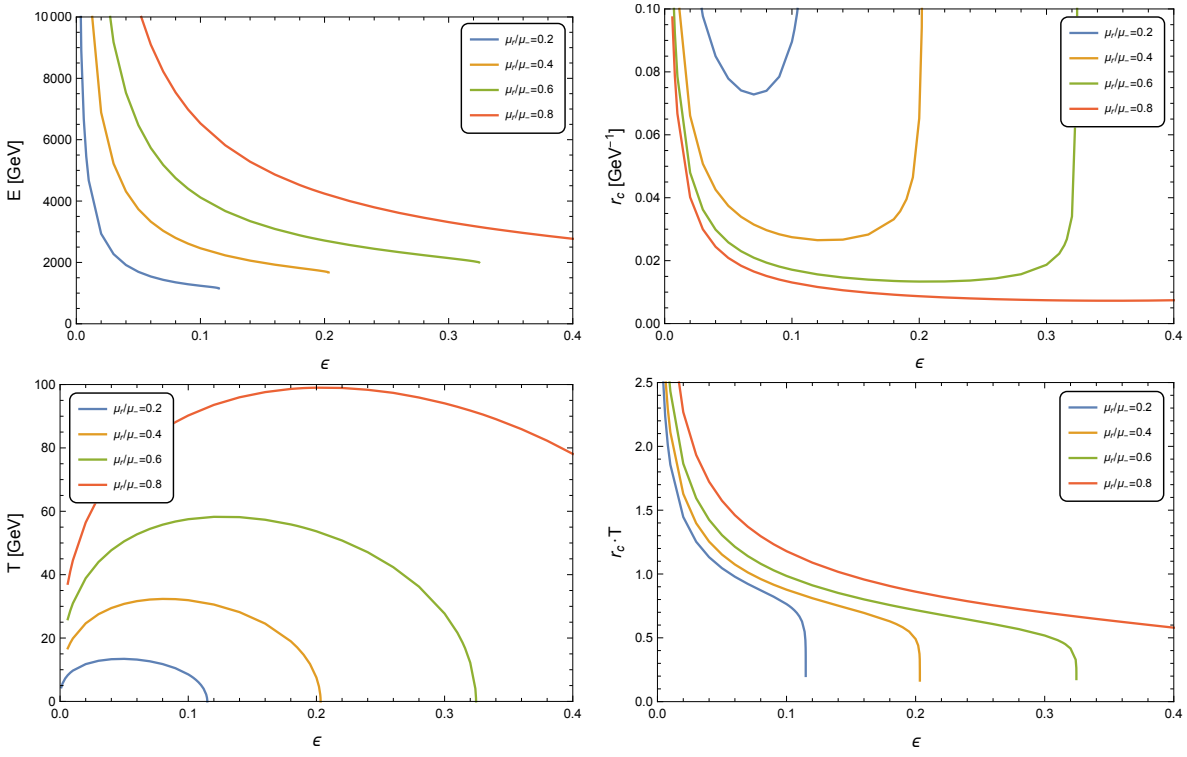

Figure 4.6: The dependence of various quantities in the bounce action S_3/T of Eq. (4.45) on ϵ for a range of release points. We take the benchmark values $\Phi_T = 1$ and $(M_\star l) = 0.55$.

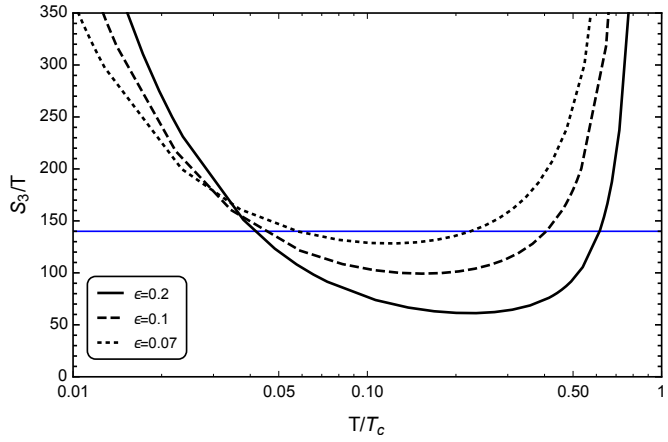

Figure 4.7: The bounce action S_3/T for various values of ϵ with the benchmark values $\Phi_T = 1$ and $(M_\star l) = 0.55$, where the blue line represents the nucleation condition. It is clear that, for positive values, decreasing ϵ increases the supercooling.

First of all, it uniquely determines the ratio between the extrema of the potential

$$\frac{\mu_-}{\mu_+} = \left(\frac{1 + \sqrt{\epsilon/(4+\epsilon)}}{1 - \sqrt{\epsilon/(4+\epsilon)}} \right)^{1/\epsilon} \quad , \tag{4.48}$$

and thus a larger ϵ pushes μ_+ closer to the minimum. This indeed facilitates the tunneling taking place, as seen in Figure 4.7. Conversely, one could attain substantial amounts of supercooling by lowering ϵ. Another important factor is the barrier height compared to the depth of the potential

$$\left| \frac{V(\mu_+)}{V(\mu_-)} \right| = \left(\frac{\mu_+}{\mu_-} \right)^4 \quad , \tag{4.49}$$

which is exact thanks to the properties of the potential. It is clear that a larger ϵ leads to a larger barrier with respect to the depth of the minimum, thus hindering the tunneling from proceeding. Hence, the size of ϵ presents two competing effects on the phase transition.

Figure 4.6 shows the effect ϵ has on the various quantities in the bounce action of Eq. (4.45). We observe rather more complex behaviors compared to the monotonic dependences on $(M_\star l)$ and Φ_T. The bubble energy decreases with increasing ϵ as μ_+ is brought closer to the minimum, until the barrier height becomes so large that the field can no longer reach $\mu = 0$. The situation for r_c and T is more interesting. Here, it is adequate to think in terms of a single particle moving in the inverted potential of Eq. (4.39). Evidently, the size of ϵ controls the *flatness* of the potential between the extrema. Increasing ϵ introduces a larger gradient in the

potential, i.e. $\partial V/\partial\mu$ becomes large between the extrema. Thus, the particle rolls faster leading r_c to decrease. Eventually, the minimum of the inverted potential becomes so deep that it becomes harder for the particle to climb out of the well. This is the reason why r_c begins to increase beyond a certain ϵ. The same physics explains the behavior of the temperature.

4.4.2 Including brane-localized curvature

We now include the effect of brane-localized curvature, represented by $\xi_{\rm IR} \neq 1$. In particular, it can take the values $0 < \xi_{\rm IR} < 1$. This changes the dynamics of the phase transition dramatically. On the one hand, having $\xi_{\rm IR} \ll 1$ significantly enhances the tunneling rate by suppressing the energy of the bubble. On the other hand, the size of Φ_T can be made larger thus prompting the phase transition to quickly proceed. To clarify the latter point, let us recall that in order to ignore back-reaction of the bulk scalar on the background geometry, the following constraints must be satisfied [102]

$$\Phi_T \ll (M_\star l)^{3/2}, \quad \Phi_P \ll (M_\star l)^{3/2} \quad . \tag{4.50}$$

If $\xi_{\rm IR} = 1$, an enormous constraint on the parameter space is imposed since a very small $(M_\star l)$ is required to have a small $\mathcal{Z}$, allowing the phase transition to proceed. The role of $\xi_{\rm IR}$ is crucial in ameliorating this tension: $(M_\star l)$ could be substantially large while the normalization factor $\mathcal{Z}$ stays $\mathcal{O}(1)$. In particular, it is now possible to increase Φ_T, consistent with Eq. (4.50), to expedite the phase transition.

We begin by finding the $(M_\star l) - \Phi_T$ parameter space for various ϵ and $\mathcal{Z}$ values, shown in Figure 4.8. We remind the reader that Φ_P is fixed by the requirement that $\mu_- = 1\,\text{TeV}$. On one hand, nucleation does not take place for parameters in the blue-shaded region. On the other, the parameters in the orange-shaded region induce large back-reaction. This latter region is found by setting $\Phi_P = (M_\star l)^{3/2}$ in Eq. (4.47) and solving for $(M_\star l)$ as a function of Φ_T, given that $\mu_- = 1$ TeV. It is always true that $\Phi_P > \Phi_T$, and hence Φ_P serves as the greater threat to the small back-reaction approximation. On the right axis, we include the ratio of the fundamental mass scales $M_{\rm IR}/M_\star$ found from Eq. (4.17). Notice this ratio has a weak dependence on $\mathcal{Z}$, and so for the range of values in Figure 4.8 we observe no significant change.

The sole effect of $\mathcal{Z}$ on the parameter space is changing the size of the blue-shaded region. Smaller $\mathcal{Z}$ significantly enhances the tunneling probability, thus shrinking the disallowed re-

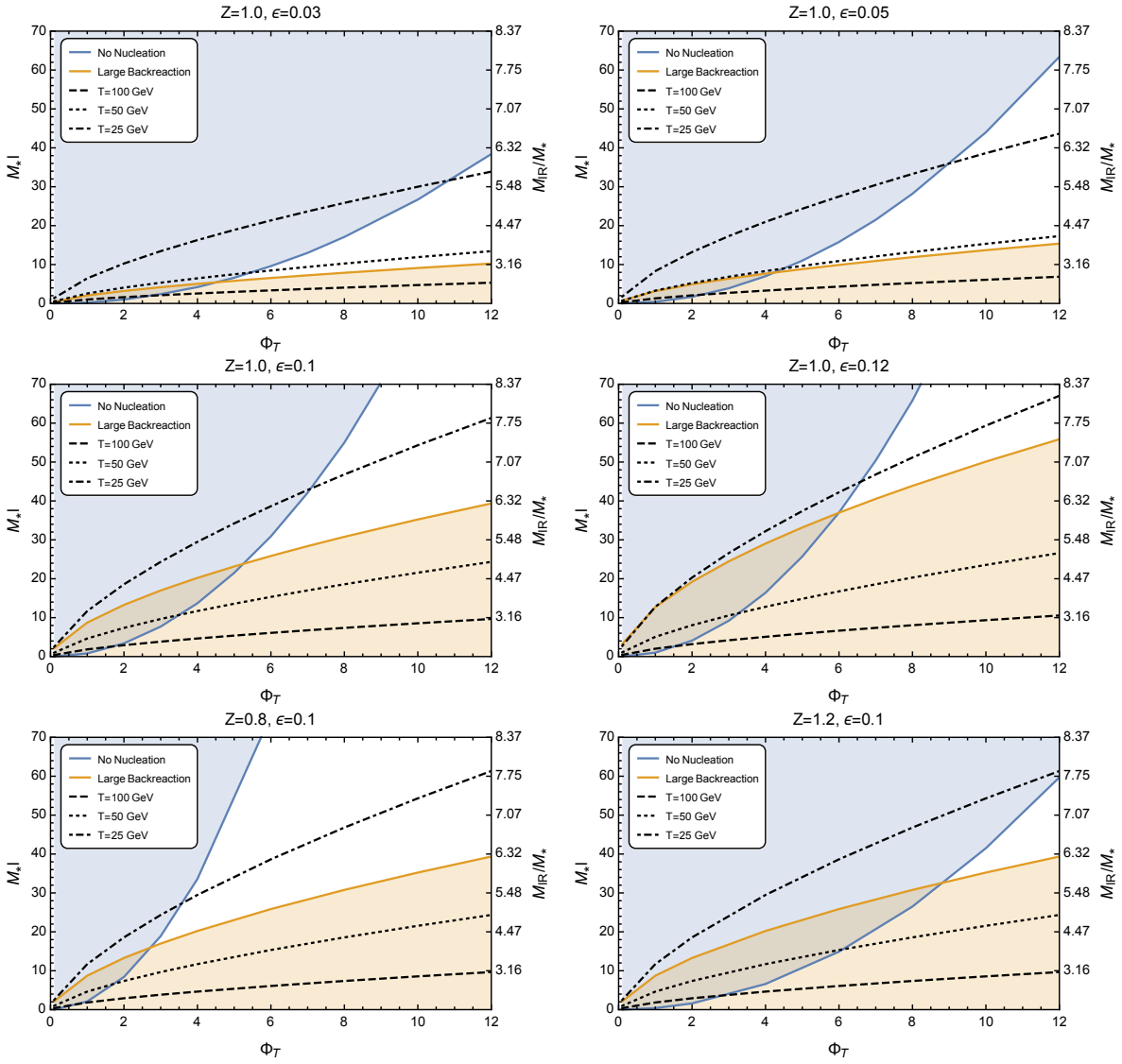

Figure 4.8: The parameter space of $(M_\star l)$ and Φ_T for varying ϵ and $\mathcal{Z}$ values. The blue-shaded region represents values at which nucleation is never achieved while the orange-shaded region represents values at which back-reaction is no longer negligible. The backreaction limit is found by setting $\Phi_P = (M_\star l)^{3/2}$ in Eq. (4.47) and solving for $(M_\star l)$. On the right axis we show the ratio of the fundamental mass scales $M_{\rm IR}/M_\star$ found from Eq. (4.17).

gion in the parameter space. Only a 20% decrease drastically enlarges the allowed parameter space as we clearly see in Figure 4.8. This behavior is quite non-trivial since this 20% decrease, for example, corresponds to an infinitesimal change in the ratio of $M_{\rm IR}/M_\star$. Indeed it is important to note that a certain level of fine-tuning is present in our approach since we always choose $M_{\rm IR}/M_\star$ to keep $\mathcal{Z}$ fixed and $\mathcal{O}(1)$. If we fix $(M_\star l)$ and change the ratio $M_{\rm IR}/M_\star$ by 1% the normalization factor $\mathcal{Z}$ changes by $\mathcal{O}(100\%)$ or so. Extrapolating the behaviour shown in Figure 4.8, the completion of the phase transition in this case would require substantially large values of both Φ_T and $(M_\star l)$.

The role of ϵ is interesting but proceeds as in previous studies. A larger ϵ induces faster nucleation as evident from our previous discussion and Figure 4.8. Yet, the orange-shaded region becomes larger with increasing ϵ as is clear from[4] Eq. (4.47). Constant-T_c curves are plotted using Eq. (4.37). Perhaps the most important effect of ϵ is to enable one to accommodate higher values of T_c, which may be crucial for some applications. For example, by decreasing ϵ one could attain higher T_c values. Notice, however, that one cannot continue pushing ϵ to lower values and expect to achieve larger T_c. Below some *optimum* ϵ, the decrease in constant-T_c curves begins to outpace that of the orange-shaded region, hindering the system from reaching higher T_c values.

We now ask ourselves the question, what is the level of supercooling throughout our available parameter space? Figure 4.9 shows color-maps for some of the allowed parameter regions in which red represents larger T_n/T_c (less supercooling) while blue represents smaller T_n/T_c (more supercooling). We immediately observe that our parameter regions allow for $T_n/T_c \sim \mathcal{O}(0.1-1)$, a significant difference to the previous results of Refs. [58, 59] in which large amounts of supercooling were unavoidable. The next question is how low a T_n/T_c could we accommodate within the allowed parameter space. It is quite interesting that $\mathcal{Z}$ has almost no effect in this regard as shown in the left plot of Figure 4.10. On the contrary, the right plot of Figure 4.10 shows that lowering ϵ allows for significantly smaller T_n/T_c. Notice that the right plot uses the lowest possible $(M_\star l)$, which implies there is more room to attain large amounts of supercooling.

To summarize, brane-localized curvature allows the phase transition to be completed at

[4] With $\xi_{\rm IR} = 1$, some previous papers [54, 57–59] have employed a brane tension term in the potential of the form $\delta T_1 \mu^4$ to allow for a negative ϵ. In particular, such a scenario relaxes back-reaction limits since $\Phi_P < \Phi_T$, which permits nucleation at $(M_\star l)$ of $\mathcal{O}(1)$.

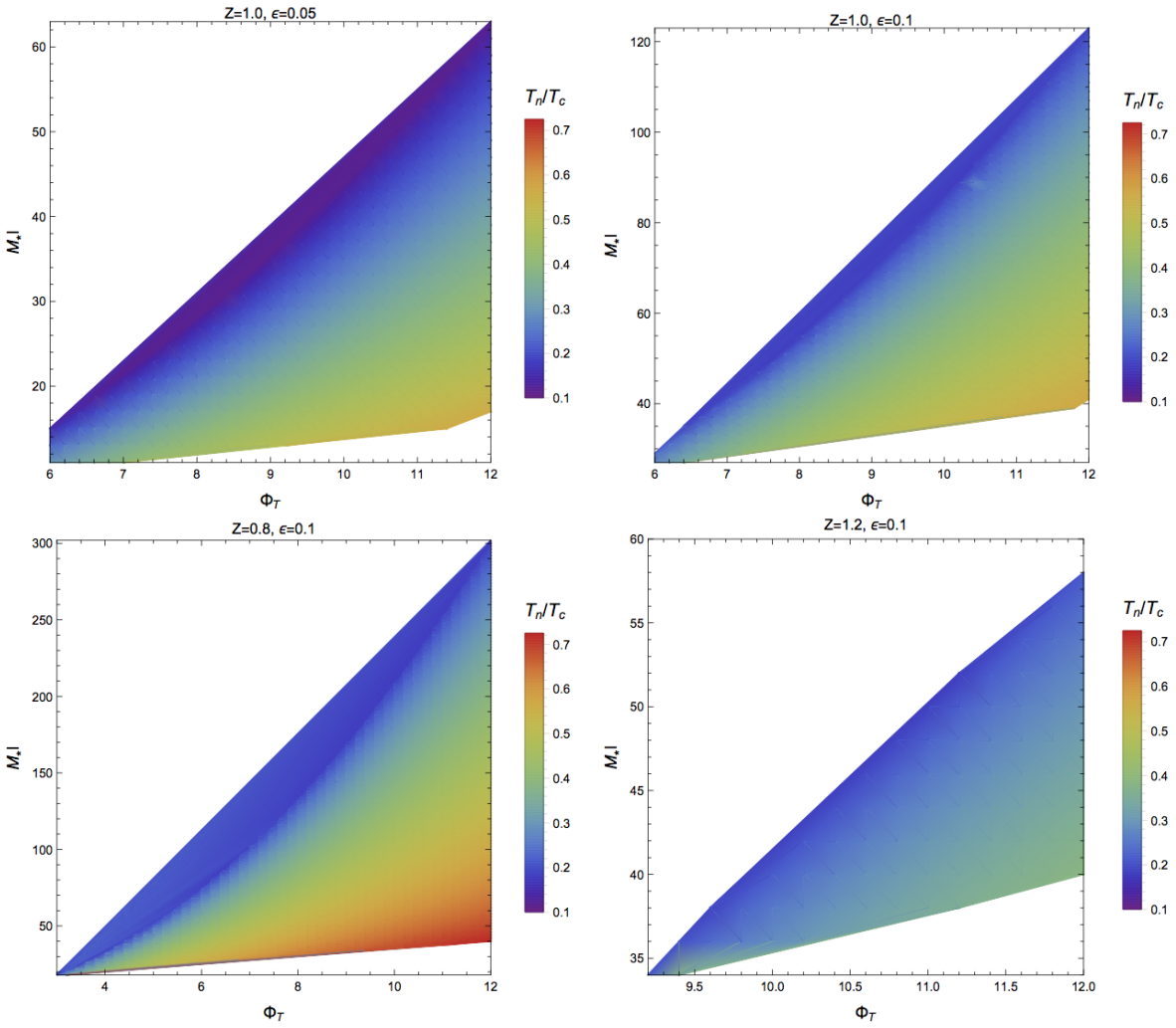

Figure 4.9: The variation in supercooling T_n/T_c over the allowed parameter regions for a selection of the parameter space plots in Figure 4.8.

much larger values of $(M_\star l)$. In particular, this implies that the holographic description is well motivated and the semi-classical treatment is well suited to describe the physics. Such large values of $(M_\star l)$ imply large values of the brane kinetic term,[5] as the parameter space discussed in this work typically requires $M_{\rm IR}/M_\star \sim \mathcal{O}(1) - \mathcal{O}(10)$, see Figure 4.8. One should inquire how natural our set-up is. First of all, the inclusion of brane-localized curvature is necessary in 5D models [118,119]. It suffices to notice that massive matter confined to the brane generates a divergent contribution proportional to Eq. (4.7). This is rather simple to understand if we realize that $M_{\rm IR}$ looks like the Planck mass in ordinary 4D gravity, and the latter receives well-known quantum corrections from massive matter (see, for example, Ref. [120]). Second, since our operator is not forbidden by any symmetries in the model, it is natural to explore renormalized values that satisfy the range of parameters we explored. Brane kinetic terms in 5D models have also been studied in the context of gauge fields, and similar conclusions were reached [121]. Finally, the presence of a brane kinetic term for gravity does not directly affect the stabilization via the Goldberger-Wise (GW) mechanism. Nevertheless, it has been shown that the presence of such terms contributes to a Casimir energy in the 5D bulk, which provides an alternative stabilization mechanism for 5D models [122]. In the future, we hope to explore alternative stabilization mechanisms within the context of our model.

4.4.3 Alternative look at the black hole contribution

It has been argued in Ref. [54] that the black hole contribution to the tunneling exponent scales as N^2. The upshot of our model is to considerably enhance, at large N, the radion tunneling by decreasing its kinetic energy. Here, one might generally worry that at large N the black hole contribution might kick in and dominate the tunneling process, upsetting some of the successes of our model. Indeed, in the absence of the exact instanton configuration, one cannot assess with certainty the dynamics of the high-temperature phase. Nevertheless, in the original analysis of Ref. [54], it was suggested to model the black hole by a field variable that describes the position of the horizon and investigate the tunneling problem by stitching together the free energies of both phases.

[5] It is clear from our plots that lowering $M_{\rm IR}$, while keeping $\mathcal{Z}$ fixed, does not allow the PT to take place. Indeed, in the extreme limit $M_{\rm IR} \to 0$, and as previous works have shown, one has to consider quite small values of $M_\star l$ and Φ_T. It is not possible to visualize in our plots this tiny corner of the parameter space, but we have indeed checked that our numerical routines reproduce the results in the literature when we take $M_{\rm IR}$ to vanish identically.

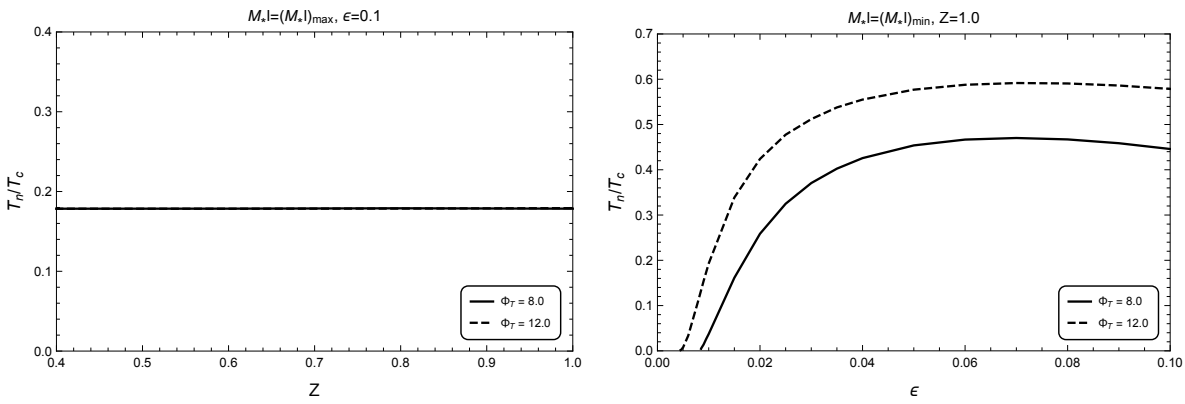

Figure 4.10: Left: The variation in the minimum T_n/T_c (which is found at the maximum $(M_\star l)$) with respect to $\mathcal{Z}$ for $\epsilon = 0.1$ and $\Phi_T = 8.0, 12.0$. Notice the two Φ_T lines are degenerate. Right: The variation in the maximum T_n/T_c (which is found at the minimum $(M_\star l)$) with respect to ϵ for $\mathcal{Z} = 1.0$ and $\Phi_T = 8.0, 12.0$.

Although our analysis followed a totally different route to model the black hole, i.e. the unconventional boundary condition Eq. (4.40), we find it advisable to present an alternative analysis within the approach of Ref. [54]. The total free energy of the system in now given by

$$V(\psi, T) = \begin{cases} V_{\rm Rad}(\psi) & \psi \geq 0 \\ V_{\rm BH}(\psi, T) & \psi < 0 \end{cases} + \frac{\pi^4}{2}(M_* l)^3 T^4 \ , \tag{4.51}$$

where the second term subtracts the energy of the false vacuum. Here, $V_{\rm Rad}(\psi)$ is given by the radion potential of Eq. (4.38) and the black hole free energy has the form [54]

$$V_{\rm BH}(T_h, T) = (M_\star l)^3 \pi^4 \left(\frac{3}{2} T_h^4 - 2\, T\, T_h^3 \right) \ . \tag{4.52}$$

A plot of the combined potential is seen in Figure 4.11. With this potential, we now have a description linking the true and false vacua, allowing a traditional bounce solution approach and removing the need for the boundary condition of Eq. (4.40). As before, the position of the radion minimum is set to be $\mu_- = 1$ TeV while that of the black hole side is simply given by T. Let us pause and comment on the traditional situation in the absence of brane-localised curvature. In that case both kinetic terms scale as N^2 and thus the contribution of each phase to the tunneling exponent strongly depends on the *width* of the potential on both sides at the time of tunneling. Since $\mu_- = 1$TeV and $T_c \ll 1$TeV, the radion motion is sufficient in analyzing the tunneling process. This simple line of reasoning fails in our model because the brane-localized curvature suppresses the dependence of the radion kinetic term on N^2, and

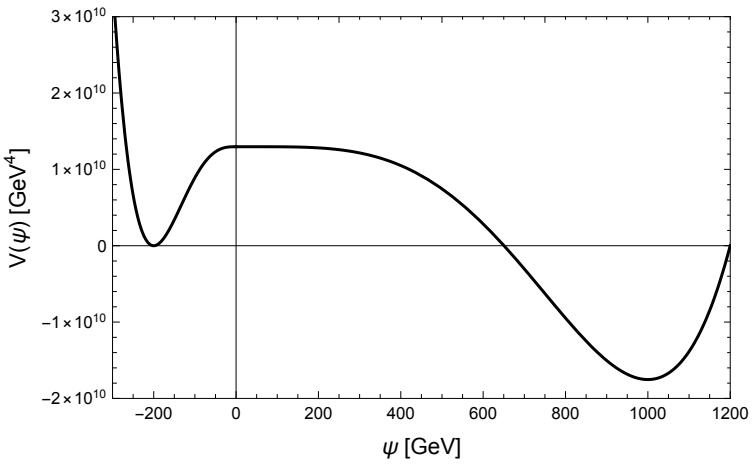

Figure 4.11: A plot of the combined potential, described by Eq. (4.51), for $\Phi_T = 1$, $\epsilon = 0.1$, $(M_\star l) = 0.55$ and $T = 200$ GeV. For this plot we ignore the kinetic terms of the fields.

thus we have to perform a full-fledged analysis of the tunneling problem. Thus the question becomes to what extent we can raise N and still tunnel, while taking the black hole into account in accordance with the prescription of Ref. [54].

We take the T_h field to have a kinetic term with prefactor $(Ml)^3$ [58]. The differing kinetic terms of the two fields change a number of important aspects of the bubble energy calculation which we outline. First, the critical temperature becomes

$$T_c = \left(\frac{-2V_{\rm Rad}(\mu_-)}{\pi^4 \mathcal{Z}^2} \right)^{1/4}, \tag{4.53}$$

where, compared to Eq. (4.37), the dependence on $(M_\star l)^{-3/4}$ is replaced by a $\mathcal{Z}^{-1/2}$ dependence.

Next we have the canonically normalized O(3) equation of motion that takes the form

$$\partial_r^2 \psi + \frac{2}{r} \cdot \partial_r \psi = \begin{cases} \frac{1}{\mathcal{Z}^2} V'_{\rm Rad}(\psi) & \psi \geq 0 \\ \frac{1}{(M_\star l)^3} V'_{\rm BH}(\psi, T) & \psi < 0, \end{cases} \tag{4.54}$$

where $V' \equiv \partial V / \partial \psi$. As per usual, an overshoot-undershoot method is employed until the correct bubble solution linking the two vacua is found. The latter is then used to calculate the corresponding bubble energy. To glean the physics, we separate the tunneling exponent into radion and black hole pieces

$$\frac{S_3}{T} = \frac{S_3^{\rm Rad}}{T} + \frac{S_3^{\rm BH}}{T} \tag{4.55}$$

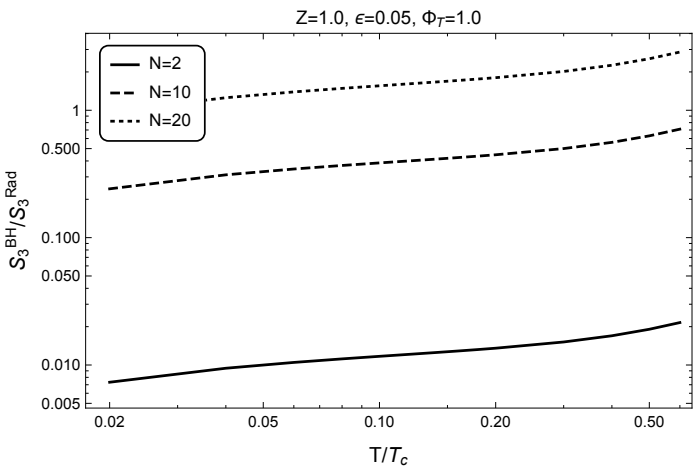

Figure 4.12: A comparison of the black hole and radion contributions to the bubble energy S_3/T, as a function of temperature, for $N = 2, 10, 20$ (corresponding to $(M_\star l) \sim 0.4, 1.4, 2.2$ respectively). Any nucleation requirements are ignored in this plot for demonstrative purposes.

with

$$\frac{S_3^{\rm Rad}}{T} = \frac{4\pi}{T} \cdot \mathcal{Z}^2 \cdot \int_0^{r_{\psi=0}} dr\ r^2 \left[\frac{1}{2}(\partial_r \psi)^2 + \frac{1}{\mathcal{Z}^2} \cdot V(\psi, T)\right] \tag{4.56}$$

$$\frac{S_3^{\rm BH}}{T} = \frac{4\pi}{T} \cdot (M_\star l)^3 \cdot \int_{r_{\psi=0}}^{\infty} dr\ r^2 \left[\frac{1}{2}(\partial_r \psi)^2 + \frac{1}{(M_\star l)^3} \cdot V(\psi, T)\right] \ . \tag{4.57}$$

Studying Eqs. (4.53)-(4.57) the dependence on some important parameters becomes clear, in particular $\mathcal{Z}$ and $(M_\star l)$ (or N). Just as before, decreasing $\mathcal{Z}$ reduces radion energy and enhances tunneling. Nevertheless, decreasing $\mathcal{Z}$ introduces a new feature by *raising* the critical temperature, which, as we discussed, increases the black hole contribution to the exponent. On the other hand $(M_\star l)$ only affects the black hole, in particular through the $(M_\star l)^3$ factor in Eq. (4.57). In Figure 4.12, we show how the black hole contribution can quickly become dominant as N increases from 2 to 20 (corresponding to a change in $(M_\star l)$ of just $\sim 0.4 - 2.2$). It therefore becomes particularly important to include black hole contributions as we investigate large N values.

To answer our basic question, we finally investigate the parameter space available in our model to achieve tunneling fully taking into account the black hole phase. Initial work made it immediately obvious that there is no available parameter space for $\mathcal{Z} \sim 1$. How much then should we suppress $\mathcal{Z}$? Remarkably, Figure 4.13 shows that a reduction by a factor of 10 is enough to yield a reasonable region of parameter space, where tunneling takes place

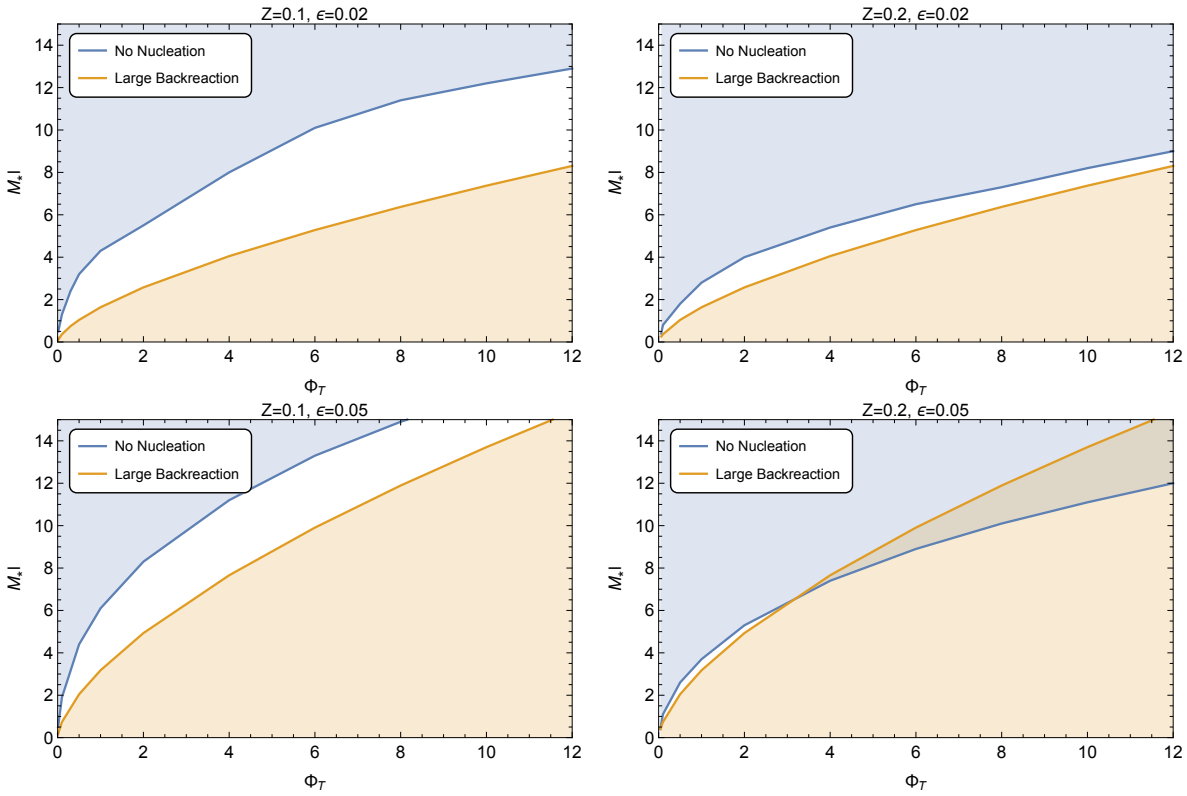

Figure 4.13: The parameter space of $(M_\star l)$ and Φ_T for varying ϵ and $\mathcal{Z}$ values for the combined potential method. The blue-shaded region represents values at which nucleation is never achieved while the orange-shaded region represents values at which back-reaction is no longer negligible. The backreaction limit is found by setting $\Phi_P = (M_\star l)^{3/2}$ in Eq. (4.47) and solving for $(M_\star l)$. Critical temperature lines, as in Figure 4.8, are no longer shown given the lack of $(M_\star l)$ dependence in Eq. (4.53).

at considerably large values of $(M_\star l)$. Whereas previously we found a parameter space that rapidly opened as Φ_T was increased, we now observe a bounded region available only in a range of Φ_T values.

4.5 Phenomenology of brane-localized curvature

In this section, we discuss the phenomenological signatures of localized brane curvature. After the phase transition is completed, the radion classically rolls down its potential until it reaches the minimum at μ_-. Fluctuations around the minimum then comprise spin-0 quanta that interact with matter on the TeV brane. We also study the KK spin-2 spectrum which is

highly dependent on the new parameter $\theta_{\rm IR}$.

4.5.1 Radion phenomenology

The first aspect one inquires about is the mass of the canonically normalized quanta, which is simply given by the second derivative of the potential at the minimum. One finds

$$\left(\frac{m_r}{\mu_-}\right)^2 = \frac{2}{\mathcal{Z}^2}\,\epsilon(4+2\epsilon)\left(2\epsilon\mathcal{F}^2 - 4\mathcal{F} - \epsilon\mathcal{F} + 4\mathcal{F}^2\right)\Phi_T^2$$
$$\approx \frac{16\Phi_T^2}{\mathcal{Z}^2}\epsilon^{3/2} \quad , \tag{4.58}$$

where

$$\mathcal{F} = \left[\frac{(4+\epsilon) + \sqrt{\epsilon(4+\epsilon)}}{2(2+\epsilon)}\right] \quad . \tag{4.59}$$

We can see that $\theta_{\rm IR}$ has a significant effect on the mass of the radion. Without brane curvature we have that $\mathcal{Z}^2 = 6(M_\star l)^3$ and the upper bound on Φ_T^2 is also $(M_\star l)^3$; hence, the radion mass will be at most $\mathcal{O}(\epsilon^{3/4}\mu_-)$. On the other hand, with $\mathcal{Z} \sim \mathcal{O}(1)$ the radion mass is $\mathcal{O}(\epsilon^{3/4}(M_\star l)^{3/2}\mu_-)$, which can easily be of the order μ_- or larger depending on the precise values chosen. In fact, in most of the allowed parameter space, Figure 4.8, we see that the radion is order a few TeV.

Let us now consider the couplings of the radion to a real scalar field ϕ on the IR brane. From Eq. (4.9), we find

$$\mathcal{L}_\phi = \frac{1}{2}\left(\frac{\mu}{k}\right)^2\left(\partial_\mu\phi\,\partial^\mu\phi - \left(\frac{\mu}{k}\right)^2 m_0^2\phi^2\right) \quad . \tag{4.60}$$

Now after the radion picks a VEV, we canonically normalize the scalar field and define the physical mass as follows

$$\phi \to \frac{\mu_-}{k}\hat{\phi}, \quad m = \frac{\mu_-}{k}m_0 \quad . \tag{4.61}$$

We examine fluctuations around the radion VEV as $\hat{\mu} = \langle\hat{\mu}\rangle + \hat{r}$, where $\langle\hat{\mu}\rangle \equiv \mu_-$ and $\hat{r}$ denotes the canonically normalized field with mass given in Eq. (4.58). We find that the interaction between this fluctuation and the brane scalar field is given by

$$\mathcal{L}_{\rm int.} = -\frac{1}{\mathcal{Z}}\frac{\hat{r}}{\mu_-}T_\mu{}^\mu \quad , \tag{4.62}$$

where our convention for the energy-momentum tensor reads

$$T_{\mu\nu} = \partial_\mu\hat{\phi}\,\partial_\nu\hat{\phi} - \frac{1}{2}\eta_{\mu\nu}\left(\partial_\lambda\hat{\phi}\,\partial^\lambda\hat{\phi} - m^2\hat{\phi}^2\right) \quad . \tag{4.63}$$

The above derivation is quite general; the radion couples to the trace of the energy momentum tensor constructed from canonically normalized fields and physical masses. What is important is the effect that the brane localized curvature has on the interaction strength. Here, we see that the effective interaction scale can be defined as $\Lambda_r \equiv \mathcal{Z}\mu_-$, whereas in the absence of brane curvature it is given by $\Lambda_r' = \sqrt{6}(M_\star l)^{3/2}\mu_-$. Thus, despite having large values of $(M_\star l)$, the radion still couples to matter with $\Lambda_r^{-1} \sim 1/\text{TeV}$ if we fix the brane curvature such that $\mathcal{Z} \sim \mathcal{O}(1)$.

With the Standard Model residing on the TeV brane, the radion phenomenology depends only on two parameters; the mass and the effective interaction scale. Much work has already been done, using results from LHC searches, to put experimental constraints on these two parameters [123–125]. Note that our discussion so far is particularly simple in that we do not consider a possible non-minimal coupling of the Higgs to the Ricci scalar, which should in principle be present. To estimate the constraints on Λ_r and m_r we can use the results from Ref. [124]. The principal decay modes of the radion are to W^+W^-, ZZ and hh, with the $ZZ \to 4l$ channel being the most constraining. Ignoring the Higgs-radion mixing, the results in [124] reveal that the bounds on Λ_r range from ~ 10 TeV for $m_r = 200$ GeV to ~ 4 TeV for $m_r = 1$ TeV. Therefore with the radion mass below 1 TeV we would expect $\Lambda_r = \mathcal{Z}\mu_- \gtrsim 4$ TeV. The results of the previous sections do not depend strongly on the exact value of μ_-; therefore, we can easily evade collider bounds by increasing the μ_- scale to $\mathcal{O}(4)$ TeV and still obtain a strong first order phase transition. Note that varying μ_- by an $\mathcal{O}(1)$ amount will have a mild effect on the phase transition parameter space, as can be seen from the nucleation condition in Eq. (4.44). A more elegant option may be to include a curvature-Higgs mixing term, in which certain values of the coupling constant can allow for lower bounds on Λ_r.

The curvature-Higgs mixing can significantly change the phenomenology of the radion; this mixing arises from a coupling of the Higgs to the Ricci scalar of the form

$$\mathcal{L} \supset \int_{-L}^{L} dy \sqrt{g_L}\, \delta(y - L)\xi_{hR}|H|^2 R(g_L) \tag{4.64}$$

where H is the Higgs doublet. For a particular value of the ξ_{hR} coupling known as the conformal point, the radion couplings to the SM fields are significantly suppressed and the bounds on the effective interaction scale are reduced. Again using the results from Ref. [124] (Figure 9) we can estimate that when ξ_{hR} takes the value associated with this conformal point, the experimental bound on Λ_r is of order 1 TeV for radion masses in the range $0.2 - 1$

TeV. A dedicated study of the radion phenomenology with a larger range of radion masses and including both the brane curvature and the curvature-Higgs mixing is required in order to obtain a complete and accurate account of the bounds on the model considered in this paper; however, this is beyond the scope of our present discussion.

4.5.2 Spin-2 phenomenology

In this section we study the spin-2 fluctuations of the metric, which we parametrize as

$$ds^2 = e^{-2ky}\left(\eta_{\mu\nu} + \tfrac{1}{M_\star^{3/2}} h_{\mu\nu}\right) dx^\mu dx^\nu - dy^2, \quad h_{\mu\nu} \equiv h_{\mu\nu}(x^\mu, y) \quad . \tag{4.65}$$

Expanding this spin-2 field in a KK decomposition, $h_{\mu\nu} = \frac{1}{\sqrt{L}} \sum_{n=0}^{\infty} f_n^g(y) h_{\mu\nu}^{(n)}(x)$, we find that in the bulk the 5D profile must obey [126]

$$\partial_y^2 f_n^g - 4k\partial_y f_n^g + m_n^2 e^{2ky} f_n^g = 0 \quad . \tag{4.66}$$

The above eigenvalue equation is obtained after a partial integration in the y-variable, which also generates brane localized terms $\sim f_n^g \partial_y f_n^g$. The boundary conditions are then determined by requiring that these terms are zero. However, the effects of the IR brane curvature must be accounted for here. Assuming that the KK gravitons are produced on-shell we can replace the second derivative of the fields, generated by the brane curvature, with their KK masses. The procedure we follow is outlined in Ref. [111]. The condition that a massless graviton exists is simply $\partial_y f_n^g = 0$ on each of the branes, while for the massive modes we have

$$\begin{aligned} \partial_y f_n^g \Big|_0 &= 0 \quad , \\ \left(e^{-2kL}\partial_y f_n^g - \tfrac{\theta_{\rm IR}}{2}\tfrac{m_n^2}{k} f_n^g\right)\Big|_L &= 0 \quad . \end{aligned} \tag{4.67}$$

The solution to Eq. (4.66) is

$$f_n^g = \frac{e^{2ky}}{N_n}\left(J_2\left(\tfrac{m_n}{k}e^{ky}\right) + \alpha_n Y_2\left(\tfrac{m_n}{k}e^{ky}\right)\right) \tag{4.68}$$

where α_n and the mass spectrum m_n are determined by the boundary conditions, Eq. (4.67), and the normalization constant N_n is determined by the orthonormality condition

$$\frac{M_\star^3}{2k}\int_{-L}^{L} dy\; e^{-2ky} f_n^g f_m^g \left(k + \theta_{\rm IR}\delta(y-L)\right) = \delta_{mn} \quad . \tag{4.69}$$

It is useful here to consider $\theta_{\rm IR}$ in terms of $\mathcal{Z}^2$, Eq. (4.17), and inspect the KK masses as a function of $(M_\star l)$ and $\mathcal{Z}$. Applying the UV boundary condition fixes

$$\alpha_n = -\frac{J_1\left(\frac{m_n}{k}\right)}{Y_1\left(\frac{m_n}{k}\right)} \quad , \tag{4.70}$$

while the IR boundary condition requires

$$J_1\left(\tfrac{m_n}{k}e^{kL}\right) - \tfrac{\theta_{\rm IR}}{2}\tfrac{m_n}{k}e^{kL}J_2\left(\tfrac{m_n}{k}e^{kL}\right) = \\ -\alpha_n\left(Y_1\left(\tfrac{m_n}{k}e^{kL}\right) - \tfrac{\theta_{\rm IR}}{2}\tfrac{m_n}{k}e^{kL}Y_2\left(\tfrac{m_n}{k}e^{kL}\right)\right) \quad . \tag{4.71}$$

Since we expect $m_n \ll k$ for the lowest-lying states and $Y_a(x)$ diverges at $x \to 0$, we can approximately take $\alpha_n = 0$ in the IR boundary condition. Therefore, the masses of the spin-2 KK modes are approximated by

$$m_n = \text{zeros}\left[J_1\left(\tfrac{m_n}{k}e^{kL}\right) - \tfrac{\theta_{\rm IR}}{2}\tfrac{m_n}{k}e^{kL}J_2\left(\tfrac{m_n}{k}e^{kL}\right)\right]. \tag{4.72}$$

In fact when $\theta_{\rm IR} = 1$, the spin-2 mass spectrum is exactly the same as that for spin-1 KK modes of a gauge field in the bulk of the RS model, i.e. $m_1/\mu_- = 2.40,\ 5.52,\ 8.65,\ 11.79$. In Figure 4.14 we show how the lightest KK graviton mass changes as we increase $(M_\star l)$ while using the brane curvature to keep $\mathcal{Z}$ at some fixed value. The values of $\mathcal{Z}$ used here extend beyond those used in our analysis in Section 4.4; however, the figure clearly shows that in the relevant parameter space the lightest KK graviton mass is significantly reduced. We clearly see that for larger values of $(M_\star l)$ the lightest KK graviton mass approaches that of the lightest KK spin-1 mass. This is strikingly different than in RS models without IR brane curvature, in which the lightest massive spin-2 mode is expected to be ~ 3.8 TeV.

The kinetic term of the KK gravitons receives a contribution proportional to $\theta_{\rm IR}$ thus changing their coupling to brane matter. In general, the effective KK graviton coupling is of the form

$$S_G^{(n)} = \frac{c_{GX}^{(n)}}{M_{Pl}}\int d^4x\, h_{(n)}^{\mu\nu}T_{\mu\nu}^X = \frac{1}{(M_\star l)^{3/2}}\frac{c_{GX}^{(n)}}{k}\int d^4x\, h_{(n)}^{\mu\nu}T_{\mu\nu}^X \tag{4.73}$$

where $T_{\mu\nu}^X$ is the stress-energy tensor of some field, and the coefficient $c_{GX}^{(n)}$ depends on the 5D properties of that field. The simplest case is matter on the TeV brane,

$$\frac{c_{GX}^{(n)}}{M_{Pl}} = \frac{f_n^g(L)}{M_{Pl}\sqrt{kL}} \simeq \frac{e^{kL}}{M_{Pl}\sqrt{1+\theta_{\rm IR}}} = \frac{1}{(M_\star l)^{3/2}\sqrt{1+\theta_{\rm IR}}}\left(\frac{1}{\mu_-}\right) \quad . \tag{4.74}$$

As expected, the coupling is proportional to 1/TeV. Opposite to the radion, notice that $\theta_{\rm IR}$ enters with a plus sign in the pre-factor of the graviton kinetic term. The effective interaction scale here can be written as $\Lambda_g = (M_\star l)^{3/2}\sqrt{1+\theta_{\rm IR}}\,\mu_-$. With the SM confined to the TeV brane the phenomenology of the KK gravitons is fixed by just their masses and matter couplings. Some work has been done recently to put bounds on m_1 and Λ_g using the

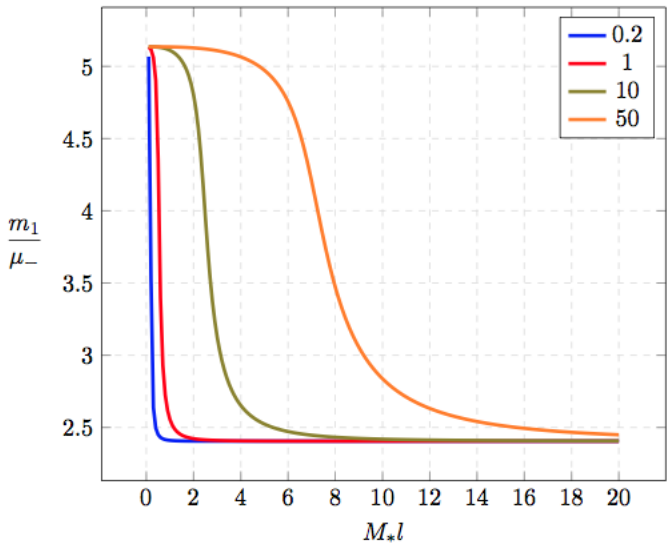

Figure 4.14: Here we show how the lightest KK graviton mass varies as we change $(M_\star l)$, while constantly modifying the brane curvature term to keep $\mathcal{Z}$ at some fixed value. We consider values of $\mathcal{Z} = 0.2, 1, 10, 50$.

recent results from LHC searches [127–129]. When both are near the TeV scale it is possible that the LHC would detect these states.

Throughout the favorable region in our parameter space, Λ_g is required to be $\mathcal{O}(10-100)$ TeV, and thus the KK gravitons are too weakly coupled to be detected in current experiments. From the definition of the radion interaction scale we see that,

$$\frac{\Lambda_r}{\Lambda_g} = \frac{\mathcal{Z}}{(M_\star l)^{3/2}\sqrt{1+\theta_{\rm IR}}} \quad . \tag{4.75}$$

The results of Section 4.4 tell us that we require $\mathcal{Z} \sim \mathcal{O}(1)$ and $\theta_{\rm IR} \simeq 1$ to obtain a strong first order phase transition to the RS background with large-N, where $N^2 = 4\pi^2(M_\star l)^3 + 1$. Therefore, at large-$N$, our model not only predicts that the radion has an $\mathcal{O}(\mu_-)$ mass and that the KK graviton mass spectrum is shifted down but also that the interaction strength of the KK gravitons is highly suppressed with respect to that of the radion.

4.6 Discussion

We considered modifying the RSI theory by adding a TeV brane-localized curvature, which leaves the background solution intact, and studied the impact on the dynamics of the holographic phase transition. The holographic interpretation is very simple: the gauge theory is

de-confined at high temperature and is dual on the gravity side to the planar AdS black hole. The low temperature phase is dual to the RSI solution with two branes stabilized properly to offer a solution to the hierarchy problem. The generic features of the transition were first considered in Ref. [54], and the physics is similar to the holographic interpretation of the Hawking-Page phase transition [103, 113].

The analysis of the phase transition is rather simplified by considering the motion of the radion in its potential that is induced by the Goldberger-Wise mechanism. Here, the contribution of the black hole phase to the tunneling rate is estimated using only the boundary condition in Eq. (4.40), which takes into account the free energy of the black hole. It would indeed be quite valuable to try to find the full gravitational and bulk scalar instanton, or at least have a better estimate of the effect of the high temperature phase on the tunneling rate.

The brane-localized curvature contributes to the kinetic energy of the radion in a fashion that makes it possible to desensitize the dependence of the tunneling rate on the fundamental combination $(M_\star l)$. Now that $(M_\star l)$ (or N) can be made large, the tunneling rate is further enhanced by propping up Φ_T, the Goldberger-Wise TeV-VEV, consistent with back-reaction constraints. Contrary to previous studies, over a wide range of parameters we find $T_n/T_c \sim \mathcal{O}(0.1-1)$.

We end by commenting on the possibility of tunneling through O(4)-symmetric bubbles. Although we did not perform a detailed study, it is likely that O(4) bubbles dominate over the O(3) ones. The physics is gleaned by inspecting the O(4) bounce action

$$S_4 = E_4 + \frac{\pi^6}{4}(M_\star l)^3 (r_c T)^4 \quad . \tag{4.76}$$

In fact, from our presented work on the O(3) case we know that the temperature roughly scales as $(M_\star l)^{-3/4}$. This implies that the second term in Eq. (4.76) is uniform with respect to $(M_\star l)$. For fixed values of $(M_\star l)$ and Φ_T, we then expect $S_4 < S_3/T$. This indeed does not invalidate any of our conclusions regarding the completion of the phase transition as the tunneling would be quicker with O(4). An in-depth study of this possibility is left to future work.

Chapter 5

An Unsatisfactory Solution

Chapter 4 and the published work [68] therein presents one solution to addressing the issues of the holographic phase transition related to a restricted parameter space, in particular a small N and negative ϵ. However, as discussed in Chatper 3, further problems remain. Most critical is the ambiguity in the kinetic term of the field describing the location of the black hole horizon, T_H, in the high temperature phase. In absence of this, a complete study of the phase transition can never be performed. Motivated by this shortcoming, work was performed to find a better description than those previously considered.

5.1 Deriving an Approximate Black Hole Kinetic Term

The premise is as follows: if T_H is indeed a field, as it has been treated, then it should be a function of the 4D spatial (brane) coordinates x, y, z (or ρ in spherical coordinates) and appear as such in the metric. Substituting this metric into the Einstein-Hilbert action should produce a kinetic-like term proportional to $(\partial T_H(\rho))^2$. From the relation in Eq. (3.42)

$$T_H \equiv \frac{r_0}{\pi l^2} \ , \tag{5.1}$$

the BH field T_H is present in the metric through r_0. The promotion $r_0 \to r_0(\rho)$ therefore represents $T_H \to T_H(\rho)$ and the AdS-S metric, Eq. (3.41), in spherical coordinates now reads

$$\begin{aligned} ds^2_{\text{AdS-S}} = \frac{r^2}{l^2}\left(1 - \frac{r_0^4(\rho)}{r^4}\right) dt^2 - \frac{l^2}{r^2}\left(1 - \frac{r_0^4(\rho)}{r^4}\right)^{-1} dr^2 \\ - \frac{r^2}{l^2}\left(d\rho^2 + \rho^2 d\theta^2 + \rho^2 \sin^2\theta \, d\phi^2\right) \ . \end{aligned} \tag{5.2}$$

Substituting into the Einstein-Hilbert action

$$S = 2M_*^3 \int dx^5 \sqrt{-g}\,(R + 12k^2)\ , \tag{5.3}$$

where the Ricci scalars of the AdS-S and AdS spacetimes are

$$R_{\text{AdS-S}} = -\frac{20}{L^2} - \frac{8l^2\, r_0(\rho)^6}{r^2(r^4 - r_0(\rho)^4)^2}\,(\partial r_0(\rho))^2\ , \tag{5.4}$$

$$R_{\text{AdS}} = -\frac{20}{L^2}\ , \tag{5.5}$$

gives the action of the corresponding AdS-S space

$$S_{\text{AdS-S}} = 64\pi M_*^3 \int d\rho \int_{r_0}^{\Lambda} dr\,\beta\,\left[-\frac{\rho^2 r^3}{l^5} - \frac{\rho^2\, r\, r_0(\rho)^6}{l(r^4 - r_0(\rho)^4)^2}\,(\partial r_0(\rho))^2\right]\ , \tag{5.6}$$

where, as in Section 3.3, Λ is a cutoff. At this point it seems promising - there is a term proportional to $(\partial r_0)^2$ that can be interpreted as the kinetic term. However, the integral over r is yet to be performed and here the prescription breaks down. Studying the coefficient of the supposed kinetic term, it is clear that upon integration the denominator becomes zero and the result is divergent.

5.2 Black Holes as Nucleation Sites

If a kinetic term cannot be derived then an alternative approach is needed. Recently there have been numerous studies [64, 66, 67] into the possibility of black holes, in particular primordial black holes (PBHs), acting as nucleation sites for bubbles during first-order phase transitions of scalar fields, like those described in Chapter 2. While the literature has so far focused on 4D zero temperature transitions, one could attempt to modify the formalism to the 5D finite temperature setting of the HPT. In doing so there are a number of issues to consider. Firstly, the HPT describes a transition from an AdS-S spacetime to RS in which there is more than a single relevant field - the black hole field T_H and the radion field μ. Secondly, in the HPT 4D bubbles nucleate and expand on the surface of the 5D BH horizon, but the nucleation site formalism describes 4D bubbles nucleating around a 4D black hole and expanding into the rest of the 4D space; these are two very different processes.

It was swiftly acknowledged these complications would prevent any reasonable progress. Nevertheless, the concept of BHs acting as seeds had left an impression. Away from any HPT considerations, could the formalism be extended to finite temperature and applied to typical

first-order cosmological phase transitions? Zero temperature studies had found significant improvements in transition rates. If the same were true in the finite temperature setting there could be remarkable consequences for not only the nature of the phase transitions, but their phenomenological predictions such as gravitational wave backgrounds.

Chapters 6 and 7 discuss work investigating and applying the concept of black holes acting as nucleation sites to finite temperature first-order phase transitions.

Chapter 6

Black Holes as Nucleation Sites

Coleman [29] and Linde [32] developed the formalism describing false vacuum decay in flat-space at zero and finite temperatures respectively. Given the vast range in scales over which phase transitions could have occurred, it is only natural to ask what effect could gravity have? This chapter introduces the second of two main topics in this thesis - black holes as bubble nucleation sites during cosmological phase transitions. After initial investigation by Hiscock [62], the topic has recently regained interest from the perspective of the decay of the current Higgs vacuum [64, 66, 67] - a zero temperature process. With the possibility of vast improvements in nucleation rates, the question is can similar improvements be found for finite temperature cosmological phase transitions? Results of such an investigation is work submitted for publication [69] presented in Chapter 7. This chapter begins simply with the effect of gravity in the absence of black holes, before quantifying the role of black holes in the thin-wall limit during zero temperature phase transitions.

6.1 Including Gravity: Coleman-de Luccia

Pioneering work from Coleman and de Luccia [61] quantified the effect of gravity on the decay of the false vacuum, subject to limitations. In general, their formalism describes tunnelling from a space of generic energy density $V(\phi_f) = \epsilon_+$ to a space of generic energy density $V(\phi_t) = \epsilon_- < \epsilon_+$, where ϕ_f and ϕ_t represent the false and true vacuum respectively. In practice, however, they focus on two special cases

1. Decay from a space of positive energy density to a space of zero energy density, $V(\phi_f) = \epsilon \to V(\phi_t) = 0$.

2. Decay from a space of zero energy density to a space of negative energy density, $V(\phi_f) = 0 \to V(\phi_t) = -\epsilon$.

Assuming that the bounce solutions remain O(4)-invariant in the presence of gravity, the most general rotationally invariant Euclidean metric is constructed

$$ds^2 = d\xi^2 + \rho(\xi)^2 d\Omega^2 \ . \tag{6.1}$$

With such a simple metric the Euclidean equations of motion are found to be

$$\phi'' + \frac{3\rho'}{\rho}\phi' = \frac{dV}{d\phi} \ , \tag{6.2}$$

where prime denotes $d/d\xi$. In the thin-wall limit this equation of motion resembles the flat-space variant, Eq. (2.13), with the subtle differences that the independent variable is now ξ, rather than r, and the thin-wall condition has changed. Following some simplification, the Euclidean action takes the form

$$S_E = 4\pi^2 \int d\xi \left(\rho^3 V - \frac{2\rho}{\kappa}\right) \ , \tag{6.3}$$

where $\kappa = 8\pi G = 1/M_P^2$. Utilising the thin-wall approximation, the bounce action B can be written in an analytic form

$$\begin{aligned} B_{\rm CdL} =& \frac{12\pi^2}{\kappa^2}\left\{\frac{1}{\epsilon_-}\left[\left(1 - \frac{1}{3}\kappa\epsilon_- r_{\rm CdL}^2\right)^{3/2} - 1\right] - \frac{1}{\epsilon_+}\left[\left(1 - \frac{1}{3}\kappa\epsilon_+ r_{\rm CdL}^2\right)^{3/2} - 1\right]\right\} \\ &+ 2\pi^2\sigma r_{\rm CdL}^3 \ , \end{aligned} \tag{6.4}$$

where $\epsilon_{+(-)}$ is the vacuum energy density outside (inside) the bubble and σ is the surface tension of the nucleated bubble. The bubble radius $r_{\rm CdL}$ is found by demanding that B be stationary, $dB_{\rm CdL}/dr_{\rm CdL} = 0$, giving the expression

$$r_{\rm CdL} = \frac{12\sigma}{\left(16(\epsilon_- - \epsilon_+)^2 + 24\kappa(\epsilon_- + \epsilon_+)\sigma^2 + 9\kappa^2\sigma^4\right)^{1/2}} \ . \tag{6.5}$$

These expressions are rather cumbersome and CdL therefore proceed to make their point using the two special cases outlined above.

In the first case of decay from a positive cosmological constant (de Sitter) to zero the critical bubble radius is now

$$r_{\rm CdL} = \frac{r_0}{1 + \frac{\epsilon r_0^2}{12 M_P^2}} \ , \tag{6.6}$$

while the bounce action takes the form

$$B_{\mathrm{CdL}} = \frac{B_0}{\left(1 + \frac{\epsilon r_0^2}{12 M_P^2}\right)^2} \ , \tag{6.7}$$

where r_0 and B_0 are the critical bubble radius, Eq. (2.17), and bounce action, Eq. (2.18), in the absence of gravitation respectively. Due to the addition in the denominators, the introduction of gravity reduces both the bubble radius and bounce action. A greater decrease in vacuum energy (larger $|\epsilon|$) results in a greater reduction in radius and bounce action. Gravity enhances the tunnelling rate for vacuum decay of de Sitter spaces.

The second case concerns decay from a zero to negative cosmological constant (Anti-de Sitter); the critical bubble radius becomes

$$r_{\mathrm{CdL}} = \frac{r_0}{1 - \frac{\epsilon r_0^2}{12 M_P^2}} \ , \tag{6.8}$$

while the bounce action takes the form

$$B_{\mathrm{CdL}} = \frac{B_0}{\left(1 - \frac{\epsilon r_0^2}{12 M_P^2}\right)^2} \ . \tag{6.9}$$

Quite simply, the denominator has changed from an addition to subtraction, yet the consequences are considerable; the inclusion of gravity now decreases the tunnelling rate, with greater decreases in vacuum energy (larger $|\epsilon|$) increasing bubble radius and bounce action. Gravity diminishes the tunnelling rate for vacuum decay of flat-spaces.

It seems, therefore, that gravity should be included whenever discussing nucleation rates in phase transitions. However, in almost all practical applications ϵ will be minimal in comparison to the Planck mass factor, M_P^2, suppressing all the gravitational terms. Any effect gravity could have is likely negligible.

While the CdL description provides valuable insight into the role gravity plays during false vacuum decay, its limitations should be kept in mind. Firstly, the assumption that the bounce solution remains O(4)-invariant is crucial to the whole formalism, allowing use of the most general rotationally invariant Euclidean metric. And while this is a reasonable assumption, the authors admit there is no theorem to back this up as in the case of scalar field theory without gravity. Second is the thin-wall limit, where simply the boundaries it sets should be remembered and considered throughout application. Finally, it should be stressed this is a formalism describing the quantum decay of a metastable state at zero-temperature, as outlined

in Section 2.1.1. Main interests here, however, concern cosmological phase transitions at finite temperature where the likely dominant processes are not described by the CdL approach. One may consider adapting the CdL formalism for this finite temperature application but one problem immediately appears. As just discussed, the formalism relies on an O(4)-invariant bounce, yet the typical thermal processes are O(3)-invariant (see Section 2.1.2); a different formalism would have to be developed.

6.2 Black Holes Nucleating Zero Temperature Phase Transitions

6.2.1 An Initial Investigation

For those with an interest in the effects of gravitation on false vacuum decay, it is a logical step to consider what role black holes could play. Hiscock [62] established the idea that a black hole could act as a nucleation site, similar to the role of an inhomogeneity in everyday phase transitions; bubbles form in a spherically symmetric fashion around the black hole and subsequently expand. Working at zero temperature with the thin-wall approximation, Hiscock studied bubble nucleation rates in the presence of a Schwarzschild black hole with an arbitrary cosmological constant (positive, zero or negative giving Schwarzschild-de Sitter, Schwarzschild and Schwarzschild-anti-de Sitter spacetimes respectively).

Similar to Chapter 2, the decay rate is given by

$$\Gamma = A\, e^{-B} \ , \tag{6.10}$$

but now without a volume factor $\mathcal{V}$; this is a decay rate and not a decay rate per unit volume. Hiscock, as is rather typical, focuses on determining the, likely dominant, exponent B. In the thin-wall approximation the bubble wall can be assumed to be infinitely thin and Israel's [63] formalism describing surface layers in general relativity can be used to derive the equations of motion describing the bubble. Demanding the black hole mass remain constant, the false (+) and true (−) vacua are described by the (Euclidean) metrics

$$ds_+^2 = f(r_+)d\tau_+^2 + f(r_+)^{-1}dr_+^2 + r_+^2 d\Omega_2^2 \ , \tag{6.11}$$

$$ds_-^2 = f(r_-)d\tau_-^2 + f(r_-)^{-1}dr_-^2 + r_-^2 d\Omega_2^2 \ , \tag{6.12}$$

with

$$f_{\pm}(r) = 1 - \frac{2GM}{r} - \frac{\Lambda_{\pm} r^2}{3} \ , \tag{6.13}$$

where M is the mass of the black hole and $\Lambda_{\pm}$ are the cosmological constants of the false and true vacua. The cosmological constants can be written in the form of energy densities with the relation $\Lambda_{\pm} = \epsilon_{\pm}/M_P^2$. Israel's formalism has two conditions: first, the induced metrics on both sides of the wall must match; second, the surface tension of the bubble wall is proportional to the difference in extrinsic curvatures. The induced metric on the wall has the form

$$ds^2_{\text{wall}} = d\lambda^2 + R^2(\lambda) d\Omega_2^2 \ , \tag{6.14}$$

where λ is the proper time on the wall, $R(\lambda)$ is the position of the wall and $d\Omega_2^2$ is the standard metric of a unit two-sphere. Explicit details can be found in Section 7.3 but, following Israel's conditions, the general result is the equation of motion

$$\begin{aligned} \dot{R}^2(\lambda) &= \frac{f_+ + f_-}{2} - \frac{(f_+ - f_-)^2}{64\pi^2 G^2 \sigma^2 R^2} - 4\pi^2 G^2 \sigma^2 R^2 \\ &\equiv U(R) \ , \end{aligned} \tag{6.15}$$

where $\dot{R} = dR/d\lambda$. With the Hiscock metric function of Eq. (6.13), the equation of motion for the bubble wall reads

$$\dot{R}^2 = 1 - \zeta^2 R^2 - \frac{2GM}{R} \ , \tag{6.16}$$

with

$$\zeta^2 \equiv \frac{\Lambda_+ - \Lambda_-}{6} + \frac{(\Lambda_+ - \Lambda_-)^2}{576\pi^2 G^2 \sigma^2} + 4\pi^2 G^2 \sigma^2 \ . \tag{6.17}$$

The "potential" $U(R)$ describing the bubble wall motion can be seen in Figure 6.1 for some example parameters. Valid solutions only exist if $\dot{R}^2 \geq 0 \Rightarrow U(R) \geq 0$. Increasing the black hole mass lowers $U(R)$ hence, there is an upper limit on M. Explicitly, the upper limit is given by $M^{\max} = (3^{3/2} G\zeta)^{-1}$. Here, there is a single valid solution, the root of the equation, at the radius R_s known as the static solution. For masses below $M^{\max}$ the equation of motion possess two zeros, $R_{\min}$ and $R_{\max}$, between which the solution oscillates with a period β_λ. These are known as oscillating solutions, examples of which can be seen in Figure 6.2. Taking $M \to 0$ recovers the CdL result with a single root $R_{\text{CdL}} = \zeta^{-1}$. Clearly, from Figure 6.1, the introduction of black holes has reduced the size of bubbles nucleated.

To understand changes in tunnelling rate provided by black holes, the Euclidean action must be calculated and compared to the CdL result. Immediately, however, there is an issue.

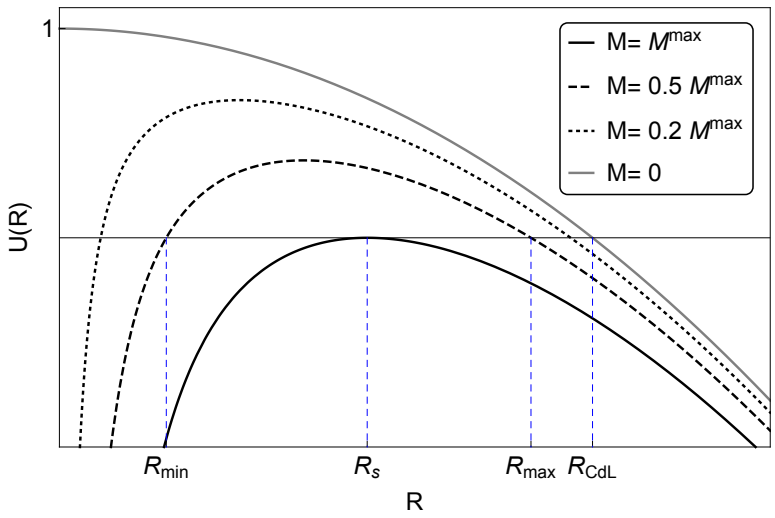

Figure 6.1: An example potential $U(R)$ of Eq. (6.15) describing the trajectory of bubbles nucleated in the Hiscock [62] formalism for varying black hole mass M. The mass has an upper limit $M^{\max}$, above which $U(R) < 0$ and there are no viable solutions.

The Euclidean times $\tau_\pm$ have respective periods $\beta_{\tau_\pm}$. If these periods are not identified with that of the event horizons then conical singularities arise at the horizons, as discussed in Section 3.3.1. In de-Sitter space there are two horizons, black hole and cosmological, and at least one conical singularity is therefore unavoidable. Hiscock, in the absence of an appropriate method to deal with them, chooses to neglect any conical singularity effects; however, later studies reveal they are important [64, 66].

Calculating the Euclidean action is split into two contributions: bulk and surface (wall). Beginning with the bulk contributions, these come from the false and true vacua. The Einstein-Hilbert action takes the forms

$$\begin{aligned} I_+^{\mathrm{B}} &= -\frac{1}{16\pi G}\int d^4x\,\sqrt{g}\,(\mathcal{R}_+ - 2\Lambda_+) \\ &= -\frac{1}{4G}\frac{2\Lambda_+}{3}\int d\tau_+\,(r_{c,+}^3 - R^3) \\ &= -\frac{1}{2G}\frac{2\Lambda_+}{3}\int dR\left(\frac{d\lambda}{dR}\right)\left(\frac{d\tau_+}{d\lambda}\right)(r_{c,+}^3 - R^3)\ , \end{aligned} \tag{6.18}$$

$$\begin{aligned} I_-^{\mathrm{B}} &= -\frac{1}{16\pi G}\int d^4x\,\sqrt{g}\,(\mathcal{R}_- - 2\Lambda_-) \\ &= -\frac{1}{4G}\frac{2\Lambda_-}{3}\int d\tau_-\,(R^3 - r_{h,-}^3) \\ &= -\frac{1}{2G}\frac{2\Lambda_-}{3}\int dR\left(\frac{d\lambda}{dR}\right)\left(\frac{d\tau_-}{d\lambda}\right)(R^3 - r_{h,-}^3)\ , \end{aligned} \tag{6.19}$$

where $r_{h,c}$ are the black hole and cosmological horizons respectively, $\mathcal{R}_\pm = 4\Lambda_\pm$ are the Ricci

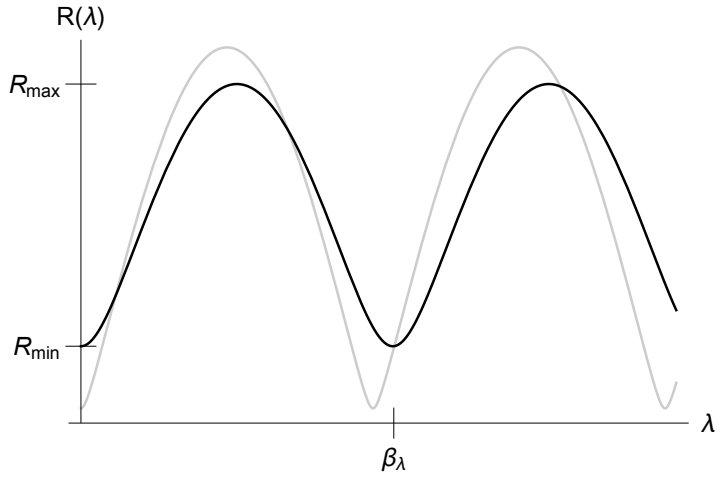

Figure 6.2: Example oscillating solutions for $M = 0.5\,M^{\max}$ (black) and $M = 0.2\,M^{\max}$ (grey). The labels correspond to the black line. The solution oscillates between $R_{\min}$ and $R_{\max}$ with a period β_λ.

scalars in each vacuum and $\sqrt{g} = r^2 \sin\theta$. It is also important to notice that one period in λ is a complete oscillation of the bubble solution, meaning $R_{\min} \to R_{\max} \to R_{\min}$. Hence, a factor of 2 appears when changing variable $\lambda \to R$, as can be seen in the final lines of Eqs. (6.18) and (6.19). The surface contribution meanwhile takes the form

$$\begin{aligned} I^{\rm S} &= \frac{1}{8\pi G}\int d^3x\,\sqrt{h}\,(K_+ - K_-) + \sigma\int d^3x\,\sqrt{h} \\ &= \frac{1}{G}\int dR\,R\left(\frac{d\lambda}{dR}\right)\left(f_+\left(\frac{d\tau_+}{d\lambda}\right) - f_-\left(\frac{d\tau_-}{d\lambda}\right)\right)\,, \end{aligned} \tag{6.20}$$

where the first term in the first line arises from the Hawking-Gibbons-York boundary term [107, 130] and the second term is the surface energy in the scalar field profile. With further details again found in Section 7.3, the relations

$$\frac{d\tau_\pm}{d\lambda} = \frac{1}{f_\pm}\left(f_\pm - U(R)\right)^{1/2}\,, \tag{6.21}$$

$$\frac{dR}{d\lambda} = \sqrt{U(R)}\,, \tag{6.22}$$

can be used to find the final forms

$$I_+^{\rm B} = -\frac{1}{G}\frac{\Lambda_+}{3}\int dR\,\frac{1}{f_+}\left(\frac{f_+}{U(R)} - 1\right)^{1/2}\left(r_{c,+}^3 - R^3\right)\,, \tag{6.23}$$

$$I_-^{\rm B} = -\frac{1}{G}\frac{\Lambda_-}{3}\int dR\,\frac{1}{f_-}\left(\frac{f_-}{U(R)} - 1\right)^{1/2}\left(R^3 - r_{h,-}^3\right)\,, \tag{6.24}$$

$$I^{\rm S} = \frac{1}{G}\int dR\,R\left[\left(\frac{f_+}{U(R)} - 1\right)^{1/2} - \left(\frac{f_-}{U(R)} - 1\right)^{1/2}\right]\,. \tag{6.25}$$

Finally, the false vacuum background must be subtracted

$$\begin{aligned} I^{\mathrm{B}}_{\mathrm{SdS}} &= -\frac{1}{4G}\frac{2\Lambda_+}{3}\int d\tau_+ \, \left(r^3_{c,+} - r^3_{h,+}\right) \\ &= -\frac{1}{G}\frac{\Lambda_+}{3}\int dR \, \frac{1}{f_+}\left(\frac{f_+}{U(R)} - 1\right)^{1/2}\left(r^3_{c,+} - r^3_{h,+}\right) \ . \end{aligned} \tag{6.26}$$

The tunnelling exponent is therefore

$$\begin{aligned} B &= I^{\mathrm{B}}_+ + I^{\mathrm{B}}_- - I^{\mathrm{B}}_{\mathrm{SdS}} + I^{\mathrm{S}} \\ &= \frac{1}{G}\int_{R_{\min}}^{R_{\max}} dR \left\{ \left(\frac{f_+}{U(R)} - 1\right)^{1/2}\left[R + \frac{\Lambda_+}{3}\frac{1}{f_+}(R^3 - r^3_{h,+})\right] \right. \\ &\qquad \left. - \left(\frac{f_-}{U(R)} - 1\right)^{1/2}\left[R + \frac{\Lambda_-}{3}\frac{1}{f_-}(R^3 - r^3_{h,-})\right]\right\} . \end{aligned} \tag{6.27}$$

While the expression in Eq. (6.27) nicely describes the bounce action for oscillating solutions, there is ambiguity in how to deal with the static solutions where the two roots $R_{\min}$ and $R_{\max}$ coalesce. Rather that integrating over R one should return to integrating over λ. In the static limit all radii become independent of λ, $R \to R_s$, and all integrals become trivial integrals over $d\lambda$. Hence, all one needs to know is the period β_λ. However, in the absence of any oscillating solution it is not clear what this should be. Hiscock attempts to approximate β_λ by expanding the potential $U(R)$ around the static solution R_s and performing the integral

$$\int d\lambda = \int dR \, \frac{1}{\sqrt{U(R)}} \ , \tag{6.28}$$

allowing him to find values for static solutions.

The results are, for example, values such as those seen in Figure 6.3. The closer the black hole mass is to the upper limit, $M^{\max}$, the greater the reduction in tunnelling exponent, with the greatest improvement at $M^{\max}$, the static solution. Hiscock made the comparison to the special cases discussed by CdL. In particular, when decaying from Schwarzschild-de Sitter to Schwarzschild ($\Lambda_+ > 0 \to \Lambda_- = 0$) the ratio B/B_{CdL} could become as low as ~ 0.56, a rather remarkable improvement in tunnelling rate.

The study of Hiscock [62] demonstrates black holes could have important consequences for false vacuum decay when acting as nucleation sites. However, his study is restricted in two important areas: the black hole mass remains constant throughout the transition and conical singularities are not accounted for.

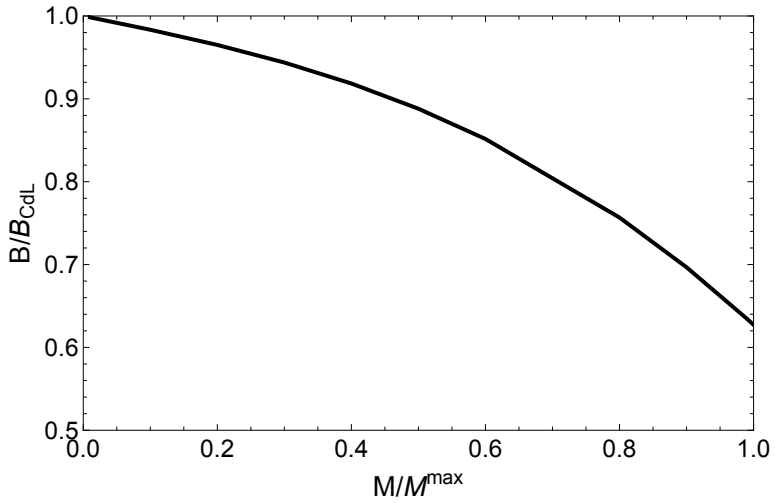

Figure 6.3: The reduction in tunnelling exponent B, compared to the absence of black holes (CdL), when introducing black holes as nucleation sites in the Hiscock [62] formalism for the example parameters $\sigma = 10^4\,\mathrm{GeV}^3$, $\epsilon_+ = 10^5\,\mathrm{GeV}^4$ and $\epsilon_- = 0$.

6.2.2 Quantifying the Conical Singularities

Following the work of Hiscock [62], there seemed to be very little interest in the possibility of black hole seeds for many years. Recently, however, Ref. [64] has revived the topic, applying the formalism to study the role of primordial black holes (PBHs) in the fate of the current Higgs vacuum [66]. Following Hiscock, Ref. [64] presents a thin-wall formalism but solves the issues of varying black hole mass and conical singularities discussed above. Importantly, it is found that the effect is larger than previously found thanks to contributions from the conical singularities.

The equation of motion is again Eq. (6.15)

$$\begin{aligned}\dot{R}^2(\lambda) &= \frac{f_+ + f_-}{2} - \frac{(f_+ - f_-)^2}{64\pi^2 G^2\sigma^2 R^2} - 4\pi^2 G^2\sigma^2 R^2 \\ &\equiv U(R)\ ,\end{aligned} \tag{6.29}$$

but now the false (+) and true (−) vacuum metric functions are

$$f_\pm(r) = 1 - \frac{2GM_\pm}{r} - \frac{\Lambda_\pm r^2}{3}\ . \tag{6.30}$$

Crucially, the seed (+) and remnant (−) black hole masses differ. The dependence of $U(R)$ on M_+ remains from Figure 6.1. Additionally, there is now a dependence on M_- which is shown in Figure 6.4. In principle, the remnant mass M_- can be larger than the seed mass

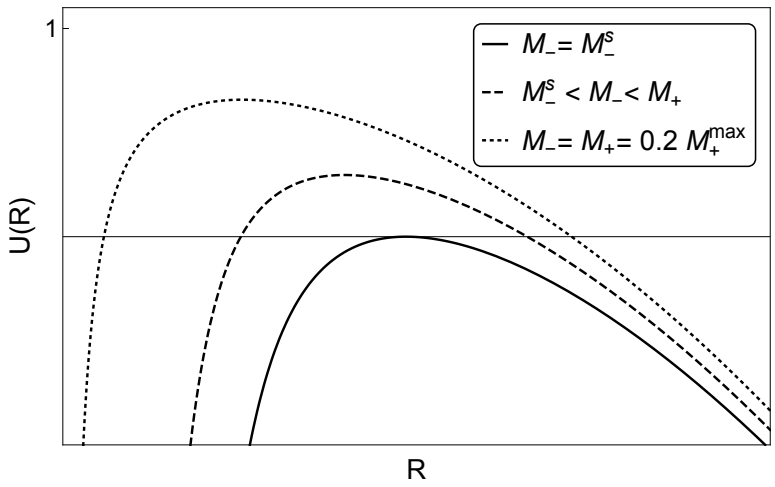

Figure 6.4: An example potential $U(R)$ of Eq. (6.29) describing the trajectory of bubbles nucleated when the black hole mass can vary between false (+) and true (−) vacuum. Here, the seed mass M_+ is kept constant while the remnant mass M_- is varied. M_- is restricted to be smaller than M_+ and larger than M_-^s, below which $U(R) < 0$ and there are no viable solutions.

M_+ and Ref. [64] presents analysis including this. However, it is shown that the greatest improvements occur at lower M_+ and M_-. Hence, for concision, here the remnant mass is chosen to be smaller than the seed mass. Keeping the seed mass constant ($M_+ = 0.2\, M_+^{\max}$), reducing M_- lowers $U(R)$, the opposite behaviour to M_+. As such, rather than setting an upper limit, the bound $\dot{R}^2 \geq 0$ provides a lower limit on the remnant mass: $M_- \geq M_-^s$. That is, for every M_+ value there is a corresponding M_- value, M_-^s, at which the only solution is $\dot{R}^2 = U(R) = 0$, the static solution. Hence, the bounds on the masses are

$$0 \leq M_+ \leq M_+^{\max} \quad , \quad M_-^s \leq M_- \leq M_+ \ . \tag{6.31}$$

Importantly, the introduction of an independent remnant mass M_- allows a static solution at all M_+. To summarise, at every M_+ there exists a static solution at $M_- = M_-^s$ and oscillating solutions elsewhere, $M_-^s < M_- \leq M_+$.

In addition to varying the black hole mass, the work of Ref. [64] crucially demonstrated how to account for the conical singularities arising from the mismatch between the periods $\beta_{\tau_\pm}$ of the Euclidean times $\tau_\pm$ and the Hawking temperatures of both horizons. As mentioned earlier in Section 3.3, the work of Ref. [65] showed that, in a 4-dimensional spacetime with

one or more conical singularities, the integral over the Ricci scalar becomes

$$\int d^4x\,\sqrt{g}\,\mathcal{R} = \sum_i 4\pi(1-\alpha_i)A_i + \int d^4x\,\sqrt{g}\,\mathcal{R}_{\rm reg}\ , \tag{6.32}$$

where $\mathcal{R}_{\rm reg}$ is the non-singular part of the Ricci scalar, α_i are the conical deficit angles and A_i is the 2-dimensional area of the corresponding conical surface.

The process of calculating the Euclidean action remains similar to the case of Hiscock but with the mentioned improvements; the bulk contributions from the false (I_+^B) and true (I_-^B) vacua but with the additional conical contributions, the surface contribution (I^S) and finally subtracting off the background ($I_{\rm SdS}^B$) again including conical contributions. The region of false vacuum is from the bubble radius R to the cosmological horizon $r_{c,+}$, hence

$$I_+^B = -4\pi(1-\alpha_{c,+})A_{c,+} + \frac{\beta_{\tau_+}}{4G}\left(-\frac{2\Lambda_+}{3}r_{c,+}^3 + 2GM_+\right) - \frac{1}{4G}\int d\tau_+\,R^2 f_+'\ , \tag{6.33}$$

where the first term is the contribution from the conical singularity with $A_{c,+}$ the area of the cosmological horizon in the false vacuum and prime denotes differentiation with respect to R. On the other hand, the region of true vacuum is from the remnant black hole horizon $r_{h,-}$ to the bubble radius R, hence

$$I_-^B = -4\pi(1-\alpha_{h,-})A_{h,-} + \frac{\beta_{\tau_-}}{4G}\left(\frac{2\Lambda_-}{3}r_{h,-}^3 - 2GM_-\right) + \frac{1}{4G}\int d\tau_-\,R^2 f_-'\ , \tag{6.34}$$

where $A_{h,-}$ is the area of the black hole horizon in the true vacuum. The conical deficits in each case read

$$\alpha_{c,+} = \frac{\beta_{\tau_+}}{\beta_{c,+}} \quad , \quad \alpha_{h,-} = \frac{\beta_{\tau_-}}{\beta_{h,-}}\ . \tag{6.35}$$

The Euclidean actions therefore become

$$\begin{aligned} I_+^B &= -\frac{A_{c,+}}{4G} + \frac{\beta_{\tau_+}}{4G}\left(\frac{A_{c,+}}{\beta_{c,+}} - \frac{2\Lambda_+}{3}r_{c,+}^3 + 2GM_+\right) - \frac{1}{4G}\int d\tau_+\,R^2 f_+' \\ &= -\frac{A_{c,+}}{4G} - \frac{1}{4G}\int d\tau_+\,R^2 f_+'\ , \end{aligned} \tag{6.36}$$

$$\begin{aligned} I_-^B &= -\frac{A_{h,-}}{4G} + \frac{\beta_{\tau_-}}{4G}\left(\frac{A_{h,-}}{\beta_{h,-}} + \frac{2\Lambda_-}{3}r_{h,-}^3 - 2GM_-\right) + \frac{1}{4G}\int d\tau_-\,R^2 f_-' \\ &= -\frac{A_{h,-}}{4G} + \frac{1}{4G}\int d\tau_-\,R^2 f_-'\ , \end{aligned} \tag{6.37}$$

where in each case the term in brackets vanishes. To complete the bulk contribution the background must be subtracted. The focus here will be on a Schwarzschild-de Sitter (SdS) background as that is most relevant for cosmological phase transitions however, Ref. [64] also

performs the subtraction for other Schwarzschild-anti-de Sitter (SAdS) backgrounds. The SdS false vacuum background covers the whole space, from $r_{h,+}$ to $r_{c,+}$, and therefore has conical contributions from both the black hole and cosmological horizons

$$\begin{aligned} I^B_{\rm SdS} &= -4\pi(1-\alpha_{h,+})A_{h,+} - 4\pi(1-\alpha_{c,+})A_{c,+} - \frac{1}{4G}\frac{2\Lambda_+}{3}\beta_{\tau_+}\left(r^3_{c,+} - r^3_{h,+}\right) \\ &= -\frac{A_{h,+}}{4G} - \frac{A_{c,+}}{4G} + \frac{\beta_{\tau_+}}{4G}\left(\frac{A_{h,+}}{\beta_{h,+}} + \frac{A_{c,+}}{\beta^{\rm cos}_+} - \frac{2\Lambda_+}{3}(r^3_{c,+} - r^3_{h,+})\right) \\ &= -\frac{A_{h,+}}{4G} - \frac{A_{c,+}}{4G}\ , \end{aligned} \tag{6.38}$$

where again the term in brackets vanishes. Subtracting this from the bulk contributions above, the final bulk contribution in the presence of conical singularities is found

$$\begin{aligned} I^B &= I^B_+ + I^B_- - I^B_{\rm SdS} \\ &= \frac{A_+ - A_-}{4G} + \frac{1}{4G}\int d\lambda\, R^2\left(f'_-\dot\tau_- - f'_+\dot\tau_+\right)\ , \end{aligned} \tag{6.39}$$

where the subscript h has been dropped on the black hole areas $A_\pm$. The surface contribution is as described in the Hiscock case and takes the form

$$I^S = \frac{1}{2G}\int d\lambda\, R\left(f_+\dot\tau_+ - f_-\dot\tau_-\right)\ . \tag{6.40}$$

Combining these bulk and surface contributions gives the final bounce action

$$B = \frac{A_+ - A_-}{4G} + \frac{1}{4G}\int d\lambda\, \left[\left(2Rf_+ - R^2 f'_+\right)\dot\tau_+ - \left(2Rf_- - R^2 f'_-\right)\dot\tau_-\right]\ , \tag{6.41}$$

which can also be expressed in terms of the bubble radius

$$\begin{aligned} B = \frac{A_+ - A_-}{4G} + \frac{1}{2G}\int_{R_{\rm min}}^{R_{\rm max}} dR\, \Bigg[& 2(R - 3GM_+)\frac{1}{f_+}\left(\frac{f_+}{U(R)} - 1\right)^{1/2} \\ & - 2(R - 3GM_-)\frac{1}{f_-}\left(\frac{f_-}{U(R)} - 1\right)^{1/2}\Bigg]\ . \end{aligned} \tag{6.42}$$

The question in regards to the static solutions can again be raised. As with the Hiscock case the integral over λ in Eq. (6.41) becomes trivial and it becomes a task of determining β_λ. Ref. [64] ignores the second term of Eq. (6.41) and takes the static bounce action to simply be the difference in black hole areas. While this is technically incorrect, numerically, for much of the parameter space, this second term is negligible and the results are valid.

Figure 6.5 shows the consequences of including conical singularities on the bounce action for the example parameters $\sigma = 10^4\,{\rm GeV}^3$, $\epsilon_+ = 10^5\,{\rm GeV}^4$ and $\epsilon_- = 0$. The black line

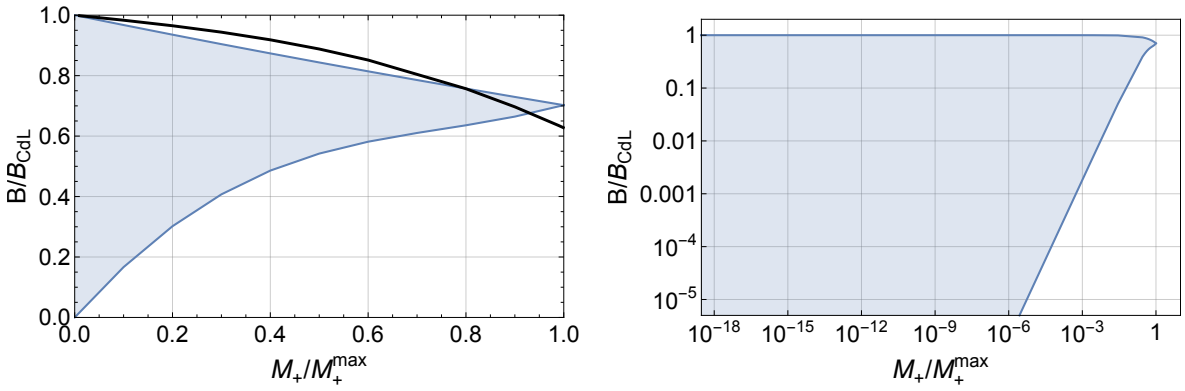

Figure 6.5: The tunnelling exponent when including black holes and their conical singularities, as given in Eq. (6.42), for the example parameters $\sigma = 10^4\,\mathrm{GeV}^3$, $\epsilon_+ = 10^5\,\mathrm{GeV}^4$ and $\epsilon_- = 0$. The black line is the result without accounting for conical singularities, as seen in Figure 6.3. The upper limit represents $M_- = M_+$ while the lower limit is the static solution $M_- = M_-^s$.

represents the values excluding conical singularities (the Hiscock approach), as shown in Figure 6.3. The lower limit is given by the static solutions $M_- = M_-^s$ and presents the greatest improvement in tunnelling rates. All other values in the blue shaded region are oscillating solutions, with the upper limit given by $M_- = M_+$. The inclusion of varying masses and conical singularities provides remarkable improvements in tunnelling rates, with B becoming arbitrarily small at small seed masses. As with the Hiscock result, the static solutions again dominate, but they are now available for any seed mass. Consequently, the greatest improvements occur at the lowest M_+ rather than highest.

Ref. [67] extended the description to thick-walled bubbles for the particular, and likely dominant, case of static solutions. The results support the thin-wall conclusion that black holes are very effective nucleation sites, extending this conclusion to a wider parameter space.

6.3 Application to Finite Temperature Phase Transitions

The studies [62, 64, 66, 67] discussed focus solely on the effect black holes have as nucleation sites on zero temperature phase transitions. However, it is also possible that a population of primordial black holes was present in the early universe, with the opportunity to seed finite temperature cosmological phase transitions. This becomes of particular importance when considering phenomenological consequences such as the resulting gravitational wave background. Significant changes in nucleation rates could propagate to important properties

such as nucleation temperature and bubble size and speed at collision. Additionally, models previously ruled out because of an inability to complete their transition could become viable, something particularly important for supercooled transitions.

Chapter 7 presents work submitted for publication applying the discussed thin-wall formalism to describe black holes acting as nucleation sites for finite temperature cosmological phase transitions. In fact, it is argued, through symmetry comparisons with flat-space transition methods, that this thin-wall formalism naturally describes a finite temperature transition. Hence, the period of the proper time on the wall β_λ should equal the inverse temperature of the universe

$$\beta_\lambda = \frac{1}{T} \, , \tag{6.43}$$

as is the case in flat-space. The study again shows that the static solutions dominate and improvements over the flat-space result can occur at smaller seed black hole masses. However, an accurate conclusion cannot be made without first considering a specific PBH distribution.

Chapter 7

Black Holes Seeding Cosmological Phase Transitions

Basem Kamal El-Menoufi[1,2], Stephan J. Huber[1], and Jonathan P. Manuel[1]

[1]Department of Physics & Astronomy, University of Sussex, Falmer, Brighton, BN1 9QH, United Kingdom

[2]Consortium for Fundamental Physics, School of Physics and Astronomy, University of Manchester, Manchester, M13 9PL, United Kingdom

Submitted for publication

arXiv:2006.16275

Abstract

We consider a generic first-order phase transition at finite temperature, and investigate to what extent a population of primordial black holes, of variable masses, can affect the rate of bubble nucleation. Using a thin-wall approximation, we construct the Euclidean configurations that describe transition at finite temperature. After the transition, the remnant black hole mass is dictated dynamically by the equations of motion. The transition exponent is computed, and displays an explicit dependence on temperature. We find the configuration with the lowest Euclidean action to be static and O(3) symmetric; therefore, the transition takes place via thermal excitation. The transition exponent exhibits a

strong dependence on the seed mass black hole, M_+, being *almost* directly proportional. A new nucleation condition in the presence of black holes is derived and the nucleation temperature is compared to the familiar flat-space result, i.e. S_3/T. For an electroweak-like phase transition it is possible to enhance the nucleation rate if $M_+ \lesssim 10^{15} M_{\rm P}$. Finally, we outline the possible transition scenarios and the consequences for the power spectrum of stochastic gravitational waves produced due to the first-order phase transition.

7.1 Introduction

Cosmological phase transitions at different epochs may have played a major role in the history of the universe, potentially occurring anywhere between the QCD ($\sim 100\,\text{MeV}$) and GUT scales ($\sim 10^{16}\,\text{GeV}$) [28]. A much studied example is the electroweak phase transition, due to which known elementary particles acquired their masses. Of particular interest are first-order phase transitions which proceed through the nucleation and expansion of bubbles; the two phases are separated by a bubble wall, inside exists the new "true" vacuum while outside the old "false" vacuum. In particle physics, there exists a continuous interest in first-order transitions because they provide departure from thermal equilibrium, as required in the process of baryogengesis [11,15,131–133]. In addition, the collision of expanding bubbles yield a stochastic background of gravitational waves that is well within the reach of LISA [17–19,21,23].

The first description of vacuum decay in continuum field theory was famously given by Coleman and Callan [29,30] and later extended by Linde [32] to the case of finite-temperature phase transitions. Therein it was determined that the probability for nucleation of the new phase, per unit time and per unit volume, is given by

$$\frac{\Gamma}{V} = A e^{-B} \,, \tag{7.1}$$

where A is a coefficient of mass dimension four and the tunneling exponent, B, is the difference between the Euclidean action of the tunneling configuration and that of the false vacuum. Due to the exponential dependence, B is the quantity mostly studied, while an estimate of A usually suffices. On one hand, vacuum decay is attributed to quantum tunneling, and therefore is appropriate for zero-temperature phase transitions. On the other hand, at finite temperature two distinct physical effects exist; the phase transition could proceed either via "thermally-assisted" quantum tunneling or by classical thermal excitation over the potential barrier.

Later on, Coleman and de Luccia (CdL) raised the question about the effect of gravitation on the dynamics of vacuum decay [61]. Assuming O(4) symmetry and using the thin-wall approximation, an appropriate limit when the reduction in vacuum energy is small compared to the height of the barrier, they found simple yet stark results. If one tunnels from a space with positive vacuum energy to a smaller, yet still positive, or zero vacuum energy then gravitation makes vacuum decay more probable. On the other hand, if one tunnels from a space with zero or negative vacuum energy then gravitation makes vacuum decay less probable. While this indeed comprised an important insight, effects of gravity remained purely academic for phenomenology. Apart from negligible corrections, the nucleation rate remained essentially unchanged from flat-space given any practical values of the surface tension and vacuum energy [61].

Notwithstanding, this might not be end for gravity. In particular, can primordial black holes (PBHs) influence cosmological phase transitions? In recent years, the interest in PBHs has rapidly intensified, see the review articles [134–136], and it seems inevitable that we revisit the dynamics of phase transitions in the presence of PBHs. The first study about the topic of black holes and phase transitions was done by Hiscock [62], and was concerned with vacuum transitions at zero temperature. He found that black holes *do* indeed increase the nucleation probability. Precisely, the presence of black holes could cause the Euclidean action to diminish by up to a factor of approximately two. However, the analysis was limited in a number of ways. Firstly, the black hole mass was kept constant throughout the transition. Secondly, conical singularities, arising from an unmatched Euclidean time period and inverse Hawking temperature, were not accounted for.

Recently, Gregory *et. al.* [64, 66, 67, 137] undertook more work in this direction that overcame the shortcomings of [62], in particular, the treatment of conical singularities. Therein, the focus was mainly on the Higgs vacuum (in)-stability in the presence of black holes[1], and they discovered that the Euclidean action could be arbitrarily reduced depending on the seed black hole mass. The central construction is based on the thin-wall approximation [29], and utilizes Israel's junction conditions [63] to smoothly glue the spacetimes that represent the two phases. Each vacuum state contains a black hole, and is therefore given by a static Schwarzschild-de-Sitter (SdS) black hole. Applying the junction conditions then yields a dynamical equation for the "bubble" wall, whose solution determines the full instanton. We

[1]The stability of the electro-weak vacuum, in pure de Sitter space, has been investigated in Ref. [138].

also note that further studies have been undertaken in Refs. [139–142] along complementary directions.

In the standard setting of early universe cosmology, there is an epoch of inflation followed by reheating. The universe then reaches a state of thermal equilibrium, after which phase transitions are likely to proceed via thermal, rather than quantum, fluctuations. In most scenarios, the phase transition proceeds thermally via finite-temperature effects in the potential. For first-order phase transitions, as the universe cools down the potential develops a barrier that separates two phases, thereby initiating the phase transition. In addition, any cosmological first-order phase transition will, through the expanding and colliding bubbles of the new phase, produce a stochastic gravitational wave (GW) background. Of particular interest are transitions happening around the electroweak scale as the expected signal of GW's is within the sensitivity of LISA [21, 23].

In this paper we investigate the potential effects of primordial black holes on the nucleation rate of a generic first-order phase transition that proceeds thermally. This situation is more complicated than the vacuum case, as it is *not* obvious a priori how to define the appropriate finite-temperature instanton, that should ultimately be used to compute the Euclidean action. In particular, which solutions of the equation of motion, describing the bubble wall motion, are relevant for the phase transition? We present a prescription that singles out the relevant tunneling configurations, the details of which are presented in Section 7.3.4. Our prescription is entirely guided by the analogy with standard finite-temperature tunneling in flat-space, which is reviewed in Section 7.2.2. Our method offers a consistent formalism to quantify the effects of PBHs on any generic cosmological first-order phase transition, at least in the thin-wall regime. This sheds new light on the features of the GW spectrum generated by the phase transition, and paves the way to study possible links with the properties of PBHs.

The paper is structured as follows. In Section 7.2 we explicitly describe the methods of tunneling, first in quantum mechanics before extending to quantum field theory. There are three generic mechanisms: zero temperature quantum tunneling through infinite-period bounces, thermally assisted quantum tunneling through finite-period bounces, and thermal excitation through static bubbles. Black holes are introduced in Section 7.3 where we begin by recapping the Israel thin-wall formalism developed by Refs. [64, 66] before moving on to quantitatively analysing the solutions and how they are applied to finite temperature cosmological phase transitions. In Section 7.4 we derive the bounce action, determine a

new nucleation criteria and then apply our approach to the example of a first-order EWPT. We outline the pathway to making phenomenological predictions in Section 7.5. Section 7.6 contemplates the various scenarios and discusses the consequences for gravitational waves. A summary is then given in Section 7.7.

7.2 Bubbles vs Bounces in QFT

7.2.1 Tunneling in Quantum Mechanics

Our knowledge about tunneling in quantum field theory comes directly from non-relativistic quantum mechanics, in particular, single particle systems. The typical potential, $V(x)$, one is interested in is shown in Figure 7.1, where a particle is initially localized to the left of the barrier at the bottom of the potential well. Quantum mechanics renders such a state unstable and it becomes paramount to compute the lifetime of unstable states. The WKB approximation offers an analytic technique to study quantum tunneling for a generic potential. The finite probability, per unit time, for the particle to quantum tunnel through the barrier is given by

$$\Gamma \simeq Ae^{-B}, \quad B := 2\int_0^a \sqrt{2V(x)}dx \quad . \tag{7.2}$$

where A is a prefactor with the dimensions of energy. There is a remarkable feature of the tunneling exponent in that it directly derives from a special solution to the Euclidean equation of motion of the system, i.e.

$$m\frac{d^2x}{d\tau^2} + \frac{(-V(x))}{dx} = 0 \quad , \tag{7.3}$$

where τ is Euclidean time. Eq. (7.3) simply describes a classical particle of mass m moving in the inverted potential of Figure 7.1. Coleman [29] observed that Eq. (7.3) admits periodic solutions known as *bounces*. To see this, we write the conservation of Euclidean energy

$$\frac{1}{2}m^2\left(\frac{dx}{d\tau}\right)^2 + (-V(x)) = 0 \quad , \tag{7.4}$$

so indeed the particle can start at the origin, slide down to reach $x = a$ and then bounce back to the origin. In particular, inspection of Eq. (7.4) reveals that the particle can only reach the origin as $\tau \to \pm\infty$ which demonstrates that the bounce has an infinite period. Hence, the bounce solution, $x_\infty(\tau)$, has the following boundary conditions

$$\lim_{\tau\to\pm\infty} x_\infty(\tau) = 0, \quad x_\infty(0) = a, \quad \frac{dx_\infty(0)}{d\tau} = 0 \quad . \tag{7.5}$$

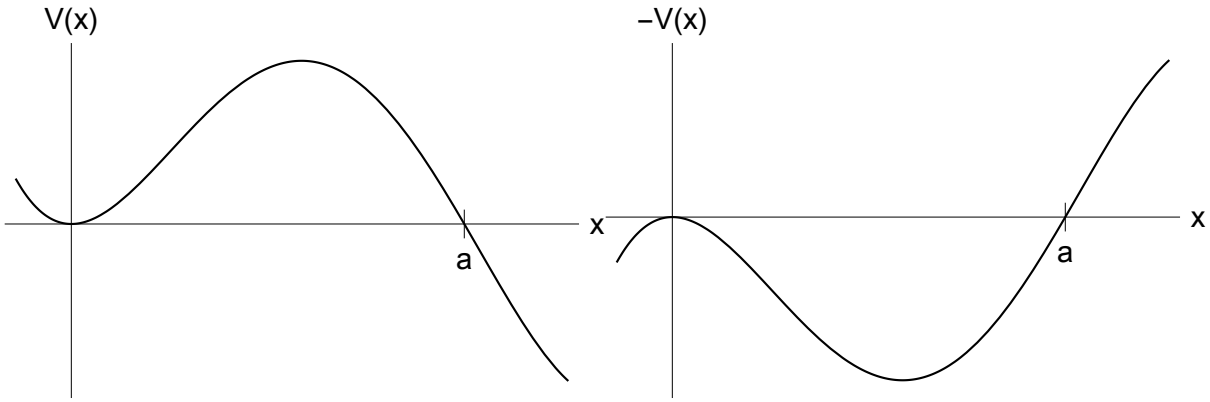

Figure 7.1: Left: A typical tunneling potential $V(x)$. Right: The inverted tunneling potential $-V(x)$.

If we now insert the bounce solutions in the Euclidean action, one recovers the exponent B in Eq. (7.2),

$$S_{\rm E} = \int_{-\infty}^{\infty} d\tau \left(\frac{1}{2} m^2 \left(\frac{dx_b}{d\tau} \right)^2 + V(x_b) \right) = B \quad . \tag{7.6}$$

In fact this is not the end of story; another class of Euclidean solutions play a dominant role in describing the decay of *thermally* excited states. These solutions also represent bounce-like behavior, but with a finite period in Euclidean time. Let us start by recalling the tunneling exponent of a thermally excited state, with energy E and inverse temperature β,

$$B(E;\beta) = \beta E + 2 \int_{x_1}^{x_2} \sqrt{2m(V(x) - E)} dx \quad , \tag{7.7}$$

where the first factor is the Boltzman suppression and (x_1, x_2) are the classical turning points, which we remind are functions of energy. Notice that the energy is kept arbitrary at this stage, but to find the appropriate decay rate in Eq. (7.2) one has to minimize the exponent in Eq. (7.7), at fixed temperature, with respect to energy. One gets

$$\frac{\partial B}{\partial E}(E_0) = 0 \quad \Rightarrow \quad \beta = 2m \int_{x_1}^{x_2} dx \frac{1}{\sqrt{2m(V(x) - E_0)}} \quad , \tag{7.8}$$

which then determines the energy as a function of temperature. Plugging E_0 back into Eq. (7.7) yields the decay rate exponent. The latter can be derived from another class of solutions to Eq. (7.3), i.e. those solutions with finite energy

$$\frac{1}{2} m^2 \left(\frac{dx}{d\tau} \right)^2 + (-V(x)) = -E \quad . \tag{7.9}$$

Clearly a solution to Eq. (7.3) with finite energy E is also a bounce, albeit with a finite period given by

$$P(E) = 2m \int_{x_1}^{x_2} dx \frac{1}{\sqrt{2m(V(x) - E)}} \quad . \tag{7.10}$$

Now Eq. (7.10) yields the energy that satisfies $P(E_0) = \beta$. It is straightforward to then obtain the finite-period bounce that we denote by $x_\beta(\tau)$. Finally, we evaluate the Euclidean action on this periodic bounce to recover Eq. (7.7)

$$S_{\rm E} = \int_{-\beta/2}^{\beta/2} d\tau \left(\frac{1}{2} m^2 \left(\frac{dx_\beta}{d\tau} \right)^2 + V(x_\beta) \right) = B(E_0; \beta) \quad . \tag{7.11}$$

As one might expect, if the temperature is high enough the particle gets excited to the top of the barrier and, therefore, *classically* transitions to the allowed region. The temperature at which this takes place can be estimated by approximating the inverted potential, at its minimum, as $V(x_0) \simeq V_0 - \frac{1}{2} m \omega_0^2 x^2$. A particle moving in the inverted potential, near $x = x_0$, then experiences a *fixed* period $2\pi/\omega_0$. Therefore, Eq. (7.3) possesses no finite-period Euclidean solutions when the temperature is such that

$$\beta < \beta_0 := \frac{2\pi}{\omega_0} \quad , \tag{7.12}$$

and the unique available solution becomes the static configuration $x_{\rm s}(\tau) = x_0$ with a tunneling exponent given by

$$S_{\rm E} = \beta V_0 \quad . \tag{7.13}$$

To summarize, we have three separate solutions to the Euclidean equation of motion and each describe a distinct physical situation. First, we have the infinite-period bounce $x_\infty(\tau)$ which describes the decay of the vacuum state. Second, the finite-period bounce $x_\beta(\tau)$ describes the decay of a thermally excited state. Third, the static solution $x_{\rm s}$ describes the classical excitation of the particle over the potential barrier.

7.2.2 Tunneling in Quantum Field Theory

The close connection between Euclidean solutions and tunneling exponents is pivotal for quantum field theory. If the potential functional in the quantum field theory exhibits a barrier, one can mimic the strategy drawn from quantum mechanics to compute the tunneling probability per unit time and per unit volume. Here we clearly need to understand what kind

of boundary conditions one has to impose on Euclidean solutions that describe the tunneling process. We write down the Euclidean equations of motion and then proceed to find bounce, as well as static, solutions. The Euclidean action evaluated on the these solutions is then interpreted as providing the decay exponent in Eq. (7.2). The justification of this procedure in QFT is best offered by the work of Coleman and Callan [29, 30], who reformulated the tunneling problem in quantum mechanics using Euclidean path integral methods.

In summary, we have three physical scenarios echoing the story in quantum mechanics. The only new input concerns the *spatial* boundary conditions imposed on the Euclidean solutions. As the solutions become extended in 3D space, we need to ensure that the action remains finite.

Infinite-period bounces & vacuum decay: First, we have a QFT of a scalar field, φ, held at zero-temperature whose Euclidean equation of motion reads

$$\frac{d^2\varphi}{d\tau^2} + \nabla^2\varphi - \frac{dV\left(\varphi\right)}{d\varphi} = 0 \quad , \tag{7.14}$$

where the potential $V(\varphi)$ has a barrier separating the two vacua. The bounce solution is fully symmetric in Euclidean time, and thus one can focus on the semi-infinite interval, $\tau \in [0, \infty)$. The temporal boundary conditions are exactly identical to Eq. (7.5)

$$\lim_{\tau\to+\infty} \varphi(\tau, \vec{x}) = \varphi_+, \quad \frac{d\varphi(0, \vec{x})}{d\tau} = 0 \quad , \tag{7.15}$$

and to ensure finiteness of the Euclidean action we further impose a spatial boundary condition

$$\lim_{|\vec{x}|\to\infty} \varphi(\tau, \vec{x}) = \varphi_+ \quad . \tag{7.16}$$

Indeed, one has to resort to numerical techniques to solve this system. Nevertheless, Coleman proved that the solution with the lowest action is O(4) invariant [29], a fact that simplifies the situation considerably. Now Eqs. (7.14)-(7.16) become

$$\frac{d^2\varphi}{d\rho^2} + \frac{3}{\rho}\frac{d\varphi}{d\rho} - \frac{dV\left(\varphi\right)}{d\varphi} = 0 \quad , \quad \lim_{\rho\to\infty} \varphi(\rho) = \varphi_+ \quad , \quad \frac{d\varphi(0)}{d\rho} = 0 \quad , \tag{7.17}$$

where the 4D radius is $\rho^2 = \tau^2 + \vec{x}^2$. The last condition in the above equation is to ensure the solution is regular at the origin $\rho = 0$. Notice that since the O(4) solution is even in τ, the second condition in Eq. (7.15) is automatically satisfied. Eq. (7.17) presents an ODE, which can be solved by numerical methods.

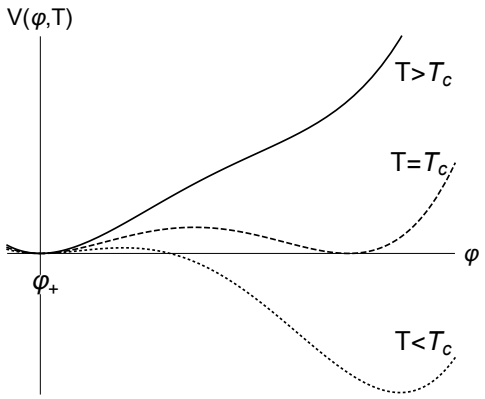

Figure 7.2: An example scalar field potential where the barrier is generated through finite temperature effects. At large temperatures there is a single minimum at φ_+, the false vacuum. As the temperature decreases a second minimum forms at φ_-, the true vacuum, the location of which is temperature dependent. At the critical temperature T_c the two minima are degenerate. Below the critical temperature the true vacuum is energetically favourable and a transition can occur.

Finite-period bounces & tunneling at finite temperature: Second, we have the situation relevant for cosmological phase transitions, whereby the theory is held at finite temperature, $\beta = 1/T$, and the thermal potential, $V(\varphi, T)$, develops a barrier as the universe cools down, see Figure 7.2. Therefore, the finite-temperature bounce satisfies

$$\frac{d^2\varphi}{d\tau^2} + \nabla^2\varphi - \frac{dV(\varphi, T)}{d\varphi} = 0 \quad , \tag{7.18}$$

with the following boundary conditions

$$\left.\frac{d\varphi(\tau, \vec{x})}{d\tau}\right|_{\tau=0} = 0 \ , \quad \lim_{|\vec{x}|\to\infty} \varphi(\tau, \vec{x}) = \varphi_+ \ , \quad \left.\frac{d\varphi(\tau, \vec{x})}{dr}\right|_{r=0} = 0 \quad . \tag{7.19}$$

The first condition clearly signifies the bouncing behavior, the second guarantees the Euclidean action is finite and the third assures the solution is regular at the origin. This set of conditions is not enough to guarantee a solution to Eq. (7.18), in other words, we need an extra condition that describes the behavior of the finite-temperature bounce as $\tau \to \pm\beta/2$. We observe that the (conserved) Euclidean Hamiltonian, for a finite-period bounce, has to be non-zero given the thermal excitation of the system. Therefore, in contrast to vacuum decay described above, a finite-temperature solution can *not* approach the false vacuum at $\pm\beta/2$. Hence, the remaining condition must instead be on the velocity of the field, i.e.

$$\lim_{\tau\to\pm\beta/2} \frac{d\varphi(\tau, \vec{x})}{d\tau} = 0 \quad , \tag{7.20}$$

which manifestly describes the bouncing behavior of the solution. As a final remark, these solutions are almost never discussed in the literature, yet, we believe the conditions in Eqs. (7.19) and (7.20) render the problem well-posed although it is not possible to make a concrete statement regarding whether a non-trivial solution exists. This can only be verified by explicit numerical methods.

Static solutions at high temperature: Lastly, we have the familiar static solution at high temperatures. The equation of motion and boundary conditions are identical to the O(4)-symmetric bounce, except the dynamics take place in three dimensions. The solution with the minimum action is O(3) invariant, i.e.

$$\frac{d^2\varphi}{dr^2} + \frac{2}{r}\frac{d\varphi}{dr} - \frac{dV(\varphi, T)}{d\varphi} = 0 \quad , \quad \lim_{r\to\infty} \varphi(r) = \varphi_+ \quad , \quad \frac{d\varphi(0)}{dr} = 0 \quad , \tag{7.21}$$

and clearly has a vanishing period. Although it is not possible in QFT to easily estimate the temperature at which the static solution dominates over the finite-period bounce, one can numerically compute the Euclidean action of both solutions as a function of temperature and utilize the smaller action as the decay exponent.

7.3 Black Holes and Cosmological Phase Transitions

In this section we consider a scalar field theory at finite temperature propagating in a background spacetime that contains a black hole. In particular, we focus on the typical situation that a potential barrier is generated by finite temperature effects as shown in Figure 7.2. Although the presentation is quite general, we have in mind an electroweak-like phase transition. As the universe cools down, the scalar field eventually tunnels and we wish to compute the tunneling exponent in the presence of a primordial population of *static* black holes. We will conduct our study with one caveat, which concerns the contribution of the thermal plasma to the equations of motion. It is well known EW-scale phase transitions occur during radiation domination. As we set to solve the equations of motion we will ignore the contribution of the thermal plasma to the energy-momentum tensor of the system. We do so for two main reasons. First, the thin-wall approximation, used throughout, requires knowing the analytic solutions for the spacetime metric in both vacuum states. However, we are not aware of any closed form solutions describing a black hole in a Friedmann–Lemaître–Robertson–Walker (FLRW) universe. Second, our main goal is to set up the appropriate formalism to compute the tun-

neling exponent for thermal transitions seeded by black holes. In particular, this enables us to conclude the dependence of the tunneling rate on both the seed mass and the temperature of the system. We do not expect the conclusions from our study to change significantly once we include the expansion of the universe in the story. Technically, the caveats just mentioned comprise an approximation that could be justified on the ground that the Hubble time is the same order of magnitude as the typical lifetime of EW-like phase transitions. Finally, we assume a bare positive cosmological constant in the gravitational sector to allow the universe, post-transition, to retain a positive vacuum energy that we try and keep close to the scale of dark energy. Altogether, we aim to include the effect of the universe expansion on the tunneling process in future work.

7.3.1 Thin-wall instantons

The goal is to solve the Euclidean equations of motion of the coupled scalar-gravity system. The analysis is considerably simplified if we adopt the thin-wall approximation. In the absence of gravity, the approximation is valid as long as the radius of the bubble is large compared the Compton wavelength of the field [29]. In the presence of black holes, however, does the same criterion validate the approximation? We will show below that this is fortunately the case.

The Euclidean equations of motion are those of a scalar field, with a finite-temperature potential, minimally coupled to general relativity

$$\begin{aligned} &G_{\mu\nu} + \Lambda_0 g_{\mu\nu} = \frac{1}{M_{\rm P}^2} T_{\mu\nu} \quad , \\ &T_{\mu\nu} = \partial_\mu\varphi\partial_\nu\varphi - g_{\mu\nu}\left(\frac{1}{2}g^{\alpha\beta}\partial_\alpha\varphi\partial_\beta\varphi + V(\varphi,T)\right) \quad , \\ &\nabla^\mu T_{\mu\nu} = 0 \quad \Rightarrow \quad \Box\varphi - \frac{dV(\varphi,T)}{d\varphi} = 0 \quad , \end{aligned} \tag{7.22}$$

where $\Box = g^{\mu\nu}\nabla_\mu\nabla_\nu$ is the covariant Laplacian and $G_{\mu\nu}$ is the Einstein tensor[2]. The equilibrium solutions are those with a homogeneous field profile permeating the most general static spherically symmetric spacetime, hence the metric has the general form

$$ds^2 = f(r)d\tau^2 + \frac{dr^2}{f(r)} + r^2\left(d\theta^2 + \sin^2\theta d\phi^2\right), \quad \varphi(\tau,\vec{x}) = \varphi_0(T) \quad . \tag{7.23}$$

In the case of interest, where the spacetime contains a black hole, Euclidean time is periodic, i.e. $0 \leq \tau \leq \beta_\tau$. Nevertheless, we do not assume any restrictions on the period of Euclidean

[2]Our convention for the Riemann tensor is that of Wald [143].

time, which renders the spacetime singular as it contains a conical singularity. The contribution of the conical singularity to the tunneling exponent will be computed according to the procedure given in [65]. The effective cosmological constant sourcing the spacetime is given by the *total* vacuum energy

$$\Lambda = \Lambda_0 + \frac{V(\varphi_0(T), T)}{M_{\rm P}^2} \quad , \tag{7.24}$$

and it proves useful to measure the cosmological constant in units of $M_{\rm P}^2$, thus we introduce

$$\epsilon_\Lambda \equiv M_{\rm P}^2 \Lambda \quad . \tag{7.25}$$

Now we wish to construct a thin-wall instanton that interpolates between the true and false vacua, given the typical scalar field finite-temperature potential in Figure 7.2. The analytic expression for such a potential will be given later on when we construct instantons for electroweak-like phase transitions. Specifically, inside the wall we have

$$ds_-^2 = f(r_-)d\tau_-^2 + f(r_-)^{-1}dr_-^2 + r_-^2 d\Omega_2^2, \quad \varphi = \varphi_0(T) \quad , \tag{7.26}$$

while outside

$$ds_+^2 = f(r_+)d\tau_+^2 + f(r_+)^{-1}dr_+^2 + r_+^2 d\Omega_2^2, \quad \varphi = 0 \quad . \tag{7.27}$$

At this stage the Euclidean periodicities $(\beta_{\tau_+}, \beta_{\tau_-})$ are arbitrary, and in general $\beta_{\tau_+} \neq \beta_{\tau_-}$. In the thin-wall approximation, the bubble wall is a hypersurface (thin layer) separating the two equilibrium vacua [62]. Spherical symmetry forces the induced metric on the wall to have the form

$$ds_{\rm wall}^2 = d\lambda^2 + R^2(\lambda)d\Omega_2^2 \quad , \tag{7.28}$$

where λ is the proper time measured by a co-moving observer with the wall and $d\Omega_2^2$ is the standard metric on a unit S^2. Indeed, λ is periodic, i.e. $0 \leq \lambda \leq \beta_\lambda$, which means the wall has topology of $S^2 \times S^1$. Notice that we have three distinct Euclidean times which, a priori, each have a unique period

$$\beta_\lambda \neq \beta_{\tau_+} \neq \beta_{\tau_-} \quad , \tag{7.29}$$

and only the dynamics will dictate any possible relation between these periods. To understand the geometry of the bubble wall, we introduce tangent vectors that span each side of the wall surface

$$e^\mu_{(1)\pm} = \dot{\tau}_\pm \frac{\partial}{\partial \tau_\pm} + \dot{R}\frac{\partial}{\partial r_\pm}, \quad e^\mu_{(2)} = \frac{\partial}{\partial \theta}, \quad e^\mu_{(3)} = \frac{\partial}{\partial \phi} \quad , \tag{7.30}$$

where an over-dot denotes differentiation with respect to λ. We can immediately work out the first junction condition [63], which requires the induced metrics on both sides of the wall to be identical. At the wall we must have $r_+ = r_- = R(\lambda)$. Additionally, we must have

$$g_{\mu\nu} e^{\mu}_{(1)\pm} e^{\nu}_{(1)\pm} = 1 \quad , \tag{7.31}$$

which yields

$$f_\pm(R)\dot{\tau}_\pm^2 + \frac{1}{f_\pm(R)}\dot{R}^2 = 1 \quad . \tag{7.32}$$

Finally, we have the normal one-forms

$$n^\pm_\mu = -\dot{R} d\tau_\pm + \dot{\tau}_\pm dr_\pm \quad , \tag{7.33}$$

which are unit normalized by virtue of Eq. (7.32), and point outward from the wall surface. The second junction condition requires the jump in the extrinsic curvature to be proportional to the surface tension of the wall as follows [63]

$$\Delta K_{ab} = -8\pi G \left(S_{ab} - \frac{1}{2} S h_{ab} \right), \quad K_{ab,\pm} = e^{\mu}_{(a)} e^{\nu}_{(a)} \nabla_\mu n_{\nu,\pm} \quad , \tag{7.34}$$

where h_{ab} is the first fundamental form or simply the induced metric in Eq. (7.28), S_{ab} is the energy-momentum tensor of the wall, and a and b run over (λ, θ, ϕ). As the scalar field tunnels through the barrier, and in the thin-wall approximation, the field gradients through the wall create a surface tension which in turn sources the wall geometry in Eq. (7.34). For a spherical wall with surface tension σ we have [62]

$$S_{ab} = -\sigma \, h_{ab} \quad , \tag{7.35}$$

where σ is typically evaluated at the critical temperature of the transition and, therefore, fully depends on the particular structure of the physics model. Using the (θ-θ) components of Eq. (7.34) we find

$$\frac{1}{R}\left(f_+(R)\dot{\tau}_+ - f_-(R)\dot{\tau}_- \right) = -4\pi G\sigma \quad , \tag{7.36}$$

and, through Eq. (7.32), we can obtain an equation for $\dot{R}$

$$\sqrt{f_+(R) - \dot{R}^2} - \sqrt{f_-(R) - \dot{R}^2} = -4\pi G\sigma R \quad . \tag{7.37}$$

The above equation is not very useful due to the square root structure, and thus we can square twice to obtain

$$\dot{R}^2 = \frac{f_+ + f_-}{2} - \frac{(f_+ - f_-)^2}{64\pi^2 G^2 \sigma^2 R^2} - 4\pi^2 G^2 \sigma^2 R^2 \quad , \tag{7.38}$$

which is our final equation of motion describing the bubble wall motion [62, 64].

7.3.2 Interlude: the Coleman-de Lucia solution

Before we analyze Eq. (7.38) in the presence of black holes, it is quite important to review the dynamics in the absence of black holes, i.e. the CdL scenario [61]. Our goal is not to go over some known results but rather to stress the physical meaning of the solution and gain the understanding that will become essential later on when we include black holes. In Eq. (7.38) the metric function is that of Euclidean de-Sitter space written in static coordinates

$$f_{\pm}(r_{\pm}) = 1 - \frac{\Lambda_{\pm} r_{\pm}^2}{3} \quad , \tag{7.39}$$

and thus

$$\dot{R}^2 = 1 - \zeta R^2 \, , \quad \zeta := 4\pi^2 G^2 \sigma^2 + \frac{4\pi G(\epsilon_+ + \epsilon_-)}{3} + \frac{(\epsilon_+ - \epsilon_-)^2}{9\sigma^2} \quad . \tag{7.40}$$

The solution of the above equation is immediate, and one can then plug back in Eq. (7.32) to find $\tau_{\pm}(\lambda)$,

$$R(\lambda) = \frac{1}{\zeta}\cos(\zeta\lambda) \, , \quad \tau_{\pm}(\lambda) = l_{\pm} \tan^{-1}\left(\frac{\sin(\zeta\lambda)}{\sqrt{\zeta^2 l_{\pm}^2 - 1}}\right) \, , \quad l_{\pm}^2 := \frac{3M_{\rm P}^2}{\epsilon_{\pm}} \quad , \tag{7.41}$$

where the solution exists if and only if $\zeta^2 l_{\pm}^2 > 1$. Therefore, in static coordinates the CdL solution is oscillatory with period $\beta_{\lambda} = 2\pi/\zeta$. Based on that one might be tempted to think that the solution possesses an O(3) symmetry, nevertheless, this is *not* true and the O(4) symmetry of the CdL solution is nothing but hidden by the choice of coordinates.

The symmetry can be made manifest in the global coordinates of Euclidean de-Sitter space, or more precisely angular coordinates on S^4. The argument goes as follows. The geometry of the thin-wall instanton is simple; we have two 4-dimensional spheres, with radii l_+ and l_-, which are glued at some polar angle that will be determined below. First, the coordinate transformation we need is of the form

$$r_{\pm} = l_{\pm}\sin(\xi_{\pm})\sin\chi, \quad \tau_{\pm} = l_{\pm}\tan^{-1}\Big[\tan(\xi_{\pm})\cos\chi\Big] \quad , \tag{7.42}$$

and leads to the following metric of Euclidean dS

$$ds_{\pm}^2 = l_{\pm}^2\Big(d\xi_{\pm}^2 + \sin^2(\xi_{\pm}) d\Omega_{(3)}^2\Big) \quad , \tag{7.43}$$

where $d\Omega_{(3)}^2$ is the metric on a unit 3-sphere. Eq. (7.43) is nothing but the standard metric on a 4-sphere with radius $l_{\pm}$. These coordinates cover the whole sphere. To prove the

O(4) invariance of the solution, we just need to show that the wall motion, represented by Eq. (7.41), becomes static in global coordinates and, in addition, find the polar angles where the two spheres are glued. From Eq. (7.41) we notice that

$$\cos^2\left(\frac{\tau_\pm(\lambda)}{l_\pm}\right)\left(R^2(\lambda)+l_\pm^2\tan^2\left(\frac{\tau_\pm(\lambda)}{l_\pm}\right)\right)=\frac{1}{\zeta^2}\quad , \tag{7.44}$$

and thus using Eq. (7.42) we find the wall to be located at

$$l_\pm\sin\xi_\pm^{\rm wall}=\frac{1}{\zeta}\quad . \tag{7.45}$$

If we recall that $\zeta^2 l_\pm^2>1$, then the above equation possesses a solution. As we anticipated each S^4 is cut at the polar angle, ξ, determined by Eq. (7.45) for each 4-sphere and then smoothly glued to form the static CdL instanton. The most important observation is that the solution manifestly displays an O(4) symmetry, and therefore it represents a tunneling configuration that proceeds via vacuum decay.

7.3.3 Including Black holes

Using the formalism outlined above we include a static black hole in the spacetime and solve Eq. (7.38). The metric is that of a static Schwarzschild de-Sitter black hole continued to Euclidean space. Hence, in Eq. (7.38) we substitute

$$f_\pm(r)=1-\frac{2GM_\pm}{r}-\frac{\Lambda_\pm r^2}{3}\quad , \tag{7.46}$$

where M is the ADM mass. As a reminder $+$ represents the false vacuum outside the bubble, while $-$ is the true vacuum inside the bubble. Therefore, M_+ is the seed black hole mass around which the bubble nucleates, M_- is the remnant black hole mass and finally $\Lambda_{+(-)}$ is the cosmological constant in the false (true) vacuum. Throughout our analysis we will instead write the cosmological constants in terms of vacuum energies, $\epsilon_\pm=M_{\rm P}^2\Lambda_\pm$, allowing a more transparent comparison to quantities from the scalar field theory. Explicitly, in our case we have

$$\Lambda_+=\Lambda_0,\quad \Lambda_-=\Lambda_0-\frac{\epsilon_\varphi}{M_{\rm P}^2}\quad , \tag{7.47}$$

where ϵ_φ is the vacuum energy density of the true vacuum. In addition, we have the Hawking temperatures for both the black hole and cosmological horizons

$$\beta_h=\frac{4\pi}{|f'(r_h)|},\quad \beta_{\rm cos}=\frac{4\pi}{|f'(r_c)|}\quad , \tag{7.48}$$

where r_h and r_c are the two positive roots of metric function. To ensure the presence of a horizon, or rather the absence of a naked singularity, we have the following inequality

$$\Lambda_{\pm} < \frac{1}{(3GM_{\pm})^2} \quad . \tag{7.49}$$

Before solving the system, we pause to comment on the validity of the thin-wall approximation, which in standard QFT just amounts to having the radius of the bubble much larger than its thickness. The thickness of the bubble, in the thin-wall approximation, is roughly given by the inverse mass of the field, while the radius of the bubble is inversely proportional to the energy density difference. Therefore, for small energy density the thin-wall approximation is valid. We want know if the presence of gravity requires any new conditions so as to validate the thin-wall approximation. To this aim, let us substitute the metric function, Eq. (7.46), into the equation of motion for the scalar field, Eq. (7.22), and find

$$\left(f(r)\,\partial_r^2 + f'(r)\partial_r + \frac{2f(r)}{r}\partial_r \right) \varphi(r) = \frac{dV\,(\varphi, T)}{d\varphi} \quad , \tag{7.50}$$

where, for simplicity, we focus on a static configuration. Operationally, the thin-wall approximation allows us to drop terms that go as $1/r$ in the equation of motion, which are negligible near the bubble wall. Inspection of Eq. (7.50) shows that the presence of the metric function does not change anything, in particular, the term with $f'(r)$ scales as $f(r)/r$ and thus can be ignored for large bubbles. Therefore, even in our case, the thin-wall approximation remains valid as long as the radius of the bubble is much larger than the wall thickness.

We finally substitute the metric function into Eq. (7.38) to find

$$\begin{aligned} \dot{R}^2 = 1 \quad & - R^2 \left[4\pi^2 G^2 \sigma^2 + \frac{4\pi G(2\epsilon_+ - \epsilon_\varphi)}{3} + \frac{\epsilon_\varphi^2}{9\sigma^2} \right] \\ & - \frac{1}{R} \left[G(M_+ + M_-) + \frac{(M_+ - M_-)\epsilon_\varphi}{6\pi\sigma^2} \right] \\ & - \frac{1}{R^4} \left[\frac{(M_+ - M_-)^2}{16\pi^2\sigma^2} \right] \\ := U(R) \quad & . \end{aligned} \tag{7.51}$$

Two parameters from the scalar field theory, the surface tension σ and the vacuum energy ϵ_φ, now appear in the equation of motion of the wall. For cosmological phase transitions the origin of the seeds will be primordial black holes. Solutions of Eq. (7.51) clearly depend on all the parameters $M_\pm$, ϵ_+, σ and ϵ_φ. Thus, for starters, it is crucial to know if there exists any *absolute* bound on any single parameter. Figure 7.3 shows the generic behavior

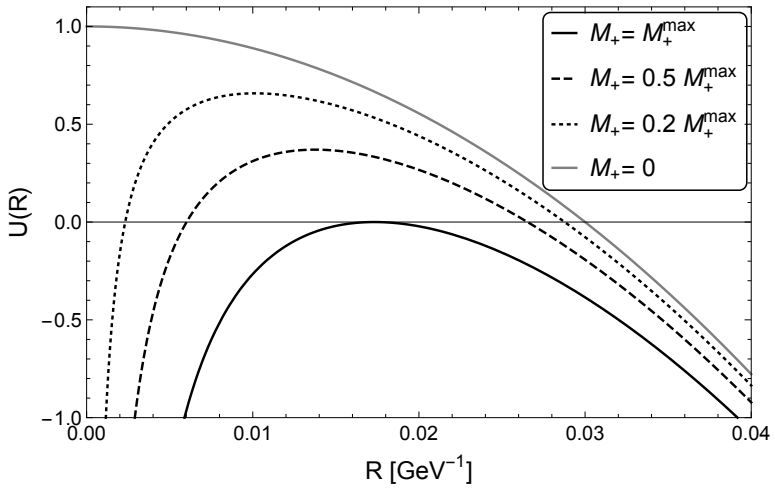

Figure 7.3: The potential $U(R)$ of Eq. (7.51) describing the bubble wall trajectory for varying seed black hole masses M_+ with $M_- = M_+$ and example parameter values $\sigma = 10^4\,\mathrm{GeV}^3$, $\epsilon_\varphi = 10^6\,\mathrm{GeV}^4$ and $\epsilon_+ - \epsilon_\varphi \sim \epsilon_{\mathrm{DE}}$ where ϵ_{DE} is the dark energy scale (setting $\epsilon_+ - \epsilon_\varphi = 0$ would not noticeably change the results). With these parameters, $M_+^{\max} = 3.5 \times 10^{17}\,M_{\mathrm{P}}$.

of the potential, $U(R)$, for an arbitrary choice of parameters. We immediately observe that for Eq. (7.51) to possess a solution the potential must be non-negative over some portion of its domain. First, let us restrict the mass of the black hole post-transition to be smaller or equal to that of the seed, $M_- \leq M_+$. Although in principle it could be larger, restricting M_- suffices for our purposes because, as we will show, the dominant tunneling configuration turns out to have the minimum accessible M_- at fixed seed M_+. Moving on, there exists an absolute bound on the seed mass as a function of the other variables, i.e $(\epsilon_+, \epsilon_\varphi, \sigma)$. It is straightforward to find this absolute value on M_+, at least numerically, by studying the single extremal point of the potential, i.e.

$$U'(R_{\mathrm{ext}}) = 0 \quad , \tag{7.52}$$

where all variables are fixed. Here, R_{ext} denotes the radius of the bubble wall at the extremal point of the potential. No solutions exist for Eq. (7.51) if and only if the value of the potential, at its critical point, is negative

$$U(R_{\mathrm{ext}}) < 0 \quad . \tag{7.53}$$

A close look at the potential illustrates the roles of $M_\pm$; increasing M_+ lowers the potential while increasing M_- raises the potential. Therefore, the maximum value of $U(R_{\mathrm{ext}})$ is obtained

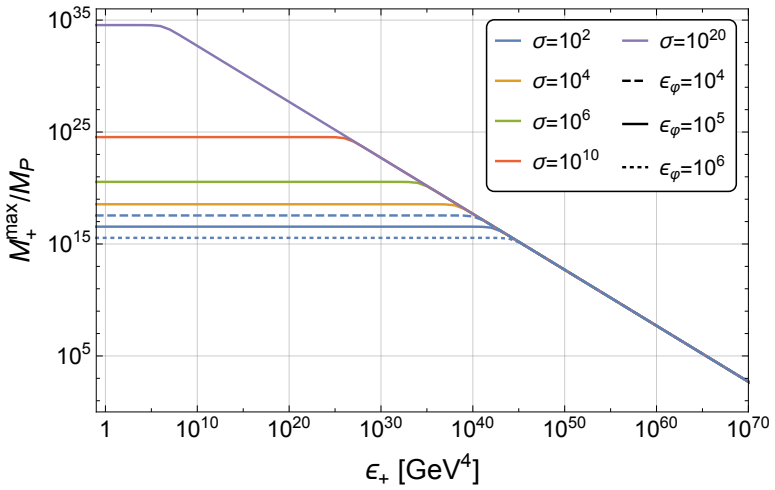

Figure 7.4: The absolute maximum seed black hole mass $M_+^{\max}$ as a function of the false vacuum energy ϵ_+ for varying surface tension σ (in GeV^3) and change in vacuum energy ϵ_φ (in GeV^4) values. Colour represents a changing σ value. Dashed, solid and dotted lines represent increases in ϵ_φ respectively. At large ϵ_+ values the dependence on σ and ϵ_φ is alleviated. Notice how, at lower ϵ_+, it is the ratio σ/ϵ_φ that determines $M_+^{\max}$ and not their separate values; for example $\sigma = 10^4$, $\epsilon_\varphi = 10^5$ and $\sigma = 10^{10}$, $\epsilon_\varphi = 10^{11}$ would have the same $M_+^{\max}$ value.

by setting M_- to its maximal value, i.e. $M_- = M_+$. Hence, using this in combination with the condition of Eq. (7.53) gives us an absolute upper bound on the seed mass, $M_+^{\max}$, that we determine numerically in Figure 7.4. Essentially, $M_+^{\max}$ remains constant up to a certain value of ϵ_+, which depends on σ and ϵ_φ, after which it decreases dramatically. Larger σ and smaller ϵ_φ reduce the plateau portion of $M_+^{\max}$. It is also important to notice that all the curves in Figure 7.4 merge at high ϵ_+ values, practically eliminating the dependence of $M_+^{\max}$ on σ and ϵ_φ. Apart from M_+, all other variables are not constrained except by the phenomenology of the underlying physics model. Inspection of exact numbers shown in Figure 7.4 implies the non-trivial constraint imposed by the physics model, through σ and ϵ_φ, on the potential relevance of primordial black holes in the phase transition process. For example, for electroweak like phase transitions, we have the typical values

$$\sigma^{\rm EW} \sim 10^4\,{\rm GeV}^3, \quad \epsilon_\varphi^{\rm EW} \sim 10^7\,{\rm GeV}^4 \quad , \tag{7.54}$$

leaving the upper limit on $M_+^{\max}$ to be around $10^{16} M_{\rm P}$ (blue curve in Figure 7.4). This shows that bubbles can only nucleate around relatively small black holes, roughly on the order of

10^{-22} solar masses ($\sim 10^8\,\mathrm{kg}$).

7.3.4 Static bubbles & periodic bounces

Before we move to construct explicit solutions of Eq. (7.51), it is imperative to pause and understand their qualtitative nature and physical meaning. In the presence of black holes, it is far from trivial to directly interpret these thin-wall instantons, and uncover the role they play in the tunneling process. To this aim, we advocate a conservative approach and rely on asserting direct correspondence with standard tunneling configurations in QFT (see Section 7.2). Generically, Eq. (7.51) displays two *disconnected* classes of solutions and we discuss each in turn.

The static branch: The first class contains static solutions, i.e. $R(\lambda) = R_{\rm s}$. For each input value of the seed mass, M_+, there exists a unique static branch where the potential vanishes at its extremal point

$$U(R_{\rm s}) = U'(R_{\rm s}) = 0 \Rightarrow \dot{R} = 0 \quad . \tag{7.55}$$

This situation is depicted by the solid black curve in Figure 7.3. We first solve Eq. (7.52) for $R_{\rm s}$, which makes the latter an explicit function of M_-, with all other parameters fixed. We then use Eq. (7.55) to determine the mass of the remnant black hole, that we denote by $M_-^{\rm s}$. With $M_-^{\rm s}$ in hand it is then straightforward to substitute back in and determine $R_{\rm s}$.

What is the physical significance of the static branch? Clearly, this class possesses a manifest O(3) spherical symmetry and is independent of Euclidean time. Using the dictionary of QFT (see Section 7.2) these solutions are the equivalent of the typical O(3) invariant *bubbles* familiar from finite-temperature phase transitions. In particular, and as we explained in Section 7.2, the transition in this case proceeds by thermal excitation over the potential barrier.

The oscillating branch: The second class of solutions emerge when $M_- \neq M_-^{\rm s}$. For each value in the admissible range, i.e.

$$M_- \in (M_-^{\rm s}, M_+] \quad , \tag{7.56}$$

the potential is positive semi-definite between $R_{\rm min}$ and $R_{\rm max}$, which satisfy

$$U(R_{\rm min}) = U(R_{\rm max}) = 0 \quad . \tag{7.57}$$

Between these two points, the wall separating the two vacua will *oscillate* indefinitely in Euclidean time, with a finite period β_λ. This period, crucially, is fully dictated by the dynamics of Eq. (7.51) and is an explicit function of the input parameters in the theory. Therefore, Eq. (7.51) possesses an infinite set of connected solutions parametrized by M_- in the admissible range. Moreover, we also stress that, by virtue of Eq. (7.32), the period of Euclidean times in both vacua, i.e. $(\beta_{\tau_+}, \beta_{\tau_-})$, are dictated dynamically.

We now ask the question: which, out of this infinite set, correspond to a valid tunneling configuration? Let us recall that the solution has an enhanced O(4) symmetry *only* in the CdL case, $M_+ = M_- = 0$, as we have demonstrated in Section 7.3.2. Based on our discussion in Section 7.2, we interpret these finite-period oscillating solutions as the equivalent of the *finite-period bounces* which describe thermally-assisted tunneling in QFT. Therefore, for each input value of M_+ we demand the period of oscillation to match the inverse temperature of the system, i.e.

$$\beta_\lambda = \frac{1}{T} \quad , \tag{7.58}$$

which presents a sufficient condition to single out a unique value for the remnant black hole mass, that we denote by M_-^β.

Quantitative analysis: We are now rightly oriented to numerically construct the solutions we are interested in. The size of ϵ_φ is born out of the underlying theory, however, ϵ_+ may be thought of as a totally free parameter. We make two choices for ϵ_+. First, in order to make contact with cosmology, ϵ_+ is fixed such that the vacuum energy after the transition matches the dark energy scale. Second, we pick a huge value of $10^{40}\,\text{GeV}^4$ to suppress the dependence of our analysis on the two other parameters, ϵ_φ and σ, as suggested by Figure 7.4.

We start by analyzing the static branch. Given an admissible value for M_+, fixing $(\epsilon_+, \epsilon_\varphi, \sigma)$, we solve Eq. (7.55) for M_-. This particular value, that we denote by M_-^s, provides a lower bound on the mass of the remnant black hole. In Figure 7.5 we provide the values of M_-^s for various parameter choices. We observe three striking features. First, M_-^s is generically very close to the seed mass M_+. Second, the difference $M_+ - M_-^s$ remains essentially constant for almost the whole admissible range of M_+. Third, increasing σ substantially increases the difference while increasing ϵ_φ decreases the difference. Note that the endpoint of each line corresponds to the configuration where $M_+ = M_+^{\max}$. Moving on, in Figure 7.6 we show the size of the static bubble, R_s, for the same parameter choices. We observe two main features.

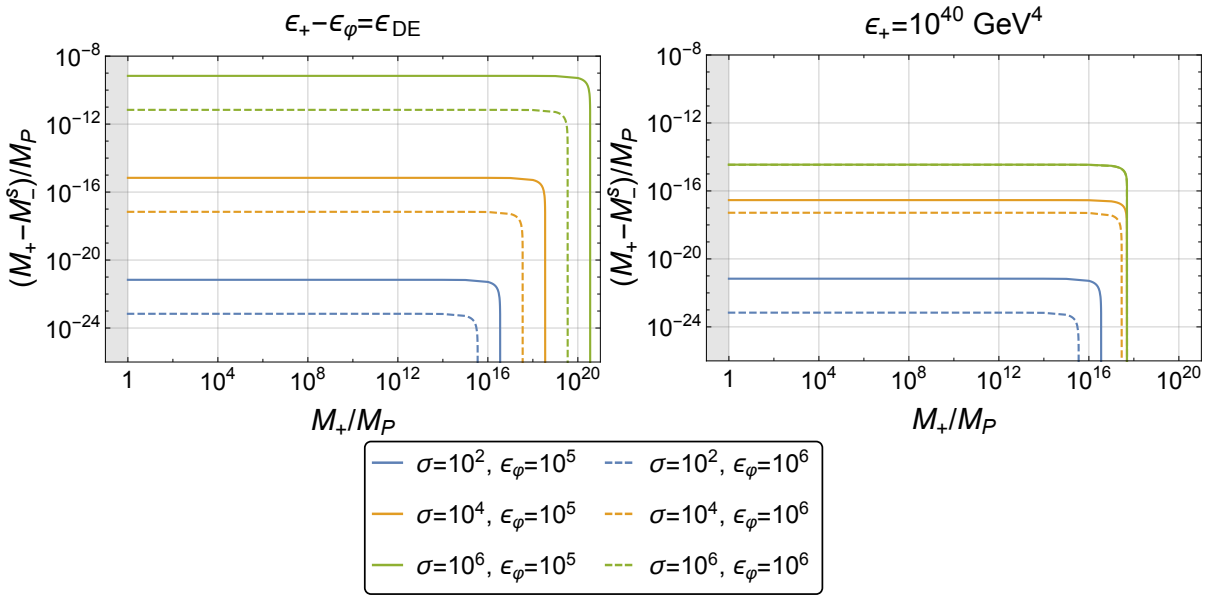

Figure 7.5: $M_+ - M_-^s$ as a function of M_+ for various σ (in GeV^3) and ϵ_φ (in GeV^4) values. The grey shaded region is sub-Planckian mass, $M_+ < M_{\rm P}$. Left: $\epsilon_+ - \epsilon_\varphi = \epsilon_{\rm DE}$. Right: $\epsilon_+ = 10^{40}\,{\rm GeV}^4$.

First, the seed black hole mass M_+ has an *insignificant* effect on $R_{\rm s}$ compared to σ and ϵ_φ. Second, increasing σ by an order of magnitude noticeably increases the size of the bubble, while increasing ϵ_φ has an equal but opposite effect.

The second class of solutions are those which are periodic. In order to show the meaning of the quantities $R_{\rm min}$, $R_{\rm max}$ and β_λ, a sketch is shown in Figure 7.7. The valid solution describing a finite-period bounce satisfies Eq. (7.58); therefore, it is essential to understand the dependence of the period β_λ on the input parameters. Figure 7.8 plots the inverse period, $1/\beta_\lambda$, as a function of M_+ for various σ and ϵ_φ values. It is important to note that $1/\beta_\lambda$ has a mild dependence on M_- as demonstrated in the bottom left plot of Figure 7.8. We observe the following features. First, $1/\beta_\lambda$ remains essentially constant with respect to M_+ until it approaches $M_+^{\rm max}$, at which point it sharply decreases to a finite minimum value. However, changing σ and ϵ_φ drastically alter $1/\beta_\lambda$ in comparison to M_+. Second, the inverse period increases by an order of magnitude if either σ decreases or ϵ_φ increases by an order of magnitude. This essentially means that the characteristics of the particle physics model controls whether or not we have a valid oscillating tunneling configuration. Given a set of $(\epsilon_+, \epsilon_\varphi, \sigma, M_+)$, the finite-period bounce satisfying the matching condition Eq. (7.58) is obtained by continuously varying M_- until M_-^β is found. If no solution is found then black

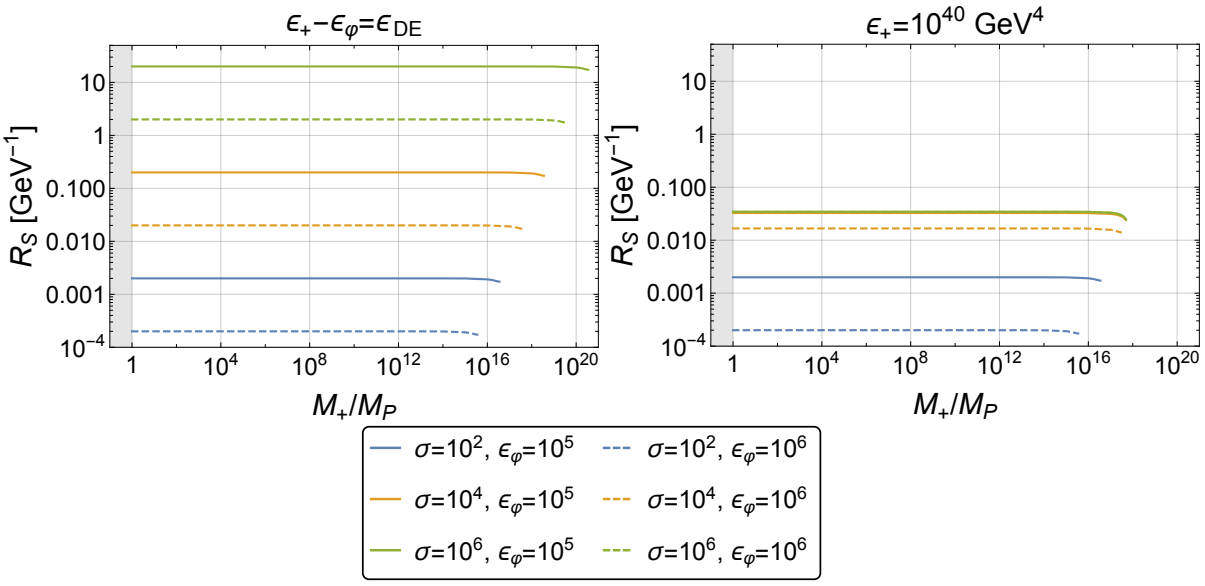

Figure 7.6: R_s as a function of M_+ for various σ (in GeV^3) and ϵ_φ (in GeV^4) values. The grey shaded region is sub-Planckian mass, $M_+ < M_P$. Left: $\epsilon_+ - \epsilon_\varphi = \epsilon_{DE}$. Right: $\epsilon_+ = 10^{40}\,\text{GeV}^4$.

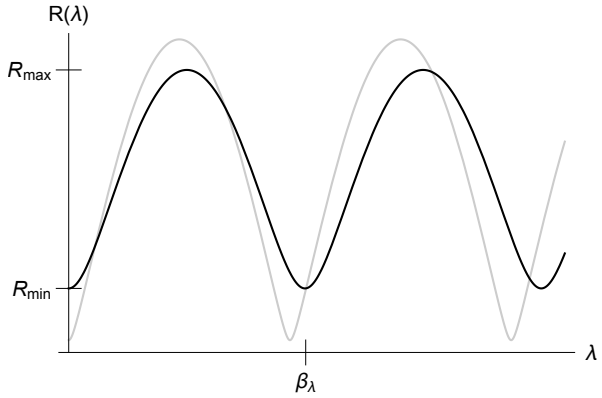

Figure 7.7: A sketch of two oscillating solutions. The labels correspond to the black line, which has a period β_λ. The minimum R_{min} and maximum R_{max} are the roots of the potential $U(R)$ given in Eq. (7.51).

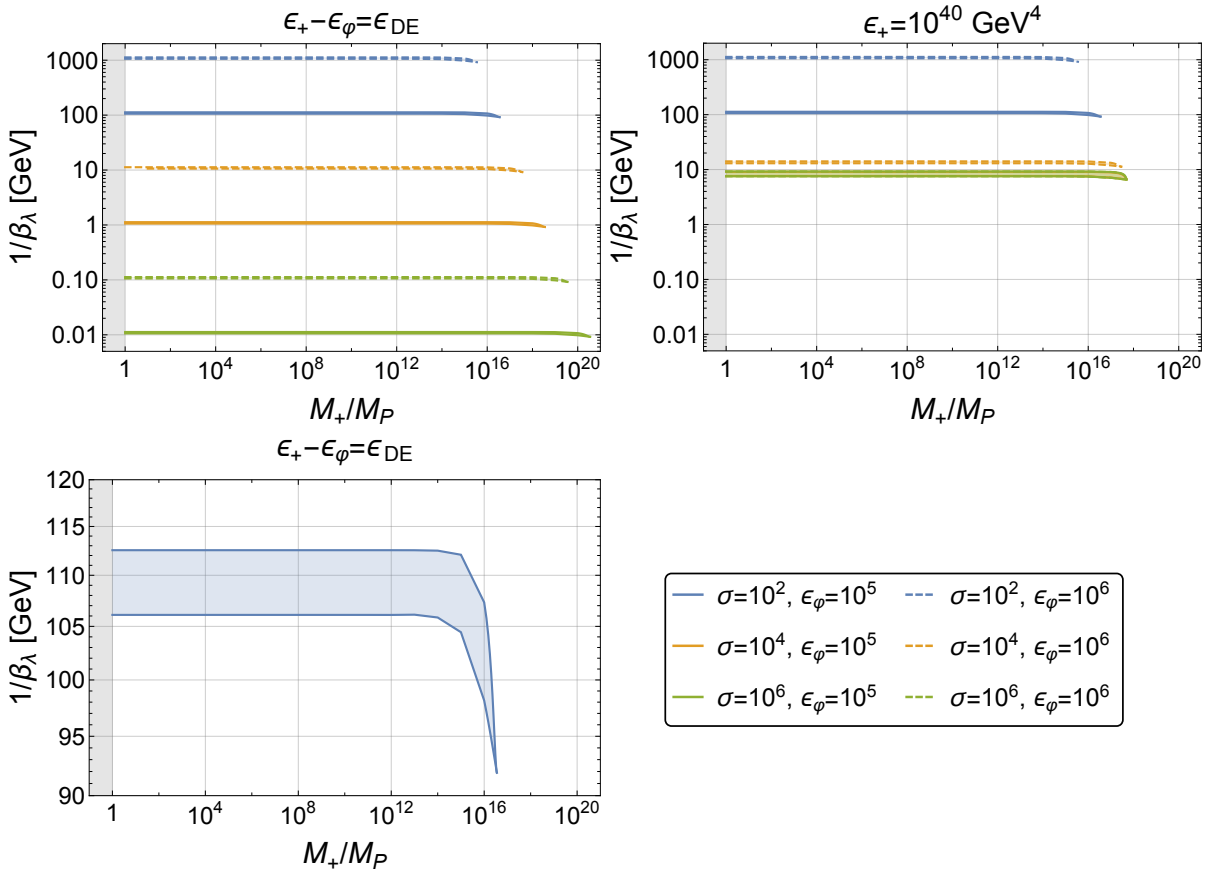

Figure 7.8: The inverse period $1/\beta_\lambda$ of the oscillating solutions as a function of M_+ for various σ (in GeV^3) and ϵ_φ (in GeV^4) values. The grey shaded region is sub-Planckian mass, $M_+ < M_P$. Top Left: $\epsilon_+ - \epsilon_\varphi = \epsilon_{DE}$. Top Right: $\epsilon_+ = 10^{40}\,\text{GeV}^4$. Bottom Left: Focus on the $1/\beta_\lambda$ region for $\sigma = 10^2$ GeV^3, $\epsilon_\varphi = 10^5$ GeV^4 and $\epsilon_+ - \epsilon_\varphi = \epsilon_{DE}$. For the $1/\beta_\lambda$ regions, the upper limit is given by approaching the static limit $M_- \to M_-^s$, while the lower limit is given by $M_- = M_+$.

holes have no effect on tunneling via finite-period bounces and we are only left with the static branch.

Finally, we would like to highlight the importance of $M_+^{\max}$. Consider the $1/\beta_\lambda$ plots of Figure 7.8. As we alluded to before, a very large value of ϵ_+ constrains the limiting values of $M_+^{\max}$ to be identical irrespective of the other parameters. That is the reason behind the difference in the top two plots of Figure 7.8, where we see the merger of many of the lines as we move from the left to the right plot. The message is clear and interesting: it is not the independent values of σ, ϵ_φ and ϵ_+ that control the period of oscillation, but rather it is the *combination* of the three parameters that sets the actual value of $M_+^{\max}$, as shown in Figure 7.4.

Qualitative final comments: Having explicitly described the solutions to Eq. (7.51) and their physical interpretations, one cannot help but inquire whether the dynamics of Eq. (7.51) admit a solution that we could interpret as a zero-temperature bounce. In standard QFT, the special feature of vacuum tunneling manifests in the O(4) symmetry of the bounce. To answer our question, therefore, one needs to inspect if a particular solution to Eq. (7.51) could possess a *hidden* O(4) symmetry.

Here we can make the analogy with the isolated case $M_- = M_+ = 0$ (CdL) that was discussed in Section 7.3.2. There, the specific sinusoidal form of the solution, Eq. (7.41), was in fact hiding the symmetry, which becomes manifest when the solution is written in global coordinates. Now in the presence of black holes, the solution $R(\lambda)$ plotted in Figure 7.7 shows that the existence of such a hidden symmetry is no longer possible. Simply put, any solution to Eq. (7.51) can generally be written as a Fourier sum, with frequencies $\omega_n = 2\pi n/\beta_\lambda$ where n is an integer. The existence of an infinite tower of Fourier modes confirms that a hidden O(4) symmetry is not possible. In essence, the wall, in the presence of black holes, is not following a simple parametric equation, in contrast to Eq. (7.44).

7.4 The Tunneling Exponent

We now move to evaluate the Euclidean action given the thin-wall solutions constructed in the last section. This is a standard computation, and the only subtlety concerns the presence of conical sections in the geometry. The latter arise due to the mismatch between the oscillation period, β_λ, and the Hawking temperatures of both horizons. In the case of the Einstein-

Hilbert action, there is a systematic technique to compute the contribution of the conical singularity to the action. In summary, consider a 4-dimensional spacetime which contains one or more conical deficit angles, α_i, the integral over the Ricci scalar curvature reads [65]

$$\int d^4x\,\sqrt{g}\,\mathcal{R} = \sum_i 4\pi(1-\alpha_i)A_i + \int d^4x\,\sqrt{g}\,\mathcal{R}_{\rm reg} \quad , \tag{7.59}$$

where $\mathcal{R}_{\rm reg}$ is the non-singular part of the Ricci scalar and A_i is the 2-dimensional area of the conical surface. In the thin-wall approximation, the bubble action is composed of two components. First, we have the *bulk* component represented by contributions of both the false and true vacua. The second component is a *surface* contribution represented by the bubble wall.

The bulk Euclidean action is very simple and reads

$$I_E^{\rm bulk}(g,\varphi) = -\frac{M_{\rm P}^2}{2}\int d^4x\,\sqrt{g}\,\left(\mathcal{R}-2\Lambda\right) \quad , \tag{7.60}$$

where the cosmological constant contains the contribution of the potential energy density of the scalar field. Let us start with the true vacuum where the only conical singularity is at the black hole horizon. The conical deficit reads

$$\alpha_h = \beta_{\tau_-}/\beta_h \quad , \tag{7.61}$$

and thus Eq. (7.60) becomes

$$I_E^{\rm bulk}(g^-,\varphi_0(T)) = -\frac{A_-}{4G} + \frac{1}{4G}\int d\tau_-\,R^2\,\frac{df_-(R)}{dR} + \frac{\beta_{\tau_-}}{4G}\left(\frac{A_-}{\beta_h} - 2GM_- + \frac{2\Lambda_- r_h^3}{3}\right) \quad . \tag{7.62}$$

In fact, using Eq. (7.48), the last term in brackets vanishes identically. In the false vacuum, we only have the cosmological horizon with a conical deficit

$$\alpha_c = \beta_{\tau_+}/\beta_c \quad , \tag{7.63}$$

and therefore

$$I_E^{\rm bulk}(g^+,0) = -\frac{A_c}{4G} - \frac{1}{4G}\int d\tau_+\,R^2\frac{df_+(R)}{dR} + \frac{\beta_{\tau_+}}{4G}\left(\frac{A_c}{\beta_c} + 2GM_+ - \frac{2\Lambda_- r_c^3}{3}\right) \quad , \tag{7.64}$$

where similarly the combination in brackets vanishes identically.

Moving on, the surface Euclidean action arises from the Hawking-Gibbons-York boundary term [107, 130] evaluated at the wall boundary

$$I_E^{\rm surf}(g) = \frac{1}{8\pi G}\int d^3x\,\sqrt{h}\,\left(K_+ - K_-\right) \quad , \tag{7.65}$$

plus the surface energy in the scalar field profile

$$I_E^{\rm surf}(g,\varphi) = \sigma \int d^3x\,\sqrt{h} = 4\pi\sigma \int d\lambda\, R^2(\lambda) \quad . \tag{7.66}$$

We can combine the two pieces above if we notice that $K_+ - K_- = -12\pi G\sigma$ by virtue of Eq. (7.34). Hence, the total wall contribution is

$$I_E^{\rm surf} = -2\pi\sigma \int d\lambda\, R^2(\lambda) = \frac{1}{2G} \int d\lambda\, R(\lambda)\left(f_+\dot{\tau}_+ - f_-\dot{\tau}_-\right) \quad , \tag{7.67}$$

where Eq. (7.36) has been used to substitute for the surface tension[3]. The complete bubble action is now easily found by subtracting off the Euclidean action of the false vacuum

$$I_{\rm SdS} = -\frac{A_+}{4G} - \frac{A_c}{4G} \quad , \tag{7.68}$$

giving

$$B = \frac{A_+ - A_-}{4G} + \frac{1}{4G} \int d\lambda\, \left[\left(2Rf_+ - R^2 f_+'\right)\dot{\tau}_+ - \left(2Rf_- - R^2 f_-'\right)\dot{\tau}_-\right] \quad . \tag{7.69}$$

This is the general form for the tunneling exponent computed in the thin-wall approximation, and has been obtained in Ref. [66]. The full numerical procedure is now clear; the solution of the equation of motion, Eq. (7.51), which satisfies the temperature matching condition, Eq. (7.58), is obtained, substituted into Eq. (7.69) and integrated over a single period β_λ. These steps are quite involved, nevertheless, the evaluation of B can be simplified somewhat by casting the integral in terms of R rather than λ. Using $d\lambda = dR\, d\lambda/dR = dR/\sqrt{U(R)}$ and Eq. (7.32) in addition to

$$\left(2Rf_\pm - R^2 f_\pm'\right) = 2(R - 3GM_\pm) \quad , \tag{7.70}$$

the tunneling exponent becomes

$$B = \frac{A_+ - A_-}{4G} + \frac{1}{2G} \int_{R_{\rm min}}^{R_{\rm max}} dR\, \left[2(R-3GM_+)\frac{1}{f_+\sqrt{U(R)}}\left(f_+ - U(R)\right)^{1/2} - \{+ \to -\}\right] \quad . \tag{7.71}$$

This form uncovers the remarkable feature that the tunneling exponent does not *explicitly* depend on the exact functional form of the wall trajectory $R(\lambda)$. Rather, it just depends on the potential $U(R)$ and the metric function. This is reminiscent of the typical situation when using the thin-wall approximation, in which the tunneling exponent becomes independent of

[3]This step is justified as long as σ is a constant that does not depend on geometry, which is true in our case.

the exact bubble profile. Let us also note that it appears as if Eq. (7.71) is independent of the temperature of the system. In reality, however, the temperature dependence is manifested in the value of M_-^β, which is determined by the matching condition of Eq. (7.58).

In the case of a static solution, Eq. (7.69) simplifies further. With $R(\lambda) \to R_s$ and $M_- \to M_-^s$, Eq. (7.32) becomes

$$\dot{\tau}_\pm = \frac{1}{\sqrt{f_\pm(R_s)}} \quad , \tag{7.72}$$

and the static bounce action takes the form

$$B_{\rm s} = \frac{A_+ - A_-}{4G} + \frac{\beta_\lambda}{2G}\left[\frac{(R_s - 3GM_+)}{\sqrt{f_+(R_s)}} - \frac{(R_s - 3GM_-^s)}{\sqrt{f_-(R_s)}}\right] \quad , \tag{7.73}$$

where it is paramount to realize that β_λ is not dictated by the dynamics any more since the wall is static. Notice that in the static case it is impossible to change variables as we have done to reach Eq. (7.71), simply because $U(R_{\rm s}) = 0$, and thus the appropriate result in this case is given by Eq. (7.73). Since the static solution is the equivalent of the O(3) symmetric configurations in flat-space QFT, it is natural to set $\beta_\lambda = 1/T$. With our mass range, Eq. (7.56), the term in square brackets in Eq. (7.73) is negative definite. Finally, it is important to realize that the β_λ-dependent term in Eq. (7.73) is absent from the corresponding action of Refs. [64, 66, 67, 137] simply because these works only consider vacuum phase transitions. In other words, there is no natural period dictated by the physics and the integral part of Eq. (7.69) can naturally be set to zero.

7.4.1 Quantitative analysis

We are now in a position to quantify the potential effect of black holes on the decay exponent of cosmological first-order phase transitions. To begin, we study the situation in the full range of M_- given by Eq. (7.56), without worrying about any matching conditions. As a means to isolate the potential effects of primordial black holes, we compare our tunneling exponent to the CdL result. This is easily obtained by plugging Eq. (7.41) in Eq. (7.69) (or Eq. (7.71) with $R_{\rm min} = 0$), setting $M_+ = M_- = 0$, and integrating. The result is

$$B_{\rm CdL} = 2\pi^2\sigma\zeta^{-3/2} + 12\pi^2 M_{\rm P}^4\left[\frac{\left(1 - f_+^{3/2}\left(1/\zeta^{1/2}\right)\right)}{\epsilon_+} - \frac{\left(1 - f_-^{3/2}\left(1/\zeta^{1/2}\right)\right)}{\epsilon_-}\right] \quad , \tag{7.74}$$

where ζ is given in Eq. (7.40). The results are shown in Figure 7.9. With the upper limit given by the maximum remnant mass $M_- = M_+$ and the lower limit by the static solutions

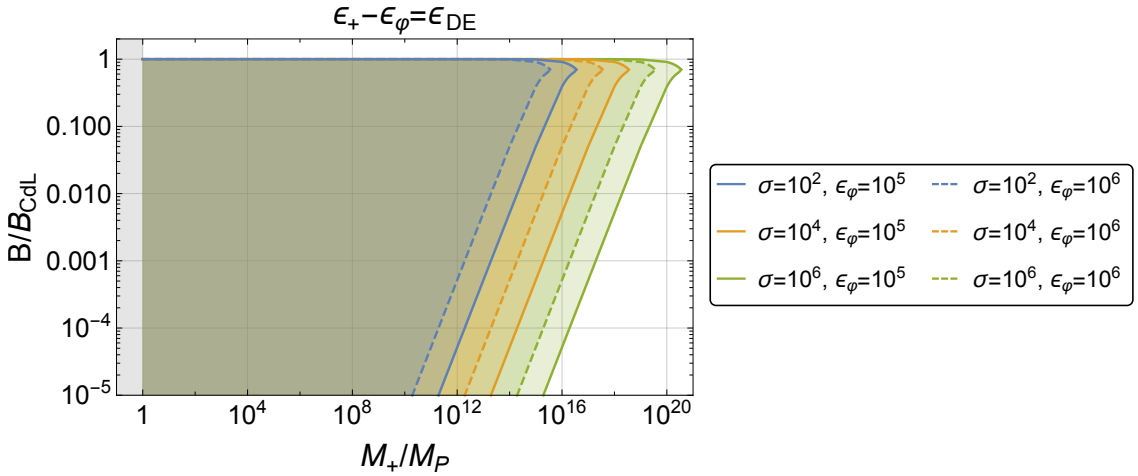

Figure 7.9: The tunneling action of Eq. (7.69) as a function of the seed black hole mass M_+, with the upper limit given by $M_+^{\max}$. The shaded regions are generated by varying M_- in the admissible range. At fixed M_+, the upper limit of any single shaded region represents the point $M_- = M_+$, while the lower limit is the static case $M_- = M_-^s$. Small seed black holes present arbitrary reduction in B. For the static solutions an example $T = 100\,\text{GeV}$ is used. Changing the temperature does not change the generic features.

$M_- = M_-^s$, the shaded region represents the range of values of B/B_{CdL} for all solutions. Immediately noticeable is the smooth transition to the CdL limit at the top of any of the shaded regions as the mass approaches zero, i.e. $M_- = M_+ \to 0$. Compared to B_{CdL}, we observe the possible reduction in B by orders of magnitude, to even an arbitrary degree at low M_+. The effect of M_- on B is quite remarkable given how small the mass difference is, as seen in Figure 7.5. In fact, the largest reduction in mass results in the greatest reduction in the tunneling exponent, namely, at fixed M_+ the smallest B is attained at M_-^{s}. Notice that the static branch of solutions is completely disconnected from the CdL limit.

Additionally, the seed mass M_+ plays a crucial role. Increasing M_+ drastically pushes up the lower limit of B, thus limiting the possible reduction. On the other hand, effects on the upper limit of B are less pronounced as we increase M_+. We do not observe any noticeable difference up until the maximum point, $M_+^{\max}$, at which B starts to slightly decrease. As expected, at $M_+^{\max}$ both the upper and lower limits on B meet at the same point. The surprising feature is that regardless of all the other parameters, the ratio B/B_{CdL} attains a common value of ~ 0.7. Finally, the effects of σ and ϵ_φ are simple yet substantial; by changing the maximum $M_+^{\max}$, as in Figure 7.4, the profile of B is shifted correspondingly.

In particular, at fixed value of $B/B_{\rm CdL}$ the largest accessible seed mass changes by orders of magnitude by varying σ and ϵ_φ. To summarise, transitions with the largest change in black hole mass, culminating in static solutions, possess the greatest prospects for improving transition rates. This improvement is reduced as the seed black hole mass M_+ is increased.

We end this section by comparing our findings to the main conclusions drawn up in Refs. [64, 66, 67, 137], although it is important to stress that we consider finite-temperature phase transitions in contrast to the vacuum case studied in those references. Yet, it is still true that our conclusions about the dominant tunneling configurations are in exact agreement with the findings of those papers. In particular, Ref. [66] found that the dominant tunneling configuration is either a static solution or an oscillating solution but without a remnant black hole ($M_- = 0$), see Figure 9 in appendix A of Ref. [66]. The delineation between the two situations, at fixed seed mass M_+, is dictated by the factor $\bar{\sigma}\ell$ in Refs. [64, 66, 67, 137]. In our case this factor is $\bar{\sigma}\ell \simeq \sigma\sqrt{\epsilon_\varphi}/M_P$, which for all our parameter space is a very tiny number. As evident from the analysis in Ref. [66], as the factor $\bar{\sigma}\ell$ approaches zero the dominant solution is just given by the static branch. This is precisely in agreement with what we observe in Figure 7.9 above.

7.4.2 Bubble nucleation criteria with black holes

Before we discuss an example electroweak phase transition, it is important to define the nucleation criteria in the presence of black holes. In a typical (flat-space) first-order cosmological phase transition proceeding through thermal excitation, the transition rate per unit volume is given by the expression

$$\frac{\Gamma}{V} = A\, e^{-B_{\rm flat}} \quad , \quad B_{\rm flat} = \frac{S_3}{T} \ , \tag{7.75}$$

where S_3 is the energy of the critical bubble and the prefactor A is of mass dimension four, commonly approximated as T^4. A successful transition is defined to be the nucleation of one bubble per Hubble time per Hubble volume. In a radiation dominated universe, this results in a nucleation condition on the exponent

$$B_{\rm flat}^{\rm nuc.} \sim 4 \log\left(\frac{M_P}{T}\right) \ . \tag{7.76}$$

If the exponent ever reaches this value or below the transition is deemed successful. For electroweak-scale transitions this takes the value $B_{\rm flat} \sim 140$.

Once black holes are included, however, one cannot define a nucleation rate per volume because the presence of the black hole breaks the spatial translation symmetry of the instanton. Therefore, there is no factor of volume, as in Eq. (7.75), and instead we have a transition rate

$$\Gamma = A\, e^{-B} \ , \tag{7.77}$$

describing nucleation around a single black hole, where the prefactor A is of mass dimension one. Unfortunately, the prefactor A is unknown. Even in the simple case where gravity is assumed *not* to be quantized, computing the determinant of one-loop fluctuations of the scalar field requires massive work since the background geometry is very involved. Still, following Ref. [64], one can attempt a rough estimate using $A \sim (GM_+)^{-1}$. An alternative nucleation condition can then be derived for the black hole case. Requiring that a single bubble be nucleated per Hubble time, the nucleation condition on B is now

$$B_{\rm BH}^{\rm nuc.} \sim \log\left(\frac{M_P^3}{T^2 M_+}\right) \ . \tag{7.78}$$

For an electroweak-scale transition and a reference mass $M_+ = 10^{14}\, M_P$ this condition is $B_{\rm BH} \sim 42$. One then might be tempted to think that black holes are not efficient in the nucleation process because a lower B is harder to achieve in general. However, given the large reductions possible in Euclidean action seen in Figure 7.9, it is likely black holes can satisfy this condition, Eq. (7.78), at a temperature higher than the usual temperatures required for flat space, thereby dominating the nucleation process.

As mentioned, Eq. (7.77) describes the rate of nucleation around a single black hole. In reality, there will be a population of primordial black holes with a given number and mass distribution. To get an idea of the true nucleation rate, Eq. (7.77) should be multiplied by the total number of black holes $N_{\rm PBH}$ in a given Hubble volume. Hence, the nucleation condition, now the probability to nucleate one bubble per Hubble time across the full population of black holes, reads

$$B_{\rm BH}^{\rm nuc.} \sim \log\left(\frac{N_{\rm PBH} M_P^3}{T^2 M_+}\right) \ . \tag{7.79}$$

A larger number of black holes, $N_{\rm PBH}$, will increase $B_{\rm BH}^{\rm nuc.}$ therefore making nucleation easier to achieve, as one would expect.

7.4.3 Electroweak-like phase transition

As we explained in Section 7.3, there are only two tunneling configurations at any fixed value of the parameters $(M_+, \epsilon_+, \epsilon_\varphi, \sigma)$. These are parametrized by M_-^β and $M_-^{\rm s}$, which represent the oscillating and static instantons of Eq. (7.51). It is crucial to note that the matched solution, M_-^β, is not guaranteed to exist because the period, β_λ, might never be equal to the inverse temperature of the system for $T < T_c$. If the two solutions exist, the decay rate will then be determined by the smaller tunneling exponent amongst both configurations. Our goal now is to compare the tunneling exponents of the two solutions. Indeed, Figure 7.9 shows that the static solution, at fixed M_+, has the lowest action, nevertheless, we aim to know the exact difference in the tunneling exponent when static solutions are compared with their oscillating counterparts which satisfy the condition Eq. (7.58).

We have in mind an electroweak-like scenario, where tunneling proceeds via the following finite-temperature potential

$$V(\varphi, T) = \frac{1}{2}\left(DT^2 - \mu^2\right)\varphi^2 - \frac{E}{3}T\varphi^3 + \frac{\lambda}{4}\varphi^4 \quad , \tag{7.80}$$

where, for definiteness, $\mu = 88\,\text{GeV}$ and $\lambda = 0.129$. The values of D and E are dependent on the details of the underlying model. We use the Standard Model value of $D = 0.34$. To replicate BSM effects and get a stronger first-order phase transition[4], the value of E is enhanced above its Standard Model value and taken to be $E = 0.21$. Consequently, we have a critical temperature $T_c = 171.3\,\text{GeV}$. The surface tension is calculated using the equation

$$\sigma = \int_{\varphi_+}^{\varphi_-} d\varphi\, \sqrt{2V(\varphi, T_c)}\ , \tag{7.81}$$

giving the value $\sigma = 2.2 \times 10^5\,\text{GeV}^3$. Finally, ϵ_φ is a function of temperature that we do not quote here. A comment is due at this stage, the formula for the surface tension in Eq. (7.81) is only valid in flat space. In the present case, one has to double check if the radius of the bubble is large enough compared to the horizon size of the remnant black hole. In our parameter space, we found that this is indeed true, and so we continue to use the simple formula in Eq. (7.81).

Unfortunately, with these typical parameters we did not find it possible to obtain a valid oscillating solution which hinders the comparison that we aim for. We circumvent this by

[4]Such an effect can easily be achieved by, for example, adding a scalar singlet to the Standard Model that does not gain a vacuum-expectation-value.

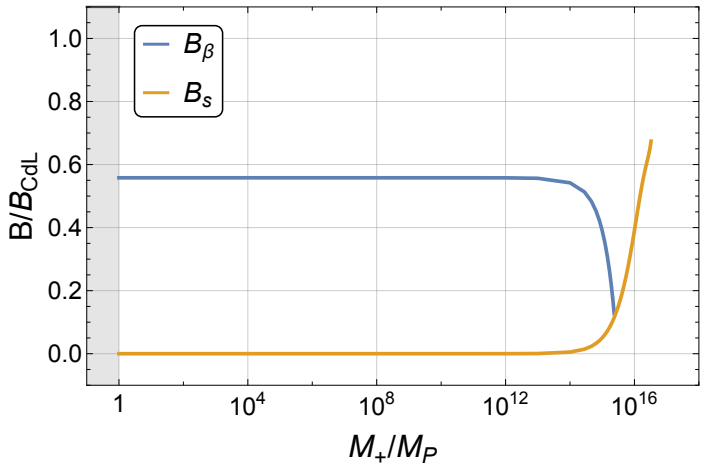

Figure 7.10: The tunneling action as a function of the seed black hole mass M_+ for some example electroweak-scale parameters $T_c = 112\,\text{GeV}$ and $\sigma = 10^4\,\text{GeV}^3$. Blue Line: Matching oscillating solutions calculated using Eq. (7.71). Orange Line: Static solutions calculated using Eq. (7.73). Matching occurs at $T = 111.4\,\text{GeV}$ where $\epsilon_\varphi = 10^7\,\text{GeV}^4$.

using $T_c = 112.8\,\text{GeV}$, $\sigma = 10^4\,\text{GeV}^3$ and a mock ϵ_φ. We have scanned the range $10^6 \leq \epsilon_\varphi \leq 10^8\,\text{GeV}^4$ to find an oscillating solution satisfying Eq. (7.58). Figure 7.8 shows that, in comparison to M_+, small changes in ϵ_φ strongly alter the inverse period of the oscillating solutions; there is likely only a small window over which matching is possible. For our example matching is satisfied at $T = 111.4\,\text{GeV}$ and $\epsilon_\varphi = 10^7\,\text{GeV}^4$. The tunneling exponent of both solutions are found and compared in Figure 7.10. We observe that the oscillating solution provides a significant reduction in B, however, static solutions always dominate as expected. Increasing M_+ has the opposite effect on the two solutions. While both remain essentially constant over small values of the seed mass, at higher M_+ the oscillating result B_β drops rapidly while the static result B_s rises. The increase in B_s can already be seen from Figure 7.9. The drop in B_β is due to the matching remnant mass, M_-^β, approaching the static limit M_-^s as M_+ increases, as illustrated by Figure 7.5. The maximum value of M_+ where matching is still attainable is definitely smaller than the absolute maximum M_+^max and represents the point where the two curves meet in Figure 7.10. To be clear, we observe that the lines never cross and the static solutions are always dominant over the periodic solutions.

Finally, we turn back to the realistic scenario of Eq. (7.80) and focus entirely on the static solutions which, as explained, provide the dominant tunneling configurations. In fact, our central equation (7.73) can be simplified further to highlight its thermodynamic meaning.

With the values $\sigma \simeq 2.7 \times 10^5\,\mathrm{GeV}^3$ and $\epsilon_\varphi \simeq 10^6\,\mathrm{GeV}^4$, notice that we possess a hierarchy $r_h \ll R_s \ll r_c$, where r_h and r_c are the black hole and cosmological horizon radii respectively (see Figure 7.6). In this case, $f_\pm(R_s) \simeq 1$ and therefore the static tunneling action becomes

$$B_s \simeq \frac{A_+ - A_-}{4G} - \frac{3\beta}{2}(M_+ - M_-^s)\ . \tag{7.82}$$

The meaning of each term is now transparent. The first is the difference in Hawking entropy between the seed and remnant black holes. While the second represents the difference between the Arnowitt-Deser-Misner (ADM) masses (or the energy) of seed and remnant black holes.

Now we can ask, how efficient are black holes in seeding the transition? To get an idea, we compare B_s to the thermal tunneling exponent in flat-space given by the familiar expression

$$B_\mathrm{flat} = \frac{S_3}{T}\quad , \tag{7.83}$$

where S_3 denotes the energy of the O(3) invariant critical bubble[5]. Figure 7.11 shows the result which exhibits interesting features that might not be expected a priori. First of all, the presence of black holes does not necessarily improve the tunneling rate. For example, if we use the maximum available value, M_+^max, no reduction is observed. Second, one has to go to relatively lower values of the seed mass in order to attain a noticeable reduction. The reduction in B, in and of itself, is a positive outcome but, as outlined in Section 7.4.2, the two scenarios have different nucleation conditions. Hence, a comparison between B_s and S_3/T is not strictly correct. Rather, the relevant comparison is that of the respective nucleation temperatures. However, even in the most restricted case of a single black hole (where the nucleation condition is $B_s \lesssim 42$ as found from Eq. (7.78)), Figure 7.11 shows that black hole initiated nucleation occurs before traditional thermal tunneling for $M_+ \lesssim 10^{15}\,M_P$. Prospects for black holes improving transition rates are certainly very promising.

The complete picture, however, can only be understood after some further considerations. Firstly, various aspects, which will be outlined in Section 7.5, constrain the phenomenological viability of seed black hole masses at formation. Secondly, knowledge of the precise mass and

[5]We note that the comparison between B_s and B_CdL is not really meaningful for phenomenology, and this is why we employ S_3/T instead. This is because the CdL result represents decay via quantum vacuum fluctuations (T=0), and is not appropriate for thermal transitions. Ideally, one might try and compute the thermal tunneling exponent in the mere presence of a cosmological constant, and compare directly to B_s. Nevertheless, we believe this will not be important since, for phenomenological purposes, B_CdL is essentially identical to the flat-space O(4)-invariant bounce action [61].

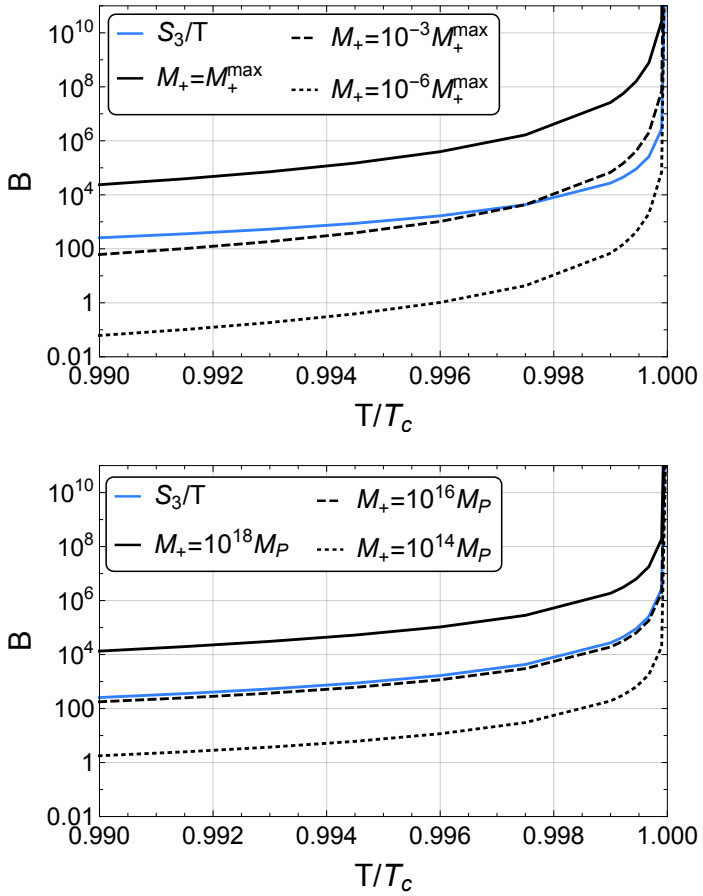

Figure 7.11: The static Euclidean action for black hole induced tunneling $B_{\rm s}$ (black lines) and the typical thermal tunneling rate S_3/T (blue line) for the example electroweak potential of Eq. (7.80), with the critical temperature $T_c = 171.3\,\text{GeV}$ and surface tension $\sigma = 2.7 \times 10^5\,\text{GeV}^3$. Note that $M_+^{\rm max}$ decreases with T due to increasing ϵ_φ. Top: M_+ is a fraction of $M_+^{\rm max}$. The solid, dashed and dotted lines represent $M_+ = M_+^{\rm max}$, $10^{-3}M_+^{\rm max}$ and $10^{-6}M_+^{\rm max}$ respectively. Bottom: M_+ is a constant value. The solid, dashed and dotted lines represent $M_+ = 10^{18}M_{\rm P}$, $10^{16}M_{\rm P}$ and $10^{14}M_{\rm P}$ respectively.

number distributions of PBHs is necessary to make accurate predictions in regards to the way the transition proceeds. While consideration of a specific PBH population is left to future work, we discuss the main transition scenarios in Section 7.6.

7.5 Routes for phenomenology

We have provided a framework for calculating the effect of black holes on generic finite temperature first-order phase transitions, encompassing arbitrary masses, cosmological constants and temperatures. Our central results for an EW-like transition, displayed in Figure 7.11, need a few more inputs in order to conduct a full phenomenological study and assess accurately the role of primordial black holes in cosmological phase transitions. This section is a presentation of what inputs we require to achieve our goal in future works.

7.5.1 Primordial Black Holes: Formation and Abundance

The first consideration needed for phenomenology is the issue of primordial black holes, in particular, their mass spectrum and abundance close to the electroweak epoch. PBHs can be formed through various mechanisms [144–147] (see reviews [136, 148]). For instance, in the case formation proceeds due to the collapse of large density perturbations during the radiation era [144, 149–153], an estimate of the mass is given by [148]

$$M_{\rm PBH} \simeq \frac{c^3 t}{G} \simeq 10^{43} \left(\frac{t_{\rm cos}}{\rm sec.}\right) M_{\rm P} \quad , \tag{7.84}$$

where $t_{\rm cos}$ denotes cosmological time. Therefore, a wide range of PBH masses becomes available between the end of inflation and the EW epoch. For instance, shortly following inflation, $t_{\rm cos} \sim 10^{-32}$ seconds and the approximate mass is $M_{\rm PBH} \simeq 10^{10} M_P$, while a PBH forming at the EW epoch is as large as $M_{\rm PBH} \simeq 10^{30} M_P$. Given the central results of Figure 7.11, we are guaranteed to find relevant PBH masses, $M_{\rm PBH} \lesssim 10^{15} M_P$, at the EW epoch.

Additionally, the observational constraints on PBH abundance need to be taken into account. For the mass range we are interested in, the most stringent constraint derives from Big Bang Nucleosynthesis (BBN) because such black holes would have evaporated at the epoch of BBN (see Figure 4 in Ref. [136]). Precisely, black holes in the mass range $\sim 10^{15} - 10^{19} M_P$ can comprise between $\sim 10^{-17} - 10^{-24}$ of the fraction of the universe's energy density at the time of their formation [136]. Therefore, for a given relevant seed mass M_+, and knowing the

relation between formation time and mass, Eq. (7.84), we can directly constrain the available number density at the EW epoch[6]. The direct consequence of this bound concerns how the phase transition actually proceeds, as we discuss in detail in Section 7.6.

7.5.2 Black Hole Decay via Hawking Radiation

It is well known that black holes decay via Hawking radiation [155, 156], endangering the completion of phase transitions seeded by black holes[7]. To claim a black hole of certain mass M_+ is relevant to the phase transition, at least one bubble per horizon volume must nucleate *before* the black hole decays via Hawking radiation. Therefore, the transition rate Γ, given in Eq. (7.77), must be greater than the Hawking evaporation rate Γ_H [64]. However, calculating Γ requires knowledge of the coefficient A. As discussed in Section 7.4.2, this is unknown once gravitational effects are included and, at best, a very rough bound on the seed mass can thus be made.

Given the known nucleation timescale of EW-like phase transitions in the absence of black holes, we can adopt a worst case scenario to estimate a lower bound on seed masses. Our logic is as follows; we are only interested in the scenario where black holes noticeably improve the transition rate. This then dictates the *worst case* transition timescale to be that of flat space, $\tau_{\rm EW} \sim 10^{-11}$ seconds. Given this strategy, we use the known lifetime of a black hole, of mass M, against Hawking evaporation (see e.g. [158]) to place a lower bound on M_+. This translates to the condition

$$M_+ \gtrsim \left(\frac{\tau_{\rm EW}}{G^2}\right)^{1/3} \simeq 10^{12} M_P \quad . \tag{7.85}$$

We remind that this is not a very strict bound because black holes of such masses, as we have shown, enhance the tunneling rate appreciably which further loosens the bound on M_+ from Hawking evaporation. Finally, we stress again that it is important to compute, or at least properly estimate, the coefficient A in order to obtain decisive bounds.

[6] Ref. [154] considered the dependence of the PBH masses and number density, at formation time, on the spectral index of primordial density fluctuations.

[7] A recent paper [157] performed an interesting study that looks in detail at the effect of Hawking radiation on the dynamics of a *vacuum* transition, considered previously in Refs. [64, 66, 67, 137].

7.6 Discussion and prospects for gravitational waves

In light of the constraints outlined in Section 7.5, we return to our electroweak-like example, Eq. (7.80), and discuss the consequences for gravitational wave production. Given that the dependence on temperature is virtually the same as in flat-space, more general conclusions can be made about the nature of the phase transition. It is clear that the interplay between a black hole seeded transition and traditional thermal excitation offers a variety of physical scenarios for nucleation. This is strictly dependent on both the seed mass M_+ as well as the number density of primordial black holes, $n_{\rm PBH}$, at the EW epoch. This latter quantity is indeed constrained by BBN observations, as we discussed. In Section 7.4.2 we derived how the condition on the Euclidean action for successful nucleation differs between the traditional case, $B^{\rm nuc.}_{\rm flat}$, and the black hole case, $B^{\rm nuc.}_{\rm BH}$. Using these conditions, and assuming that the corresponding Euclidean actions B_s and S_3/T indeed have the same dependence on T (as observed in Figure 7.11), we now describe these possible scenarios and the consequences for the resulting gravitational wave spectrum [21, 23].

Typical thermal excitation dominates: First is the simple case where black holes play no role and the traditional thermal excitation dominates. In terms of the nucleation conditions, that is $B_s \gg B^{\rm nuc.}_{\rm BH}$ and $S_3/T \leq B^{\rm nuc.}_{\rm flat}$. Such a scenario is most likely at large seed masses M_+.

Black holes dominate, many black holes: The second scenario is the opposite; there are many black holes and the transition proceeds solely via nucleation around them. This corresponds to a large $n_{\rm PBH}$ with $B_s \leq B^{\rm nuc.}_{\rm BH}$ and $S_3/T \gg B^{\rm nuc.}_{\rm flat}$. Consequently, the bubble properties are heavily influenced by the distribution of black holes - a large number of black holes, and therefore nucleation sites, results in smaller bubbles at collision. Hence, a gravitational wave spectrum with a higher frequency and reduced amplitude is produced.

Black holes dominate, few black holes: The third case is again a transition seeded exclusively by black holes but now with a small number of black holes. That is small $n_{\rm PBH}$ with $B_s < B^{\rm nuc.}_{\rm BH}$ and $S_3/T \gg B^{\rm nuc.}_{\rm flat}$. Fewer bubbles are nucleated and they therefore have a larger radius upon collision. The result could be a strong gravitational wave signal at lower frequencies.

Mixed: Lastly, there could be a crossover scenario where both typical thermal excitation and black hole nucleation can occur. That is $B_s \sim B_{\rm BH}^{\rm nuc.}$ and $S_3/T \sim B_{\rm flat}^{\rm nuc.}$. The outcome here is again highly dependent on the distribution of black holes. If there are few, the typical thermal transition is likely to dominate and proceed as normal. If there are many, then black hole nucleation could dominate resulting in many, smaller bubbles. As previously mentioned, this produces a gravitational wave spectrum with a higher frequency and reduced amplitude.

Having described the possible scenarios, we can now reconsider our basic EW-like transition of Section 7.4.3, described by Eq. (7.80). Clearly, with our values of the coefficients D and E it is true that $S_3/T \sim B_{\rm flat}^{\rm nuc.}$ and therefore we are in the mixed case. It remains then to decide if black holes can dominate the nucleation process. This requires that we know both the average number of bubbles with a flat space core and the average number of black holes $N_{\rm PBH}$ in the mass range $10^{12} - 10^{15} M_P$.

The average number of bubbles with a flat space core can be calculated quite easily knowing the average bubble radius. Using Ref. [23], we get $N_{\rm bubbles} \simeq 10^{10}$ (this number is based on using a bubble wall velocity of $v_{\rm wall} = 1/3$). On the other hand, the BBN constraints can be used directly to set an upper bound on the total number of black holes per Hubble volume at the EW epoch, given the relevant mass range $10^{12} - 10^{15} M_P$. The quantity constrained by BBN is the fraction of the universe's mass in PBHs at their formation time [136],

$$\beta(M) \equiv \frac{\rho_{\rm PBH}(t_{\rm form})}{\rho(t_{\rm form})} \simeq \frac{M}{T_{\rm form}} \frac{n_{\rm PBH}(t)}{s(t)} \ , \tag{7.86}$$

where $s(t)$ is the entropy density and the ratio $n_{\rm PBH}/s$ is conserved. For our mass range, we read off the bound $\beta(M) \lesssim 10^{-17}$ from Ref. [136]. Using Eq. (7.84) to relate the formation time to the mass, we find simply

$$N_{\rm PBH} \lesssim 10^{13} \ . \tag{7.87}$$

We observe the total number of black holes could be orders of magnitude larger than the average number of bubbles with a flat space core, $N_{\rm bubbles}$. This means there is a real possibility for black hole seeds to dominate the transition. Notwithstanding, one still needs a dedicated study to simulate the seeded bubble collisions in order to predict the resulting gravitational wave spectrum.

7.7 Summary

In this study we have provided a basis for quantifying the effect of black holes acting as nucleation sites for bubbles during a finite-temperature cosmological phase transition. Using a thin-wall formalism, the equation of motion describing the bubble wall is derived building on earlier works [62,64]. There are two types of solution - oscillating and static. By comparing to the typical flat-space solutions, it is clear that these correspond to thermally-assisted quantum tunneling and thermal excitation respectively. While a static solution is always available, an oscillating solution is only valid when the inverse of its period, β_λ^{-1}, matches the temperature, T, of the universe.

We then calculate the transition exponent, given by the Euclidean action, including the conical singularities arising from a mismatch between the Hawking temperature of the black holes and the periods of Euclidean time. It turns out that the static solutions are always dominant (have the lowest action). The static action is given in Eq. (7.73) and simply requires four input parameters: the seed black hole mass M_+, false vacuum energy density ϵ_+, bubble surface tension σ and the change in vacuum energy density ϵ_φ. While the last two parameters, σ and ϵ_φ, are provided by the scalar field theory describing the transition, M_+ and ϵ_+ are free parameters. A quantitative analysis across the parameter space revealed that reducing the seed mass M_+ reduces the action, becoming arbitrarily small at lower masses.

While a reduction in transition exponent is promising for improving transition rates, it does not tell the full story - a comparison to typical thermal excitation in flat-space must be made. In particular, the nucleation temperatures of the two methods must be compared. Importantly, the criterion for successful nucleation is altered in the presence of black holes and this new form is given in Eq. (7.79). To provide a realistic example, the formalism was applied to an electroweak-like phase transition described by Eq. (7.80). Focusing on the dominant static solutions, Figure 7.11 shows that although black hole seeds do not always improve nucleation rates (larger seed masses), enhancements are observed for seed masses $M_+ \lesssim 10^{15}\, M_P$.

It is clear that black holes acting a nucleation sites could have significant consequences for finite temperature cosmological phase transitions, offering improvements to transition rates by greatly reducing the transition exponent. In Section 7.6, we outlined the various transition scenarios based on a comparison between the two tunneling mechanisms which are expected

to coexist. For our EW example, we found that BBN constraints are not too stringent and indeed black holes can play a dominant role in cosmological phase transitions.

Chapter 8

Conclusion

This work has broadly focused on bubble nucleation rates during first-order cosmological phase transitions, and the role this plays in determining a successful transition, in two main applications - the restricted holographic phase transition and the prospect of black holes acting as nucleation sites.

To begin, the established description of vacuum decay in first-order phase transitions was covered in Chapter 2. Three methods of transition - zero temperature bounce, finite temperature bounce and thermal excitation - were introduced and the steps for calculating the transition rate detailed, with particular focus on the transition exponent B. While numerical methods are needed for a full description, the thin-wall approximation provides an illuminating analytical description; in particular, elucidating the importance of the surface tension σ and vacuum energy difference ϵ_φ. For transitions around the electroweak scale, it was shown that $B \lesssim 140$ is the necessary nucleation condition to determine success across the relevant parameter space. The chapter concludes by outlining how to calculate the resulting gravitational wave spectrum, dependent on the features of the transition - one of the most important phenomenological outcomes.

With a description of vacuum decay established, the first of two main topics in this thesis was introduced in Chapter 3 - the holographic phase transition. The foundation is the Randall-Sundrum (RS) extra dimensional model in which a single, warped, spatial extra-dimension bordered by branes is added as a means of solving the hierarchy problem, with the Standard Model confined to one of these branes. The size of the new dimension is dynamically determined by a scalar field known as the radion μ. Finite temperature studies had shown that the model was not stable at high temperatures until it was realised, through

the use of holography, that at such temperatures the stable state is in fact a five-dimensional (5D) Schwarzschild-anti-de Sitter geometry in which the Standard Model brane is replaced by a black hole horizon. As the universe cooled the RS setup became energetically favourable and a phase transition occurred. From the four-dimensional (4D) viewpoint, as informed by holography, this corresponds to a conformal field theory (CFT) transitioning from a de-confined to a confined phase. However, the transition remains rather unconventional - the governing potential has a "nearly conformal" structure, characterised by a large separation in minima when compared to the size of the maximum. The result is a highly supercooled phase transition where the nucleation temperature T_N can be orders of magnitude smaller than the critical temperature T_c. Consequently, the transition often struggles to achieve $B \lesssim 140$ and complete. A key reason is the parameter N. From the 4D perspective this is the size of the CFT gauge group; from the 5D perspective it is related to the combination $M_* l$ where M_* is the 5D Planck mass and l is the inverse of the curvature of the anti-de Sitter space. A small N improves transition rates, yet a large N is necessary for the semi-classical description of gravity to remain valid. This tension hinders the prospects of the transition. Consequently, previous studies had been restricted to low N where the validity of the theory can be questioned.

Chapter 4 presents published work solving the tension in N through the introduction of brane-localised curvature. This addition simply alters the kinetic term of the radion field μ. The added freedom, facilitated through a new parameter θ_{IR}, can allow successful phase transitions with $N \sim 10^2$. Additionally, this was achieved with a positive mass squared, ϵ, for the bulk scalar field. Previous studies, meanwhile, had required a negative ϵ due to benefits this provides for transition rates.

Nevertheless, a bigger issue with the holographic phase transition remains. As also outlined in Chapter 3, the description of the high temperature, black hole phase is incomplete. Conventional phase transitions are described by a single scalar field present across both phases. The holographic phase transition, however, is described by two separate 4D fields corresponding to the two phases. The first is the Hawking temperature of the black hole T_H which describes the position of the black hole horizon in the high temperature phase. The second is the previously mentioned radion μ, related to the size of the extra dimension. Numerous methods have been used to incorporate and combine the two sides, yet all are approximations and have their drawbacks. A common approach is to combine the two fields into a single new field, with the potential of each describing a separate region in field space of a new combined

potential. The major issue here lies in a lack of knowledge in regards to the true form for the kinetic term of the black hole field T_H. Chapter 5 is a short chapter outlining an attempt to derive an approximate kinetic term for T_H by promoting it to a function of the brane spatial coordinates. Unfortunately, the result is always divergent and a more appropriate form could not be found. However, further attempts lead to an alternative approach considering the black hole instead as a nucleation site for bubbles. While complexities remain over how, or even if, such an approach is relevant for the holographic phase transition, it was realised that black holes acting as nucleation sites had yet to be considered in the context of conventional finite temperature, first-order, cosmological phase transitions.

With this realisation, discussion moved to the second of the two main topics in this thesis - black holes as bubble nucleation sites in cosmological phase transitions. Chapter 6 introduced the idea as so far studied in the literature - during zero temperature phase transitions. The premise is first put into context by considering false vacuum decay in the presence of gravity. It turns out that decay from a positive vacuum energy (de Sitter space) facilitates nucleation. However, improvements are likely to be negligible for any conventional transition. The concept of black hole seeds is then introduced. Using a thin-wall based approach, an initial study found that the tunnelling action B could be reduced by almost a factor of two, having an important impact on transition rates. Yet, this initial investigation was constrained to a constant black hole mass and ignored contributions from conical singularities. Recently, however, new work alleviated these issues and found arbitrary reductions in B at small seed masses. It seems that black holes could have a remarkable impact on phase transitions.

Nevertheless, previous studies had only been concerned with zero temperature transitions. Chapter 7 details work submitted for publication on applying this formalism to finite temperature cosmological phase transitions. It was argued that, through symmetry comparisons with the standard flat-space QFT solutions, it is necessary to consider black holes as nucleation sites in a finite temperature context. This offers a natural period for the Euclidean time - the inverse of the temperature of the system, as is the case in the well established flat-space formalism. Investigation demonstrated that the main influence of temperature is in determining the change in vacuum energy, $\epsilon_\varphi(T)$, as given by the underlying finite temperature potential for the scalar field. It is again found that arbitrary reductions in Euclidean action B are possible for small seed black hole masses. However, to understand if improvements have been made over a typical thermal transition it is necessary to compare nucleation temperatures.

A new nucleation condition in the presence of black holes is derived which depends on the mass and total number of black holes. The formalism was applied to an example electroweak phase transition where it was shown, even in the most limiting case of a single black hole, black hole nucleation dominates for seed masses $M_+ \lesssim 10^{15}\, M_P$. While limits from primordial nulceosynthesis and Hawking decay provide upper and lower bounds on initial masses respectively, the picture is only complete once an accurate description of the primordial black hole population is considered. Depending on the prominence of black hole nucleation in the transition, the resulting gravitational wave spectrum could be significantly altered due to differences in bubble sizes and velocities at collision.

The work of this thesis has attempted to answer some issues relating to the holographic phase transition and the role played by black holes in bubble nucleation. Nevertheless, there of course remain many more unanswered questions. In regards to the holographic phase transition, Chapters 3 and 4, the most remarkable breakthrough would be a full gravitational instanton linking the two phases. In the absence of this, likely, incredibly difficult solution, some improvement in the kinetic term for the T_H field would allow studies to take a united approach in treating the high temperature phase and have greater confidence in their results. In terms of modifying the transition, changes to the potential of the bulk scalar field, both in the bulk and near the branes, as well as moving away from the small mass squared (ϵ) limit look promising.

In regards to black holes acting as nucleation sites for finite temperature transitions, the work of Chapter 7 presents a truly initial investigation, and is by no means the end. Primarily, robust application requires an understanding of the number and mass distributions of primordial black holes at the time of transition. This is the natural starting point for further improvements. Additionally, true understanding of the bubble nucleation rate requires knowledge of the pre-factor A, a quantity currently only very roughly estimated, and not just the transition exponent B. Finally, extending the formalism beyond the thin-wall regime would be a significant step, allowing application in far wider regions of parameter space.

Bibliography

[1] D. A. Kirzhnits and A. D. Linde, "Macroscopic Consequences of the Weinberg Model," *Phys. Lett.* **42B** (1972) 471–474.

[2] D. A. Kirzhnits, "Weinberg model in the hot universe," *JETP Lett.* **15** (1972) 529–531. [Pisma Zh. Eksp. Teor. Fiz.15,745(1972)].

[3] L. Dolan and R. Jackiw, "Symmetry Behavior at Finite Temperature," *Phys. Rev.* **D9** (1974) 3320–3341.

[4] S. Weinberg, "Gauge and Global Symmetries at High Temperature," *Phys. Rev.* **D9** (1974) 3357–3378.

[5] D. A. Kirzhnits and A. D. Linde, "Symmetry Behavior in Gauge Theories," *Annals Phys.* **101** (1976) 195–238.

[6] A. D. Linde, "Phase Transitions in Gauge Theories and Cosmology," *Rept. Prog. Phys.* **42** (1979) 389.

[7] R. Durrer and A. Neronov, "Cosmological Magnetic Fields: Their Generation, Evolution and Observation," *Astron. Astrophys. Rev.* **21** (2013) 62, `arXiv:1303.7121 [astro-ph.CO]`.

[8] A. D. Sakharov, "Violation of CP Invariance, C asymmetry, and baryon asymmetry of the universe," *Pisma Zh. Eksp. Teor. Fiz.* **5** (1967) 32–35. [Usp. Fiz. Nauk161,no.5,61(1991)].

[9] S. Weinberg, "Cosmological Production of Baryons," *Phys. Rev. Lett.* **42** (1979) 850–853.

[10] A. D. Sakharov, "Baryonic Asymmetry of the Universe," *Sov. Phys. JETP* **49** (1979) 594–599. [Zh. Eksp. Teor. Fiz.76,1172(1979)].

[11] V. A. Kuzmin, V. A. Rubakov, and M. E. Shaposhnikov, "On the Anomalous Electroweak Baryon Number Nonconservation in the Early Universe," *Phys. Lett.* **155B** (1985) 36.

[12] A. Riotto, "Theories of baryogenesis," in *Proceedings, Summer School in High-energy physics and cosmology: Trieste, Italy, June 29-July 17, 1998*, pp. 326–436. 1998. arXiv:hep-ph/9807454 [hep-ph].

[13] M. Trodden, "Electroweak baryogenesis," *Rev. Mod. Phys.* **71** (1999) 1463–1500, arXiv:hep-ph/9803479 [hep-ph].

[14] J. M. Cline, "Baryogenesis," in *Les Houches Summer School - Session 86: Particle Physics and Cosmology: The Fabric of Spacetime Les Houches, France, July 31-August 25, 2006*. 2006. arXiv:hep-ph/0609145 [hep-ph].

[15] D. E. Morrissey and M. J. Ramsey-Musolf, "Electroweak baryogenesis," *New J. Phys.* **14** (2012) 125003, arXiv:1206.2942 [hep-ph].

[16] J. M. Cline, "Is electroweak baryogenesis dead?," *Phil. Trans. Roy. Soc. Lond.* **A376** no. 2114, (2018) 20170116, arXiv:1704.08911 [hep-ph]. [,339(2017)].

[17] C. J. Hogan, "Gravitational radiation from cosmological phase transitions," *Mon. Not. Roy. Astron. Soc.* **218** (1986) 629–636.

[18] A. Kosowsky, M. S. Turner, and R. Watkins, "Gravitational waves from first order cosmological phase transitions," *Phys. Rev. Lett.* **69** (1992) 2026–2029.

[19] M. Kamionkowski, A. Kosowsky, and M. S. Turner, "Gravitational radiation from first order phase transitions," *Phys. Rev.* **D49** (1994) 2837–2851, arXiv:astro-ph/9310044 [astro-ph].

[20] J. R. Espinosa, T. Konstandin, J. M. No, and G. Servant, "Energy Budget of Cosmological First-order Phase Transitions," *JCAP* **1006** (2010) 028, arXiv:1004.4187 [hep-ph].

[21] C. Caprini *et al.*, "Science with the space-based interferometer eLISA. II: Gravitational waves from cosmological phase transitions," *JCAP* **1604** no. 04, (2016) 001, arXiv:1512.06239 [astro-ph.CO].

[22] D. J. Weir, "Gravitational waves from a first order electroweak phase transition: a brief review," *Phil. Trans. Roy. Soc. Lond.* **A376** no. 2114, (2018) 20170126, arXiv:1705.01783 [hep-ph].

[23] C. Caprini *et al.*, "Detecting gravitational waves from cosmological phase transitions with LISA: an update," *JCAP* **03** (2020) 024, arXiv:1910.13125 [astro-ph.CO].

[24] F. Wilczek, "Application of the renormalization group to a second order QCD phase transition," *Int. J. Mod. Phys.* **A7** (1992) 3911–3925. [Erratum: Int. J. Mod. Phys.A7,6951(1992)].

[25] K. Rajagopal and F. Wilczek, "Static and dynamic critical phenomena at a second order QCD phase transition," *Nucl. Phys.* **B399** (1993) 395–425, arXiv:hep-ph/9210253 [hep-ph].

[26] T. Schäfer and E. V. Shuryak, "Instantons in QCD," *Rev. Mod. Phys.* **70** (1998) 323–426, arXiv:hep-ph/9610451 [hep-ph].

[27] S. Dimopoulos and H. Georgi, "Softly Broken Supersymmetry and SU(5)," *Nucl. Phys.* **B193** (1981) 150–162.

[28] A. Mazumdar and G. White, "Review of cosmic phase transitions: their significance and experimental signatures," *Rept. Prog. Phys.* **82** no. 7, (2019) 076901, arXiv:1811.01948 [hep-ph].

[29] S. R. Coleman, "The Fate of the False Vacuum. 1. Semiclassical Theory," *Phys. Rev.* **D15** (1977) 2929–2936. [Erratum: Phys. Rev.D16,1248(1977)].

[30] C. G. Callan, Jr. and S. R. Coleman, "The Fate of the False Vacuum. 2. First Quantum Corrections," *Phys. Rev.* **D16** (1977) 1762–1768.

[31] A. D. Linde, "Fate of the False Vacuum at Finite Temperature: Theory and Applications," *Phys. Lett.* **100B** (1981) 37–40.

[32] A. D. Linde, "Decay of the False Vacuum at Finite Temperature," *Nucl. Phys.* **B216** (1983) 421. [Erratum: Nucl. Phys.B223,544(1983)].

[33] K. Kajantie, M. Laine, K. Rummukainen, and M. E. Shaposhnikov, "Is there a hot electroweak phase transition at m(H) larger or equal to m(W)?," *Phys. Rev. Lett.* **77** (1996) 2887–2890, arXiv:hep-ph/9605288.

[34] M. Gurtler, E.-M. Ilgenfritz, and A. Schiller, "Where the electroweak phase transition ends," *Phys. Rev. D* **56** (1997) 3888–3895, arXiv:hep-lat/9704013.

[35] K. Rummukainen, M. Tsypin, K. Kajantie, M. Laine, and M. E. Shaposhnikov, "The Universality class of the electroweak theory," *Nucl. Phys. B* **532** (1998) 283–314, arXiv:hep-lat/9805013.

[36] Y. Aoki, F. Csikor, Z. Fodor, and A. Ukawa, "The Endpoint of the first order phase transition of the SU(2) gauge Higgs model on a four-dimensional isotropic lattice," *Phys. Rev. D* **60** (1999) 013001, arXiv:hep-lat/9901021.

[37] F. Csikor, Z. Fodor, and J. Heitger, "Endpoint of the hot electroweak phase transition," *Phys. Rev. Lett.* **82** (1999) 21–24, arXiv:hep-ph/9809291.

[38] J. Espinosa and M. Quiros, "The Electroweak phase transition with a singlet," *Phys. Lett. B* **305** (1993) 98–105, arXiv:hep-ph/9301285.

[39] J. Choi and R. Volkas, "Real Higgs singlet and the electroweak phase transition in the Standard Model," *Phys. Lett. B* **317** (1993) 385–391, arXiv:hep-ph/9308234.

[40] M. Carena, M. Quiros, and C. Wagner, "Opening the window for electroweak baryogenesis," *Phys. Lett. B* **380** (1996) 81–91, arXiv:hep-ph/9603420.

[41] D. Delepine, J. Gerard, R. Gonzalez Felipe, and J. Weyers, "A Light stop and electroweak baryogenesis," *Phys. Lett. B* **386** (1996) 183–188, arXiv:hep-ph/9604440.

[42] S. Ham, Y. Jeong, and S. Oh, "Electroweak phase transition in an extension of the standard model with a real Higgs singlet," *J. Phys. G* **31** no. 8, (2005) 857–871, arXiv:hep-ph/0411352.

[43] J. R. Espinosa and M. Quiros, "Novel Effects in Electroweak Breaking from a Hidden Sector," *Phys. Rev. D* **76** (2007) 076004, arXiv:hep-ph/0701145.

[44] S. Profumo, M. J. Ramsey-Musolf, and G. Shaughnessy, "Singlet Higgs phenomenology and the electroweak phase transition," *JHEP* **08** (2007) 010, arXiv:0705.2425 [hep-ph].

[45] S. J. Huber and M. Sopena, "An efficient approach to electroweak bubble velocities," arXiv:1302.1044 [hep-ph].

[46] **LIGO Scientific, Virgo** Collaboration, B. P. Abbott *et al.*, "Observation of Gravitational Waves from a Binary Black Hole Merger," *Phys. Rev. Lett.* **116** no. 6, (2016) 061102, arXiv:1602.03837 [gr-qc].

[47] **LISA** Collaboration, P. Amaro-Seoane *et al.*, "Laser Interferometer Space Antenna," arXiv:1702.00786 [astro-ph.IM].

[48] N. Arkani-Hamed, S. Dimopoulos, and G. R. Dvali, "The Hierarchy problem and new dimensions at a millimeter," *Phys. Lett.* **B429** (1998) 263–272, arXiv:hep-ph/9803315 [hep-ph].

[49] L. Randall and R. Sundrum, "A Large mass hierarchy from a small extra dimension," *Phys. Rev. Lett.* **83** (1999) 3370–3373, arXiv:hep-ph/9905221 [hep-ph].

[50] P. Binetruy, C. Deffayet, and D. Langlois, "Nonconventional cosmology from a brane universe," *Nucl. Phys.* **B565** (2000) 269–287, arXiv:hep-th/9905012 [hep-th].

[51] J. M. Cline, C. Grojean, and G. Servant, "Cosmological expansion in the presence of extra dimensions," *Phys. Rev. Lett.* **83** (1999) 4245, arXiv:hep-ph/9906523 [hep-ph].

[52] C. Csaki, M. Graesser, L. Randall, and J. Terning, "Cosmology of brane models with radion stabilization," *Phys. Rev.* **D62** (2000) 045015, arXiv:hep-ph/9911406 [hep-ph].

[53] J. Lesgourgues, S. Pastor, M. Peloso, and L. Sorbo, "Cosmology of the Randall-Sundrum model after dilaton stabilization," *Phys. Lett.* **B489** (2000) 411, arXiv:hep-ph/0004086 [hep-ph].

[54] P. Creminelli, A. Nicolis, and R. Rattazzi, "Holography and the electroweak phase transition," *JHEP* **03** (2002) 051, arXiv:hep-th/0107141 [hep-th].

[55] J. M. Maldacena, "The Large N limit of superconformal field theories and supergravity," *Int. J. Theor. Phys.* **38** (1999) 1113–1133, arXiv:hep-th/9711200 [hep-th]. [Adv. Theor. Math. Phys.2,231(1998)].

[56] T. Konstandin and G. Servant, "Cosmological Consequences of Nearly Conformal Dynamics at the TeV scale," *JCAP* **1112** (2011) 009, arXiv:1104.4791 [hep-ph].

[57] L. Randall and G. Servant, "Gravitational waves from warped spacetime," *JHEP* **05** (2007) 054, arXiv:hep-ph/0607158 [hep-ph].

[58] G. Nardini, M. Quiros, and A. Wulzer, "A Confining Strong First-Order Electroweak Phase Transition," *JHEP* **09** (2007) 077, arXiv:0706.3388 [hep-ph].

[59] T. Konstandin, G. Nardini, and M. Quiros, "Gravitational Backreaction Effects on the Holographic Phase Transition," *Phys. Rev.* **D82** (2010) 083513, arXiv:1007.1468 [hep-ph].

[60] E. Megías, G. Nardini, and M. Quirós, "Cosmological Phase Transitions in Warped Space: Gravitational Waves and Collider Signatures," *JHEP* **09** (2018) 095, arXiv:1806.04877 [hep-ph].

[61] S. R. Coleman and F. De Luccia, "Gravitational Effects on and of Vacuum Decay," *Phys. Rev.* **D21** (1980) 3305.

[62] W. A. Hiscock, "CAN BLACK HOLES NUCLEATE VACUUM PHASE TRANSITIONS?," *Phys. Rev.* **D35** (1987) 1161–1170.

[63] W. Israel, "Singular hypersurfaces and thin shells in general relativity," *Nuovo Cim.* **B44S10** (1966) 1. [Nuovo Cim.B44,1(1966)].

[64] R. Gregory, I. G. Moss, and B. Withers, "Black holes as bubble nucleation sites," *JHEP* **03** (2014) 081, arXiv:1401.0017 [hep-th].

[65] D. V. Fursaev and S. N. Solodukhin, "On the description of the Riemannian geometry in the presence of conical defects," *Phys. Rev.* **D52** (1995) 2133–2143, arXiv:hep-th/9501127 [hep-th].

[66] P. Burda, R. Gregory, and I. Moss, "Vacuum metastability with black holes," *JHEP* **08** (2015) 114, arXiv:1503.07331 [hep-th].

[67] P. Burda, R. Gregory, and I. Moss, "The fate of the Higgs vacuum," *JHEP* **06** (2016) 025, arXiv:1601.02152 [hep-th].

[68] B. M. Dillon, B. K. El-Menoufi, S. J. Huber, and J. P. Manuel, "Rapid holographic phase transition with brane-localized curvature," *Phys. Rev. D* **98** no. 8, (2018) 086005, arXiv:1708.02953 [hep-th].

[69] B. K. El-Menoufi, S. J. Huber, and J. P. Manuel, "Black holes seeding cosmological phase transitions," arXiv:2006.16275 [hep-th].

[70] M. Laine and A. Vuorinen, "Basics of Thermal Field Theory," *Lect. Notes Phys.* **925** (2016) pp.1–281, arXiv:1701.01554 [hep-ph].

[71] C. Grojean and G. Servant, "Gravitational Waves from Phase Transitions at the Electroweak Scale and Beyond," *Phys. Rev.* **D75** (2007) 043507, arXiv:hep-ph/0607107 [hep-ph].

[72] M. Hindmarsh, S. J. Huber, K. Rummukainen, and D. J. Weir, "Numerical simulations of acoustically generated gravitational waves at a first order phase transition," *Phys. Rev.* **D92** no. 12, (2015) 123009, arXiv:1504.03291 [astro-ph.CO].

[73] M. Hindmarsh, S. J. Huber, K. Rummukainen, and D. J. Weir, "Shape of the acoustic gravitational wave power spectrum from a first order phase transition," *Phys. Rev.* **D96** no. 10, (2017) 103520, arXiv:1704.05871 [astro-ph.CO].

[74] G. D. Moore and T. Prokopec, "How fast can the wall move? A Study of the electroweak phase transition dynamics," *Phys. Rev.* **D52** (1995) 7182–7204, arXiv:hep-ph/9506475 [hep-ph].

[75] G. D. Moore and T. Prokopec, "Bubble wall velocity in a first order electroweak phase transition," *Phys. Rev. Lett.* **75** (1995) 777–780, arXiv:hep-ph/9503296 [hep-ph].

[76] D. Bodeker and G. D. Moore, "Can electroweak bubble walls run away?," *JCAP* **0905** (2009) 009, arXiv:0903.4099 [hep-ph].

[77] A. Megevand and A. D. Sanchez, "Velocity of electroweak bubble walls," *Nucl. Phys.* **B825** (2010) 151–176, arXiv:0908.3663 [hep-ph].

[78] D. Bodeker and G. D. Moore, "Electroweak Bubble Wall Speed Limit," *JCAP* **1705** no. 05, (2017) 025, arXiv:1703.08215 [hep-ph].

[79] G. C. Dorsch, S. J. Huber, and T. Konstandin, "Bubble wall velocities in the Standard Model and beyond," *JCAP* **1812** no. 12, (2018) 034, arXiv:1809.04907 [hep-ph].

[80] A. Kosowsky, "Gravitational radiation from strongly first-order cosmological phase transitions," in *The Fermilab Meeting DPF 92. Proceedings, 7th Meeting of the American Physical Society, Division of Particles and Fields, Batavia, USA, November 10-14, 1992. Vol. 1, 2*, pp. 1415–1417. 1992.

[81] A. Kosowsky and M. S. Turner, "Gravitational radiation from colliding vacuum bubbles: envelope approximation to many bubble collisions," *Phys. Rev.* **D47** (1993) 4372–4391, arXiv:astro-ph/9211004 [astro-ph].

[82] C. Caprini, R. Durrer, and G. Servant, "Gravitational wave generation from bubble collisions in first-order phase transitions: An analytic approach," *Phys. Rev.* **D77** (2008) 124015, arXiv:0711.2593 [astro-ph].

[83] S. J. Huber and T. Konstandin, "Gravitational Wave Production by Collisions: More Bubbles," *JCAP* **0809** (2008) 022, arXiv:0806.1828 [hep-ph].

[84] C. Caprini and R. Durrer, "Gravitational waves from stochastic relativistic sources: Primordial turbulence and magnetic fields," *Phys. Rev.* **D74** (2006) 063521, arXiv:astro-ph/0603476 [astro-ph].

[85] M. Hindmarsh, "Sound shell model for acoustic gravitational wave production at a first-order phase transition in the early Universe," *Phys. Rev. Lett.* **120** no. 7, (2018) 071301, arXiv:1608.04735 [astro-ph.CO].

[86] M. Hindmarsh, S. J. Huber, K. Rummukainen, and D. J. Weir, "Gravitational waves from the sound of a first order phase transition," *Phys. Rev. Lett.* **112** (2014) 041301, arXiv:1304.2433 [hep-ph].

[87] A. Kosowsky, A. Mack, and T. Kahniashvili, "Gravitational radiation from cosmological turbulence," *Phys. Rev.* **D66** (2002) 024030, arXiv:astro-ph/0111483 [astro-ph].

[88] C. Caprini, R. Durrer, and G. Servant, "The stochastic gravitational wave background from turbulence and magnetic fields generated by a first-order phase transition," *JCAP* **0912** (2009) 024, arXiv:0909.0622 [astro-ph.CO].

[89] P. Binetruy, A. Bohe, C. Caprini, and J.-F. Dufaux, "Cosmological Backgrounds of Gravitational Waves and eLISA/NGO: Phase Transitions, Cosmic Strings and Other Sources," *JCAP* **1206** (2012) 027, arXiv:1201.0983 [gr-qc].

[90] V. A. Rubakov, "Large and infinite extra dimensions: An Introduction," *Phys. Usp.* **44** (2001) 871–893, arXiv:hep-ph/0104152 [hep-ph]. [Usp. Fiz. Nauk171,913(2001)].

[91] G. Gabadadze, "ICTP lectures on large extra dimensions," *ICTP Lect. Notes Ser.* **14** (2003) 77–120, arXiv:hep-ph/0308112 [hep-ph].

[92] C. Csaki, "TASI lectures on extra dimensions and branes," in *From fields to strings: Circumnavigating theoretical physics. Ian Kogan memorial collection (3 volume set)*, pp. 605–698. 2004. arXiv:hep-ph/0404096 [hep-ph]. [,967(2004)].

[93] C. Csaki, J. Hubisz, and P. Meade, "TASI lectures on electroweak symmetry breaking from extra dimensions," in *Physics in D ¿= 4. Proceedings, Theoretical Advanced Study Institute in elementary particle physics, TASI 2004, Boulder, USA, June 6-July 2, 2004*, pp. 703–776. 2005. arXiv:hep-ph/0510275 [hep-ph].

[94] A. Perez-Lorenzana, "An Introduction to extra dimensions," *J. Phys. Conf. Ser.* **18** (2005) 224–269, arXiv:hep-ph/0503177 [hep-ph].

[95] R. Rattazzi, "Cargese lectures on extra-dimensions," in *Particle physics and cosmology: The interface. Proceedings, NATO Advanced Study Institute, School, Cargese, France, August 4-16, 2003*, pp. 461–517. 2003. arXiv:hep-ph/0607055 [hep-ph].
http://weblib.cern.ch/abstract?CERN-PH-TH-2006-029-JOURNAL-REF:-PARTICLE-PHYSICS.

[96] C. Csáki and P. Tanedo, "Beyond the Standard Model," in *Proceedings, 2013 European School of High-Energy Physics (ESHEP 2013): Paradfurdo, Hungary, June 5-18, 2013*, pp. 169–268. 2015. arXiv:1602.04228 [hep-ph].

[97] I. Antoniadis, N. Arkani-Hamed, S. Dimopoulos, and G. R. Dvali, "New dimensions at a millimeter to a Fermi and superstrings at a TeV," *Phys. Lett.* **B436** (1998) 257–263, arXiv:hep-ph/9804398 [hep-ph].

[98] M. Gabella, "The randall-sundrum model,".

[99] C. Charmousis, R. Gregory, and V. A. Rubakov, "Wave function of the radion in a brane world," *Phys. Rev.* **D62** (2000) 067505, arXiv:hep-th/9912160 [hep-th].

[100] W. D. Goldberger and I. Z. Rothstein, "Quantum stabilization of compactified AdS(5)," *Phys. Lett. B* **491** (2000) 339–344, arXiv:hep-th/0007065.

[101] J. Garriga, O. Pujolas, and T. Tanaka, "Radion effective potential in the brane world," *Nucl. Phys. B* **605** (2001) 192–214, arXiv:hep-th/0004109.

[102] W. D. Goldberger and M. B. Wise, "Modulus stabilization with bulk fields," *Phys. Rev. Lett.* **83** (1999) 4922–4925, arXiv:hep-ph/9907447 [hep-ph].

[103] E. Witten, "Anti-de Sitter space and holography," *Adv. Theor. Math. Phys.* **2** (1998) 253–291, arXiv:hep-th/9802150 [hep-th].

[104] N. Arkani-Hamed, M. Porrati, and L. Randall, "Holography and phenomenology," *JHEP* **08** (2001) 017, arXiv:hep-th/0012148 [hep-th].

[105] R. Rattazzi and A. Zaffaroni, "Comments on the holographic picture of the Randall-Sundrum model," *JHEP* **04** (2001) 021, arXiv:hep-th/0012248 [hep-th].

[106] G. T. Horowitz and R. C. Myers, "The AdS / CFT correspondence and a new positive energy conjecture for general relativity," *Phys. Rev.* **D59** (1998) 026005, arXiv:hep-th/9808079 [hep-th].

[107] G. W. Gibbons and S. W. Hawking, "Action Integrals and Partition Functions in Quantum Gravity," *Phys. Rev.* **D15** (1977) 2752–2756.

[108] W. D. Goldberger and M. B. Wise, "Phenomenology of a stabilized modulus," *Phys. Lett.* **B475** (2000) 275–279, arXiv:hep-ph/9911457 [hep-ph].

[109] O. DeWolfe, D. Z. Freedman, S. S. Gubser, and A. Karch, "Modeling the fifth-dimension with scalars and gravity," *Phys. Rev.* **D62** (2000) 046008, arXiv:hep-th/9909134 [hep-th].

[110] C. Csaki, M. L. Graesser, and G. D. Kribs, "Radion dynamics and electroweak physics," *Phys. Rev. D* **63** (2001) 065002, arXiv:hep-th/0008151.

[111] H. Davoudiasl, J. L. Hewett, and T. G. Rizzo, "Brane localized curvature for warped gravitons," *JHEP* **08** (2003) 034, arXiv:hep-ph/0305086 [hep-ph].

[112] E. Witten, "Anti-de Sitter space, thermal phase transition, and confinement in gauge theories," *Adv. Theor. Math. Phys.* **2** (1998) 505–532, arXiv:hep-th/9803131 [hep-th]. [,89(1998)].

[113] S. W. Hawking and D. N. Page, "Thermodynamics of Black Holes in anti-De Sitter Space," *Commun. Math. Phys.* **87** (1983) 577.

[114] M. Carena, J. D. Lykken, and M. Park, "The Interval approach to braneworld gravity," *Phys. Rev.* **D72** (2005) 084017, arXiv:hep-ph/0506305 [hep-ph].

[115] D. P. George and K. L. McDonald, "Gravity on a Little Warped Space," *Phys. Rev.* **D84** (2011) 064007, arXiv:1107.0755 [hep-ph].

[116] B. M. Dillon, D. P. George, and K. L. McDonald, "Regarding the Radion in Randall-Sundrum Models with Brane Curvature," *Phys. Rev.* **D94** no. 6, (2016) 064045, arXiv:1605.03087 [hep-ph].

[117] S. Bruggisser, B. Von Harling, O. Matsedonskyi, and G. Servant, "Electroweak Phase Transition and Baryogenesis in Composite Higgs Models," *JHEP* **12** (2018) 099, arXiv:1804.07314 [hep-ph].

[118] G. R. Dvali, G. Gabadadze, and M. Porrati, "4-D gravity on a brane in 5-D Minkowski space," *Phys. Lett.* **B485** (2000) 208–214, arXiv:hep-th/0005016 [hep-th].

[119] M. Carena, A. Delgado, J. D. Lykken, S. Pokorski, M. Quiros, and C. E. M. Wagner, "Brane Effects on Extra Dimensional Scenarios: A Tale of Two Gravitons," *Nucl. Phys.* **B609** (2001) 499–517, arXiv:hep-ph/0102172 [hep-ph].

[120] N. D. Birrell and P. C. W. Davies, *Quantum Fields in Curved Space*. Cambridge Monographs on Mathematical Physics. Cambridge Univ. Press, Cambridge, UK, 1984. http://www.cambridge.org/mw/academic/subjects/physics/

theoretical-physics-and-mathematical-physics/
quantum-fields-curved-space?format=PB.

[121] M. Carena, T. M. P. Tait, and C. E. M. Wagner, "Branes and Orbifolds are Opaque," *Acta Phys. Polon.* **B33** (2002) 2355, arXiv:hep-ph/0207056 [hep-ph].

[122] E. Ponton and E. Poppitz, "Casimir energy and radius stabilization in five-dimensional orbifolds and six-dimensional orbifolds," *JHEP* **06** (2001) 019, arXiv:hep-ph/0105021 [hep-ph].

[123] A. Ahmed, B. M. Dillon, B. Grzadkowski, J. F. Gunion, and Y. Jiang, "Implications of the absence of high-mass radion signals," *Phys. Rev.* **D95** no. 9, (2017) 095019, arXiv:1512.05771 [hep-ph].

[124] A. Chakraborty, U. Maitra, S. Raychaudhuri, and T. Samui, "Mixed Higgs–radion states at the LHC – a detailed study," *Nucl. Phys.* **B922** (2017) 41–61, arXiv:1701.07471 [hep-ph].

[125] A. Angelescu, G. Moreau, and F. Richard, "Scalar production in association with a Z boson at the LHC and ILC: The mixed Higgs-radion case of warped models," *Phys. Rev.* **D96** no. 1, (2017) 015019, arXiv:1702.03984 [hep-ph].

[126] H. Davoudiasl, J. L. Hewett, and T. G. Rizzo, "Phenomenology of the Randall-Sundrum Gauge Hierarchy Model," *Phys. Rev. Lett.* **84** (2000) 2080, arXiv:hep-ph/9909255 [hep-ph].

[127] B. M. Dillon and V. Sanz, "Kaluza-Klein gravitons at LHC2," *Phys. Rev.* **D96** no. 3, (2017) 035008, arXiv:1603.09550 [hep-ph].

[128] B. M. Dillon, C. Han, H. M. Lee, and M. Park, "KK graviton resonance and cascade decays in warped gravity," *Int. J. Mod. Phys.* **A32** no. 33, (2017) 1745006, arXiv:1606.07171 [hep-ph].

[129] E. Alvarez, L. Da Rold, J. Mazzitelli, and A. Szynkman, "Graviton resonance phenomenology and a pseudo-Nambu-Goldstone boson Higgs at the LHC," *Phys. Rev.* **D95** no. 11, (2017) 115012, arXiv:1610.08451 [hep-ph].

[130] J. W. York, Jr., "Role of conformal three geometry in the dynamics of gravitation," *Phys. Rev. Lett.* **28** (1972) 1082–1085.

[131] M. E. Shaposhnikov, "Possible Appearance of the Baryon Asymmetry of the Universe in an Electroweak Theory," *JETP Lett.* **44** (1986) 465–468. [Pisma Zh. Eksp. Teor. Fiz.44,364(1986)].

[132] M. E. Shaposhnikov, "Baryon Asymmetry of the Universe in Standard Electroweak Theory," *Nucl. Phys.* **B287** (1987) 757–775.

[133] T. Konstandin, "Quantum Transport and Electroweak Baryogenesis," *Phys. Usp.* **56** (2013) 747–771, arXiv:1302.6713 [hep-ph].

[134] M. Sasaki, T. Suyama, T. Tanaka, and S. Yokoyama, "Primordial black holes—perspectives in gravitational wave astronomy," *Class. Quant. Grav.* **35** no. 6, (2018) 063001, arXiv:1801.05235 [astro-ph.CO].

[135] B. Carr, F. Kuhnel, and M. Sandstad, "Primordial Black Holes as Dark Matter," *Phys. Rev. D* **94** no. 8, (2016) 083504, arXiv:1607.06077 [astro-ph.CO].

[136] B. Carr, K. Kohri, Y. Sendouda, and J. Yokoyama, "Constraints on Primordial Black Holes," arXiv:2002.12778 [astro-ph.CO].

[137] P. Burda, R. Gregory, and I. Moss, "Gravity and the stability of the Higgs vacuum," *Phys. Rev. Lett.* **115** (2015) 071303, arXiv:1501.04937 [hep-th].

[138] A. Rajantie and S. Stopyra, "Standard Model vacuum decay with gravity," *Phys. Rev. D* **95** no. 2, (2017) 025008, arXiv:1606.00849 [hep-th].

[139] D. Canko, I. Gialamas, G. Jelic-Cizmek, A. Riotto, and N. Tetradis, "On the Catalysis of the Electroweak Vacuum Decay by Black Holes at High Temperature," *Eur. Phys. J. C* **78** no. 4, (2018) 328, arXiv:1706.01364 [hep-th].

[140] D. Gorbunov, D. Levkov, and A. Panin, "Fatal youth of the Universe: black hole threat for the electroweak vacuum during preheating," *JCAP* **1710** no. 10, (2017) 016, arXiv:1704.05399 [astro-ph.CO].

[141] K. Mukaida and M. Yamada, "False Vacuum Decay Catalyzed by Black Holes," *Phys. Rev.* **D96** no. 10, (2017) 103514, arXiv:1706.04523 [hep-th].

[142] N. Oshita, M. Yamada, and M. Yamaguchi, "Compact objects as the catalysts for vacuum decays," *Phys. Lett. B* **791** (2019) 149–155, arXiv:1808.01382 [gr-qc].

[143] R. M. Wald, *General Relativity*. Chicago Univ. Pr., Chicago, USA, 1984.

[144] B. J. Carr and S. W. Hawking, "Black holes in the early Universe," *Mon. Not. Roy. Astron. Soc.* **168** (1974) 399–415.

[145] M. Crawford and D. N. Schramm, "Spontaneous Generation of Density Perturbations in the Early Universe," *Nature* **298** (1982) 538–540. [,333(1982)].

[146] S. W. Hawking, I. G. Moss, and J. M. Stewart, "Bubble Collisions in the Very Early Universe," *Phys. Rev.* **D26** (1982) 2681.

[147] S. W. Hawking, "Black Holes From Cosmic Strings," *Phys. Lett.* **B231** (1989) 237–239.

[148] A. M. Green, "Primordial Black Holes: sirens of the early Universe," *Fundam. Theor. Phys.* **178** (2015) 129–149, arXiv:1403.1198 [gr-qc].

[149] B. J. Carr, "The Primordial black hole mass spectrum," *Astrophys. J.* **201** (1975) 1–19.

[150] J. C. Niemeyer and K. Jedamzik, "Near-critical gravitational collapse and the initial mass function of primordial black holes," *Phys. Rev. Lett.* **80** (1998) 5481–5484, arXiv:astro-ph/9709072 [astro-ph].

[151] J. C. Niemeyer and K. Jedamzik, "Dynamics of primordial black hole formation," *Phys. Rev.* **D59** (1999) 124013, arXiv:astro-ph/9901292 [astro-ph].

[152] A. M. Green, A. R. Liddle, K. A. Malik, and M. Sasaki, "A New calculation of the mass fraction of primordial black holes," *Phys. Rev.* **D70** (2004) 041502, arXiv:astro-ph/0403181 [astro-ph].

[153] S. Young, C. T. Byrnes, and M. Sasaki, "Calculating the mass fraction of primordial black holes," *JCAP* **1407** (2014) 045, arXiv:1405.7023 [gr-qc].

[154] D.-C. Dai, R. Gregory, and D. Stojkovic, "Connecting the Higgs Potential and Primordial Black Holes," *Phys. Rev. D* **101** no. 12, (2020) 125012, arXiv:1909.00773 [hep-ph].

[155] S. W. Hawking, "Black hole explosions," *Nature* **248** (1974) 30–31.

[156] S. W. Hawking, "Particle Creation by Black Holes," *Commun. Math. Phys.* **43** (1975) 199–220. [,167(1975)].

[157] T. Hayashi, K. Kamada, N. Oshita, and J. Yokoyama, "On catalyzed vacuum decay around a radiating black hole and the crisis of the electroweak vacuum," *JHEP* **08** (2020) 088, arXiv:2005.12808 [hep-th].

[158] B. J. Carr, K. Kohri, Y. Sendouda, and J. Yokoyama, "New cosmological constraints on primordial black holes," *Phys. Rev.* **D81** (2010) 104019, arXiv:0912.5297 [astro-ph.CO].